67 7 0 1 9 9 Copy 339

[redacted]

553973
76P

[redacted]

NASA MEMO 2-19-59A

NASA

MEMORANDUM

Classification changed to declassifie
effective 1 April 1963 under
authority of NASA CCN 2 by
J. J. Carroll. JC

N 63 13883

AN EXPERIMENTAL INVESTIGATION OF CIRCULAR INTERNAL-COMPRESSION INLETS WITH TRANSLATING CENTERBODIES EMPLOYING BOUNDARY-LAYER REMOVAL AT MACH NUMBERS FROM 0.85 TO 3.50

By Frank A. Pfyl and Earl C. Watson

Ames Research Center
Moffett Field, Calif.

CASE FILE
COPY

[redacted]

NATIONAL AERONAUTICS AND
SPACE ADMINISTRATION
WASHINGTON
March 1959

[redacted]

UNC[redacted]SIFIED

NATIONAL AERONAUTICS AND SPACE ADMINISTRATION

MEMORANDUM 2-19-59A

AN EXPERIMENTAL INVESTIGATION OF CIRCULAR INTERNAL-COMPRESSION INLETS WITH TRANSLATING CENTERBODIES EMPLOYING BOUNDARY-LAYER REMOVAL AT MACH NUMBERS FROM 0.85 TO 3.50*

By Frank A. Pfyl and Earl C. Watson

SUMMARY

The performance characteristics of axially symmetric internal-compression inlets with translating centerbodies are presented for a Mach number range of 0.85 to 3.5 and for Reynolds numbers between 0.6 and 5.2 million (based on inlet diameter). The study chiefly concerns the effect of boundary-layer removal on the total-pressure recovery for a number of internal shapes. A limited amount of data shows the effect of flow-deflector plates on angle-of-attack performance and data showing inlet flow distortion and unsteadiness characteristics also are included.

Seven inlets were investigated and each is designated herein as either straight, ogival, or isentropic, according to the shape of its supersonic diffuser. The straight inlets were designed with internal surfaces having straight-line elements. The internal surfaces of the ogival inlet have contours which result from design considerations based on a one-dimensional flow analysis in conjunction with the requirement of a nearly linear pressure gradient. The isentropic inlets were designed by the method of characteristics to avoid the formation of internal shock waves.

The results of the investigation showed that at Mach number 2.5 the pressure recovery of a straight inlet with zero boundary-layer removal was 76 percent, whereas, with boundary-layer removal equal to approximately 8 percent of the entering inlet mass flow the pressure recovery was 88 percent. Although different in internal shape, the best straight and isentropic inlets had approximately the same pressure recovery at Mach number 2.5 when boundary-layer bleed was applied. However, in the case of the

*Title, Unclassified

[redacted]

ogival inlet the pressure recovery was poorer than that of the straight and isentropic inlets. The initial rate of pressure recovery decay with angle of attack for the straight inlets increased with increasing Mach number. With one inlet, a flow deflector plate was effective in maintaining the pressure recovery up to at least 9° angle of attack, and it improved the total-pressure distribution. A study of the internal-pressure oscillations on two of the straight inlets showed that no air-flow unsteadiness occurred during supercritical inlet operation (terminal shock inside inlet). A test with one inlet indicated that the maximum obtainable pressure recovery generally increased with increasing values of Reynolds number from 2.7 to 5.2 million.

INTRODUCTION

Presented in reference 1 are the results of an exploratory experimental investigation of a type of internal-compression inlet which has a translating centerbody. The data showed that the pressure recovery was comparable to that for single-cone external-compression inlets and the discussion indicated that zero external wave drag was possible. Although such findings were gratifying, the analysis presented in reference 1 as well as subsequent studies of the data indicated certain deficiencies of the inlet which, if eliminated, could possibly improve the characteristics considerably. For example, it was known from studies of total-pressure measurements near the throat region that because of terminal-shock-wave interactions, the boundary layer thickened excessively behind the wave and caused large total-pressure losses. Also, an analysis of the data indicated that a constant-area section in the region of minimum-flow area was desirable. Furthermore, studies of the internal lines of the inlet showed that small changes to the shape would possibly permit a sizable reduction in the starting Mach number of the inlet and hence an improvement in off-design characteristics. Lastly, it was suspected that the pressure recovery of the inlet might be very sensitive to angle of attack.

In conjunction with the above analyses, related studies of research efforts on other types of internal-compression inlets reported in references 2 to 6 have shown that large benefits accrued from the use of boundary-layer removal and that the limits of maximum pressure recovery for internal-compression inlets were high with respect to those for external-compression inlets. Consequently, investigations of the inlets of the type introduced in reference 1 designed to operate up to Mach numbers of 2.5 were continued. The experimental studies, reported herein, have been exploratory in nature since a complete study could not be made of the many design variables believed to influence the characteristics of internal-compression inlets. Thus, although several modifications to the internal lines were investigated, only one type of boundary-layer-removal system and a single method for improving the angle-of-attack characteristics were tested.

[redacted]

Several Ames facilities were used in the course of these investigations to obtain data over a Mach number range from 0.85 to 3.5. Measurements were made of the total-pressure recovery at a position where the compressor of a jet engine might be located, and in the region of the inlet throat. In addition measurements of the static-pressure fluctuations within the inlet were made. Although the principal portion of the data was obtained at 0° angle of attack, some measurements were made at angles of attack up to 12°. In addition to the experimental measurements, a brief analysis of the drag characteristics of the inlet which included considerations of the boundary-layer-removal system was made and is included herein.

SYMBOLS

A area, sq in.

$\frac{A_{min}}{A_i}$ contraction ratio (the minimum internal flow area at constant centerbody position divided by the area of the annulus at the lip leading edge)

D annulus entrance diameter at the lip leading edge, in.

D_A local internal diameter of annulus, in.

D_B local diameter of centerbody, in.

f frequency, cps

L longitudinal distance from the compressor station (positive direction downstream), in.

$\frac{m_b}{m_\infty}$ $\frac{\text{mass of boundary-layer air removed}}{\rho_\infty A_i V_\infty}$

$\frac{m_i}{m_\infty}$ $\frac{\text{mass flow entering inlet}}{\rho_\infty A_i V_\infty}$

M Mach number

p_t total pressure, lb/sq ft

$\Delta\overline{p}$ root-mean square of the static-pressure fluctuations, lb/sq ft

R Reynolds number, based on inlet diameter

V velocity, ft/sec

X longitudinal distance from the annulus leading edge (positive direction downstream), in.

$\frac{y}{Y}$ vertical distance from centerbody surface to probe divided by throat height at probe station

α angle of attack, deg

ρ mass density of air, slugs/cu ft

Inlet Designations

I isentropic inlets (design of internal shape to avoid the formation of shock waves)

O ogival inlet (internal contours designed to approximate a uniform longitudinal pressure gradient)

P inlet having holes in the centerbody and annulus to provide perforated surfaces

S straight inlets (internal contours composed of straight-line elements)

Subscripts

c compressor entrance station

i inlet station (lip leading edge)

l local condition

∞ free-stream condition

APPARATUS, MODELS, AND PROCEDURE

Test Facilities

Three different facilities were used for the investigation of the inlet models: the Ames 6- by 6-foot, 8- by 7-foot, and 8- by 8-inch supersonic wind tunnels. A description of each tunnel can be found in references 7, 8, and 1, respectively. [redacted]

Models

Of the seven models tested, three were of large scale (inlet diameter = 12.5 in.) for tests in the 6- by 6-foot and 8- by 7-foot wind tunnels and four were of small scale (inlet diameter = 2.5 in.) for tests in the 8- by 8-inch wind tunnel. A photograph of one of the large models mounted in the test section of the 6- by 6-foot wind tunnel is shown in figure 1 (the model mounting in the 8- by 7-foot wind tunnel was similar). In figure 2 one of the small models is shown mounted in the 8- by 8-inch wind tunnel. Assembly drawings of a large and a small model are shown in figure 3.

Inlet Design

Details of the seven inlets are shown in figure 4. Four straight inlets, identified by the letter S, were designed with internal surfaces having straight-line elements. One inlet, identified by the letter O, had approximately ogival internal surfaces and was, therefore, termed the ogival inlet. It was designed with curved longitudinal surface elements resulting from design considerations based on a one-dimensional flow analysis in conjunction with the requirement of a nearly linear axial pressure gradient. Two inlets designed by the method of characteristics to avoid the formation of internal shock waves are termed isentropic inlets and are identified by the letter I.

The design considerations for internal-compression inlets with translating centerbodies which were discussed previously in reference 1 were employed in the inlets of the present investigation. The longitudinal distributions of area ratio for the inlets discussed herein differed somewhat from those of reference 1, however, as the result of several contour modifications made to improve the performance of the latter configurations. Small scale inlets S4, O1, and I1 were the same as those tested in reference 1 except that the annuli were changed to provide nearly constant area sections near the throat regions, and the centerbodies were shortened in each case to provide larger base areas for removal of boundary-layer air. Because of these modifications, the starting Mach numbers of these inlets were higher than those of reference 1. The small-scale isentropic inlet, I2, was similar in shape to inlet I1 (and also to the inlet of ref. 4) but provided area ratios to allow starting near a Mach number of 1.5. Of the large-scale models, inlets S1 and S3 were similar in design to inlet S4, but both required changes to the subsonic diffuser contours because of structural requirements. In addition, inlet S1 contours were altered to provide a nearly constant area section as well as to permit a starting Mach number near 1.5. Inlet S2, on the other hand, differed greatly from the above inlets in that it was designed for

efficient supersonic compression at a Mach number of about 2.0. For the inlets of the present investigation A_l/A_i is shown in figure 5, and the contraction ratio A_{min}/A_i is plotted in figure 6. For convenience, the important design parameters and test variables for each inlet are given in the following table.

Inlet	Wind tunnel	Range of test variables			Design parameters			
		M_∞	$R \times 10^{-6}$	α, deg	Centerbody apex, X/D	$\frac{A_{min}}{A_i}$	Constant area length[1] (inlet diameters)	M_{start}
S1	8- by 7-foot	2.47-3.50	0.60-1.07	0-12	0	0.374	0.80	1.5
S2	6- by 6-foot	0.85-2.25	2.5-2.9	0	0	.649	0	1.85
S3	6- by 6-foot	2.34	1.15	0-11.6	0	.390	.20	1.85
S4	8- by 8-inch	2.1-3.0	2.5-3.9	0	0	.373	.84	2.3
O1	8- by 8-inch	1.7-3.0	2.0-3.9	0	-0.2[2]	.373	.84	2.0
I1	8- by 8-inch	2.1-3.0	2.5-3.9	0	0	.373	.84	2.3
I2	8- by 8-inch	1.8-3.0	2.0-5.2	0	-0.46[2]	.404	.84	1.5

[1]With the exception of inlets S2 and S3, allowances were made for boundary-layer growth.
[2]For inlets O1 and I2 the centerbodies could be retracted to X/D values of 0.

The location and size of the holes in the annulus and centerbody of the inlets employing boundary-layer removal are given in figure 7. For each inlet the upstream row of holes in both the annulus and centerbody coincided with the beginning of the constant area section of the inlet when the centerbody was positioned for maximum pressure recovery at M = 2.5 and without boundary-layer removal. Note in figure 5, for the inlets employing boundary-layer removal, that at each centerbody apex position the region of perforations on the centerbody (indicated by dash lines) is shown with respect to the region of perforations on the annulus. The holes were sized to permit removal of approximately 8 percent of the inlet flow. For the small models the air removed through the annulus was ejected to the free stream at 90° to the center line of symmetry, whereas for the large model the removed air was expanded rearward through a nozzle to a supersonic Mach number. In all bleed configurations, the air removed through the centerbody perforated surface was ejected at the base of the model. Inlets employing boundary-layer removal are identified herein by a letter P following the letter-digit combination.

Drawings of the angle-of-attack, flow-deflector plates used on models S1 and S3 are presented in figure 8.

Instrumentation and Measurements

Total-pressure recovery.- For both the large and small models, the total-pressure recovery at the assumed location of the engine compressor face was measured with total-pressure tubes arranged on an equal-area basis as shown in figures 3(a) and 3(b). The rake of the large model had 36 total- and 6 static-pressure tubes and the rake of the small model had 20 total- and 4 static-pressure tubes. For both cases, the pressure tubes were connected to mercury filled multitube manometers and the data were recorded photographically. From such data total-pressure distribution was obtained. The manometers also contained integrating tubes which were used in conjunction with automatic recording and computing equipment to obtain average values of the total pressures. (Static-pressure measurements in the main duct of the large and small models were not used in these tests.)

Mass flow through boundary-layer removal system.- Because of space limitations in the small models, only one static- and one total-pressure tube could be placed in the centerbody boundary-layer-removal system to measure the mass flow. As shown in figure 3(b), the tubes were near the exit of the centerbody boundary-layer-removal duct. The mass flow through the annulus boundary-layer-removal system was not measured directly. However, an estimate was made, assuming that the pressure recovery across the holes was the same as those measured in the centerbody and that the flow through all holes was choked. Therefore, the mass flow through the annulus was assumed proportional to the ratio of the perforated area of the annulus to that of the centerbody.

No measurements were made of the boundary-layer-removal mass flow of the large model, S1, because measuring tubes could not be installed in the exit passages.

Total-pressure surveys.- Surveys of the total-pressure distribution in the vicinity of the inlet throat were made for inlets S4 and I2 using a total-pressure probe and a wall static-pressure orifice. When possible, two surveys were made, one with the terminal shock positioned ahead of the probe, and the other with it behind the probe. In the latter case the flow was supersonic at the probe and in the calculation of stream total pressure, the Rayleigh pitot relationship and the assumption of constant static pressure across the duct were used.

Static-pressure pulsations.- A pressure cell (a bonded strain-gage type) was installed flush with the duct surface near the compressor inlet station of inlets S2 and S3 (see fig. 3(a)) to measure the static-pressure pulsations in the duct when flow unsteadiness occurred. The output signal of the pressure cell was passed through a complete carrier-amplification system (system response flat to 3000 cps) and then recorded in two

different ways. In one case the root-mean-square value of the amplified signal was observed with a calibrated AC-DC thermocouple-type milliammeter. This method provided a convenient indication of the energy level of the flow unsteadiness. In the other, the signal was recorded on a magnetic tape so as to permit analysis of the unsteadiness characteristics at the conclusion of the test.

Procedure

The procedure for obtaining pressure-recovery data was the same for the large and the small models. In most cases data were obtained for supercritical inlet operations. However, depending on the Mach number and inlet, some data were taken for subcritical inlet operation. After an inlet had been started (by extending the centerbody), the centerbody was retracted to one of several positions near the most rearward one for which any further retraction would expel the terminal shock from within the inlet. At each centerbody position the back pressure was then increased by closing the exit plug. The pressure recovery increased with forward translation of the exit plug until the point was reached where the terminal shock was expelled. The pressure recovery obtained just prior to expulsion of the terminal shock was considered the maximum obtainable for that centerbody position. The pressure recovery values presented herein for subcritical inlet operation are the maximum obtainable for the specified centerbody positions.

RESULTS

The average total-pressure recoveries obtained for the internal-compression inlets at 0° angle of attack are shown in figures 9 through 11. Specifically, the variation of maximum pressure recovery with contraction ratio, A_{min}/A_i, is presented in figure 9 for each inlet at each Mach number investigated. These curves generally show that for each Mach number the highest pressure recovery, with or without boundary-layer control, occurred at a contraction ratio other than the lowest attainable. It should be noted that while a peak value of pressure recovery was always obtained for each Mach number, sufficient data to define clearly the entire curve are lacking in some cases. The highest values obtained at each Mach number for the inlets with and without boundary-layer removal are presented in figure 10 to show the variation of maximum pressure recovery with Mach number. Tests which varied the Reynolds number at $M_{\infty} = 2.5$ were made with inlet I2P and the results are presented in figure 11.

Total-pressure surveys in the transonic region of internal-compression inlets are useful for determining the efficiency of the compression process in the supersonic region of the inlet. The results of surveys obtained at $M_{\infty} = 2.5$ for two inlets (S4 and I2) with and without boundary-layer removal

are shown in figure 12. The data are presented for the terminal shock downstream of the survey probe and, where possible, for it upstream of the probe. By this technique a comparison can be made between losses arising from supersonic compression alone and those arising from the entire compression process up to and including the terminal shock system.

The results showing the effect of angle of attack on pressure recovery are presented in figure 13 for several inlets. Data for the inlets with and without flow-deflector plates are included.

It is desirable that the air delivered to the compressor by the inlet system have small variations in the distribution of total pressure as well as high average pressure recovery. Therefore, contours of local total-pressure ratio for several inlets are presented in figure 14 to show typical total-pressure distribution. In addition to total-pressure distortion the character of flow unsteadiness is important to the designer. The results showing the magnitude of unsteadiness (expressed by the parameter, $\Delta\overline{p}/p_{t_\infty}$) as well as the predominant frequency of the disturbance are presented in figures 15 and 16.

DISCUSSION

Total-Pressure Recovery

Effect of boundary-layer removal.- The importance of the application of boundary-layer control to most air-induction systems has been well established as a requisite to the attainment of high pressure recovery. Some of the general flow characteristics associated with the removal of boundary-layer air through holes, scoops, and nozzles are presented in references 9, 10, and 11, and several studies of specific scoop-type, boundary-layer-removal systems in internal-compression inlets are presented in references 2, 3, 4, and 6. However, there is little published data available which can be used to select the location or the type of bleed system for three-dimensional internal-compression inlets.

The over-all improvement in pressure recovery obtained by removal of the low-energy boundary-layer air with the perforated inlets of this test was large and can be seen most conveniently in figure 10. The largest gain at $M_\infty = 2.5$ was obtained with inlet S4P - from 77 percent without boundary-layer removal (inlet S4) to 88 percent; the corresponding geometric contraction ratios were 0.470 and 0.420, respectively. The total boundary-layer air removed through the centerbody and annulus perforations of the small inlets near $M_\infty = 2.5$ was estimated, as discussed in Inlet Design section, to be about 8 percent of the inlet capture mass flow.

Some understanding of the effects of boundary-layer control can be obtained from the results of the total-pressure surveys in the throat region (fig. 12). Considering first the data wherein the terminal shock is aft of the probe, the results show that boundary-layer control reduced the total-pressure losses near both surfaces for inlet S4P but had no appreciable effect on the total-pressure losses for inlet I2P. This may be the reason why boundary-layer control was more beneficial in the case of inlet S4P than I2P. However, in addition to the possible gain from boundary-layer control resulting from a reduction of losses near the inlet surfaces, it is believed that the major benefit of boundary-layer control is that it increases the stability of the terminal shock location in the throat region. Therefore, it may be that because of a more stable shock location it was possible to operate an inlet with boundary-layer control, in contrast to an inlet with none, at a lower geometric contraction ratio and at a lower Mach number ahead of a terminal shock of correspondingly lower total-pressure losses. Small total-pressure losses across the terminal shock wave when boundary-layer control was used are evident from a comparison of the total-pressure surveys made with the terminal shock wave behind and ahead of the probe (see figs. 12(b) and 12(d)). When comparing the results of inlets S4P and I2P it should be noted that although their total-pressure profiles were different for operation with no boundary-layer removal, their profiles were nearly the same when maximum pressure recovery was attained with boundary-layer control.

It is evident that if the losses in total pressure were decreased for operation when terminal shock was aft of probe (see figs. 12(b) and (d)) by further improvements in boundary-layer control, associated gains in the pressure recovery at the compressor station could be expected. Most consideration should be given to improving the flow near the annulus, since that is where the largest region of loss occurred.

The shrouded, perforated large inlet S1P (see fig. 7(a)) was designed with a practical annulus flow-removal system in which the boundary-layer air was exited nearly axially. Of the several exit openings in the shroud tested, satisfactory operation occurred only with the largest opening which provided an exit nozzle throat area 25 percent greater than the total area of the annulus holes. This indicates that low pressure recovery was obtained across the 90° perforated holes. With the use of slanted holes higher plenum pressure recovery might have been attained thus requiring smaller exit openings. It should be noted here that because of operational limitations of the large model no boundary-layer air could be removed through the centerbody at $M_\infty = 2.47$; at the higher Mach numbers the boundary-layer air removed through the constricted exit passage of the centerbody, in percent of inlet flow, was probably much less than that exited from the small models (S4P, O1P, I1P, and I2P).

The present tests have shown that removal of moderate amounts of boundary-layer air for this type of inlet significantly improves the pressure recovery up to Mach numbers of about 3.0. Other types of

internal-compression inlets removing generally larger amounts of boundary-layer air have provided high pressure recovery over the Mach number range of this test. Some results of tests of other types of inlets as well as the results of tests of several of the present inlets are shown together in figure 17. It is evident that with boundary-layer control the pressure recovery of internal-compression inlets can exceed the values defined by the envelope of the best external-compression inlets. Also, the data of reference 3 indicate the pressure recovery that may be attained with the present type of inlet, provided efficient methods are found for properly controlling boundary-layer air.

In figure 17 and also in figure 10 it can be seen that a rapid decrease in pressure recovery occurred above $M_\infty = 2.0$ for inlet S2 (consider only supercritical flow operation) and above $M_\infty = 2.5$ for inlets S4P, I1P, and I2P. A partial explanation for this behavior of these inlets becomes apparent by studying the contraction-ratio data presented in figure 18. For inlet S2 the contraction ratio could not be reduced below the value attained at $M_\infty = 2.0$ (a centerbody travel limitation) and consequently a rapid decrease in pressure recovery would be expected at Mach numbers above 2.0. The minimum available contraction ratio that could have been obtained with inlets S4P and I2P was never quite reached. However, because the contraction ratio for maximum pressure recovery remained essentially constant with Mach numbers above 2.5 and no increase in boundary-layer removal was noted, it would be expected that a rapid decrease in pressure recovery with increasing Mach number above 2.5 would occur. It is believed, therefore, that while all the pressure-recovery data are of academic interest, those data presented for Mach numbers above that where the rapid decrease of pressure recovery occurs are not to be considered representative of the pressure recovery that might be obtained with an inlet of the present type designed for higher Mach numbers.

Effect of internal shape.- A comparison between the best straight inlet, S4P, and the best isentropic inlet, I2P, shows that their pressure-recovery characteristics were quite similar for a wide range of Mach numbers (see fig. 17). In addition, it was previously shown that at $M_\infty = 2.5$ their total-pressure profiles in the throat were nearly the same. Of interest, then, is the physical difference between these inlets at $M_\infty = 2.5$. For convenience, figure 19 is included and it can be seen therein that the main difference in the internal-area distribution is ahead of the minimum throat area. It can be concluded that the differences in shapes in the supersonic region represented by these two inlets had no significant effect on the pressure recovery attained at $M_\infty = 2.5$.

It should not be inferred from the above that any shape in the supersonic region will be satisfactory. The data for isentropic inlets I1P and I2P show considerable differences in the pressure-recovery characteristics (see figs. 10(e) and (f)). A preliminary theoretical flow analysis

of isentropic shapes has shown that small changes in the contours influence the flow field considerably and may cause coalescence of Mach lines which result in strong shock waves and concomitant total-pressure losses. Thus, until more conclusive theoretical analyses can be made information leading to satisfactory isentropic designs will remain meager.

Additional effects of shape in the supersonic region are apparent from the data obtained with inlets O1 and O1P. The poor pressure-recovery characteristics of this type inlet are believed to be related, for the most part, to the relatively large internal lip angle. Several tests were conducted in which the annulus of inlet I2P was used in conjunction with the ogival centerbody. At $M_\infty = 2.5$ and with boundary-layer control the pressure recovery for this inlet was 83 percent - an increase of approximately 9 percent over that obtained with inlet O1P with about the same amount of boundary-layer air removed. It may be that relatively large lip angles can promote shock-induced boundary-layer separation on the centerbody and cause serious losses in pressure recovery.

Experimental investigations in a constant-area channel (refs. 9 and 10) have shown the advantages of high ratios of throat length to the length of the terminal-shock region. As noted previously, inlets S4, O1, and I1 provided an increase in the length of the transonic region over that for the corresponding inlets of reference 1. Comparisons of the data of reference 1 and those for the present tests shown together in figures 10(c), (d), and (e) are inconclusive as to the effect the added constant-area section had on pressure recovery. The results of reference 4 show that there was little, or no improvement in pressure recovery at $M_\infty = 2.5$ with the addition of a lengthened, constant-area throat section.

The importance of subsonic diffusion has been emphasized in many publications and, in general, the findings indicate that both the local and equivalent-conical subsonic diffusion angles must be kept low. In addition, the length of the diffuser should be kept as short as possible to keep the friction losses low. One of the ratios that strongly influences the subsonic diffuser shape is A_c/A_i. For the inlets of the present investigation this ratio was 1.0, a value typical of that used for an engine designed for Mach numbers of about 2.0. For the geometric characteristics of these inlets the equivalent subsonic diffuser angle could be as large at 10°. Had a lower value of A_c/A_i been used (such as 0.60 or 0.70 which are values typical for engines designed for Mach numbers near 3.0), the subsonic diffuser could have been either shorter, or have had smaller diffusion angles. In contrast to inlet I2P the isentropic inlet of reference 4 had a value of A_c/A_i equal to 0.653. Also, its subsonic diffuser (see fig. 19 for difference in area variation and length between I2P and the inlet of reference 4) was short and had a small diffuser angle, thereby conforming to the requirements of an

efficient subsonic diffuser. The data of figure 17 show that at $M_\infty = 2.5$ the pressure recovery obtained with this inlet was 0.910 and with inlet I2P it was 0.864. This difference in pressure recovery is believed to be attributed to both the differences in subsonic diffusers and the differences in bleed systems.

In the design of the internal shape of internal-compression inlets the starting Mach number must be considered. The significance of this can be shown by the data for inlets S2 and I2P (figs. 10(b) and (f), respectively). The discontinuity in the curve (fig. 10(b), inlet S2) showing an abrupt increase in pressure recovery between Mach numbers of 1.8 and 1.9 occurs because inlet S2 was unable to "swallow" the terminal shock at $M = 1.8$, whereas at $M = 1.9$ the inlet started. Notice, however, that no discontinuity occurred for inlet I2P (fig. 10(f)) which was designed to start near a Mach number of about 1.5 ($M = 1.8$ was the lower Mach number limit of the small tunnel).

Effect of angle of attack.- One important characteristic to a designer is the rate at which the pressure recovery decays with increasing angle of attack $\left[\frac{\Delta(p_{t_c}/p_{t_\infty})_{max}}{\Delta\alpha}\right]_{\alpha\approx 0^\circ}$. As shown in figure 20 for three of the inlets investigated herein, the rate of pressure-recovery decay with angle of attack was relatively small for Mach numbers less than about 2.5, whereas it was large at Mach numbers near 3.0. The results of the tests of reference 6 also included in figure 20 show a similar effect of Mach number. From these results it is apparent that circular inlets may be more sensitive to asymmetric flow at Mach numbers above approximately 2.5 than below.

One way of improving pressure recovery at angle of attack is to position the inlet properly to take advantage of the compression afforded by the flow field of a wing or body. Another may be with the use of flow-deflector plates which, in some cases, could provide a flow field approximating that under a wing or body. For inlet S3, which was tested only with a concave plate (see fig. 8(a)) the data show that at $M_\infty = 2.34$ the flow-deflector plate was effective in maintaining the pressure recovery up to at least 9° angle of attack, the limit of the test (fig. 13(b)). Without the plate the pressure recovery decreased rapidly with an increase in angle of attack above 4°. Inlets S1 and S1P were tested with three different plates (concave, straight, and convex) at M_∞ of 2.74 and 3.0. These plates were not as effective at these Mach numbers as was the plate used with inlet S3 at $M_\infty = 2.34$; the sudden reduction in pressure recovery began at an angle of attack of about 3.0°. It is believed that the main reason for the ineffectiveness of the plates at high angles of attack for inlets S1 and S1P must be connected with the presence of the space between the leading edge of the inlet and the trailing edge of the plates (inlet S3, with flow-deflector plate, did not have a space). Observation of the manometer tubes during the tests of inlets S1 and S1P

indicated that a large region of total-pressure loss occurred near the top of the duct at the compressor station when the angle of attack was increased above 3°. Apparently large flow disturbances occurred in the region of the space, entered the inlet, and strongly influenced the internal flow to produce this large loss. (The testing at angles of attack was limited to low Reynolds number, and Mach numbers above 2.5, because of excessive model oscillations which apparently were produced by vibrations of the model-support system.)

Effect of Reynolds number.- The flight Reynolds number (based on inlet diameter) for a full-scale inlet operating over a wide range of Mach numbers and altitudes may vary from about 3 to 5 million. Hence, tests were made with inlet I2P at $M_\infty = 2.5$ to investigate the effects of Reynolds number over this range. Calculations indicated that the flow removed through the centerbody was nearly constant for this range of Reynolds number ($m_b/m_\infty = 0.04$). The data obtained with the centerbody and exit plug set for positions of maximum pressure recovery (fig. 11(b)) show that although a slight discontinuity occurs in both the pressure recovery and the contraction-ratio curves at $R = 3.8$ million, the pressure recovery generally increased with increasing values of Reynolds number from 2.7 to 5.2 million. In the tests of reference 4 (at lower Reynolds numbers, 0.24 to 0.96 million) similar trends of pressure recovery and contraction ratio were also observed, but the rates of change were greater than those obtained in the present tests.

Flow Distortion and Unsteadiness

Flow distortion.- The effect of increasing angle of attack on flow distortion is shown in figure 14(a) for inlet S3. At 0° the contours were symmetrical, and the maximum difference was 0.09; however, at angles of attack above 5.75° there were large radial and circumferential variations in the total-pressure ratio. Figure 14(b) was included to show that the flow-deflector plate, in addition to improving the average pressure recovery, also improved the total-pressure distribution at angle of attack. Although the largest difference in total-pressure ratio was about the same with or without the plate, the circumferential distribution was greatly improved. Examination of the data for inlets S4 and S4P (fig. 14(c)) shows that at $M_\infty = 2.5$ boundary-layer removal also improved the over-all total-pressure distortion as well as the average pressure recovery.

Unsteadiness.- In the present tests the unsteadiness was first observed with the schlieren system and during its occurrence measurements were made of the amplitude and frequency of the static-pressure fluctuations near the compressor station. No measurable unsteadiness was observed with the inlet started and the terminal shock inside near the throat region. However, for subcritical inlet operation, unsteadiness usually occurred when the centerbody was positioned so that there was

interaction between the normal shock and the centerbody boundary layer. The predominant frequency of the disturbance is included for the data points for which it could be obtained (see figs. 15 and 16). (It should be noted that the unsteadiness data in figs. 15 and 16 cannot be correlated with the pressure-recovery data of figs. 9(b) and 9(c).) The unsteadiness data show that, generally, the magnitude of the pressure disturbance increased with increasing values of contraction ratio, that is, with extension of the centerbody. This should be expected because with increasing centerbody extension the adverse interaction between the normal shock and the boundary layer on the centerbody should increase above that which would occur with the centerbody nearly retracted. However, in some cases when schlieren observations indicated an increase in buzz with increasing centerbody extension, the pressure cell showed no increase in pressure fluctuation. This may occur if the subsonic flow behind the external normal shock is accelerated sufficiently inside the inlet to choke the minimum area. Then pressure pulsations that might enter the inlet would be damped.

Drag

Drag considerations are of basic importance in comparisons of air-induction systems. During the present investigation, however, no drag measurements were made because of the difficulty of measuring the small drag values experienced by the internal-compression inlet. For example, calculations of the external-wave-drag coefficient of a typical internal-compression inlet pod using the method of characteristics indicate a value of only 0.009[1] because of the low external lip angle of the inlet. A comparable external-compression inlet, on the other hand, would have a wave-drag coefficient of the order of 0.100 to 0.250 depending on the value of the lip angle selected (in this case 15° to 28°).

As the present report and reference 3 both show, proper application of boundary-layer control may provide a significant increase in pressure recovery. However, the momentum loss of the air removed through the control system must be known to properly determine whether the increase in pressure recovery results in an over-all performance gain. Again, in the present investigation the magnitude of this drag component was not measured. However, calculations show that a drag coefficient of approximately 0.016 may be obtained, assuming a bleed mass-flow ratio of 0.08 and a total pressure loss of 0.40 p_{t_∞} in a system in which the air is discharged at 15° to the free stream (convergent-divergent exit nozzle).

[1]The drag coefficient is based on the area of the annulus at the lip leading edge ($M_\infty = 2.5$, $D_i/(D_{max})_{exit} = 0.742$, length of pod = 6.74 inlet diameters and mass-flow ratio of 1.0). See reference 12 for method used in determining the wave drag.

It should be noted that the amount of air removed in the present investigation was small. For inlets in which large amounts of boundary-layer air are removed to attain high pressure recovery, such as those considered in reference 3 ($m_b/m_\infty = 0.28$), the drag coefficient would be large, and might approach values of the order of 0.06 for the same assumptions used in the above analysis of the present inlets.

A further source of drag is skin friction on the external surface. For a typical installation of an internal-compression inlet (see footnote 1), a drag coefficient of 0.040 was calculated. (An all-turbulent boundary-layer flow was assumed and a Reynolds number of 1.0 million based on the inlet diameter was used.) This value would be approximately the same whether the inlet was of the internal-compression or external-compression type and would probably be unaffected by the amount of air removed through the boundary-layer-control system.

SUMMARY OF RESULTS

Tests were conducted with seven circular, axially symmetric, internal-compression inlets, some of which were equipped with systems for removing internal boundary-layer air. The following results were obtained from the investigation conducted with these inlets for Mach numbers between 0.85 and 3.5, for Reynolds numbers (based on inlet diameter) between 0.6 and 5.2 million, and for angles of attack up to 12°:

1. At a Mach number of 2.5 the largest gain in pressure recovery resulting from boundary-layer removal was obtained with a straight inlet designed to perform up to Mach numbers of about 2.5. The pressure recovery was 77 percent of the free-stream value without boundary-layer removal, and 88 percent with about 8 percent of the inlet capture flow removed through perforated surfaces.

2. The differences in internal shape of the best straight and best isentropic inlet, each with perforations, had no significant effect on the pressure recovery at a Mach number of 2.5. However, in the case of the ogive inlet the pressure recovery was poorer than those of the straight and isentropic inlets.

3. Analysis of angle-of-attack data revealed that the initial rate of pressure-recovery decay with angle of attack increased with increasing Mach number. With one inlet a flow-deflector plate, placed above the inlet to project ahead of the entrance, was effective in maintaining nearly constant pressure recovery for angles of attack up to at least 9°, the limit of the test. Further, the total-pressure distribution was improved over the angle-of-attack range.

4. The distortion at the compressor station was small for all inlets tested for angles of attack up to about 6°.

5. No air-flow unsteadiness was observed during supercritical inlet operation. However, high-level flow unsteadiness occurred at some subcritical inlet conditions.

6. A test with one inlet indicated that the maximum obtainable pressure recovery increased generally with increasing values of Reynolds number from 2.7 to 5.2 million.

Ames Research Center
National Aeronautics and Space Administration
Moffett Field, Calif., Nov. 20, 1958

REFERENCES

1. Mossman, Emmet A., and Pfyl, Frank A.: An Experimental Investigation at Mach Numbers From 2.1 to 3.0 of Circular-Internal-Contraction Inlets With Translating Centerbodies. NACA RM A56G06, 1956.

2. Kepler, C. E.: Performance of a Variable-Geometry Chin Inlet at Mach Numbers from 1.6 to 3.0. Research Dept. Rep. R-0955-24, United Aircraft Corporation, Oct. 1957.

3. Gunther, Fred: Combined Bimonthly Summary No. 56, Oct. 1 to Dec. 1, 1956, and No. 60, June 1, to Aug. 1, 1957, CIT., Pasadena, Calif.

4. Bowditch, David N., and Anderson, Bernhard H.: Performance of an Isentropic, All-Internal Contraction, Axisymmetric Inlet Designed for Mach 2.50. NACA RM E58E16, 1958. (Same data presented in Rozycki, R. C.: Experimental Investigation of Isentropic Internal Contraction Inlets at Mach Numbers From 2.0 to 2.7. Rep. LR12565, Lockheed Aircraft Corporation, Oct. 10, 1957)

5. Rodean, H. C.: Maximum Limits of Total Pressure Recovery For Supersonic Inlets. Eng. Dept. Rep. 10912, Chance Vought Aircraft, Inc., May 1, 1957.

6. Obery, Leonard J., and Stitt, Leonard E.: Performance of External-Internal Compression Inlet With Abrupt Internal Turning at Mach Numbers 3.0 and 2.0. NACA RM E57H07a, 1957.

7. Phelps, E. Ray, and Boyd, John W.: A Wind-Tunnel Investigation of the Effects of Conical Camber For An Airplane Configuration Having a Triangular Wing of Aspect Ratio 2.2. NACA RM A57A10, 1957.

8. Manual For Users of the Unitary Plan Wind Tunnel Facilities of the National Advisory Committee For Aeronautics. NACA, Washington, 1956.

9. McLafferty, G. H., Krasnoff, E. L., Ranard, E. D., Rose, W. G., and Vergara, R. D.: Investigation of Turbojet Inlet Design Parameters. Research Dept. Rep. R-0790-13, United Aircraft Corporation, Dec. 1955.

10. McLafferty, George: A Study of Perforation Configurations For Supersonic Diffusers. Research Dept. Rep. R-53372-7, United Aircraft Corporation, Dec. 1950.

11. Cnossen, J. W.: Studies of Boundary-Layer Removal Scoops For High-Performance Supersonic Inlets. Research Dept. Rep. R-0955-21, United Aircraft Corporation, Oct. 1957.

12. Presley, Leroy L., and Mossman, Emmet A.: A Study of Several Theoretical Methods for Computing the Zero-Lift Wave Drag of Open-Nosed Bodies of Revolution in the Mach Number Range of 2.0 to 4.0. NACA TN 4368, 1958.

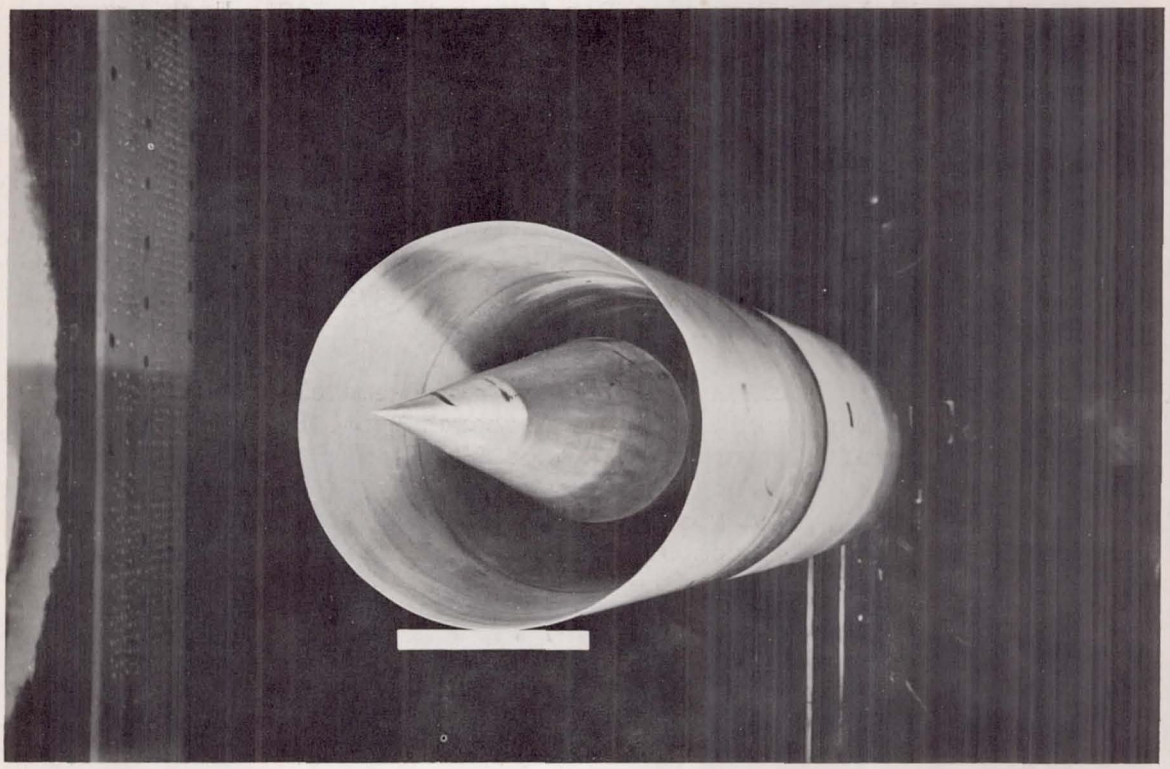

A-21318

(a) Front view

Figure 1.- Photographs of one of the large internal-compression inlets mounted in the Ames 6- by 6-foot wind tunnel.

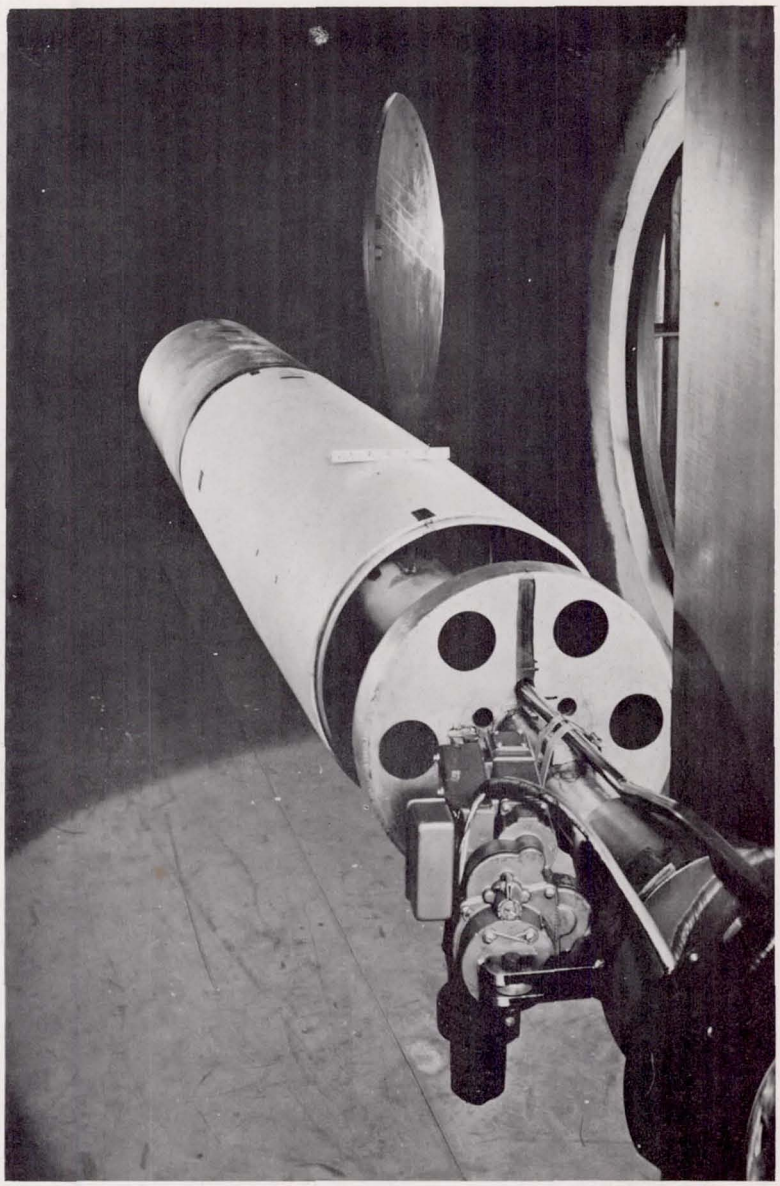

A-21317

(b) Rear view.

Figure 1.- Concluded.

CONFIDENTIAL

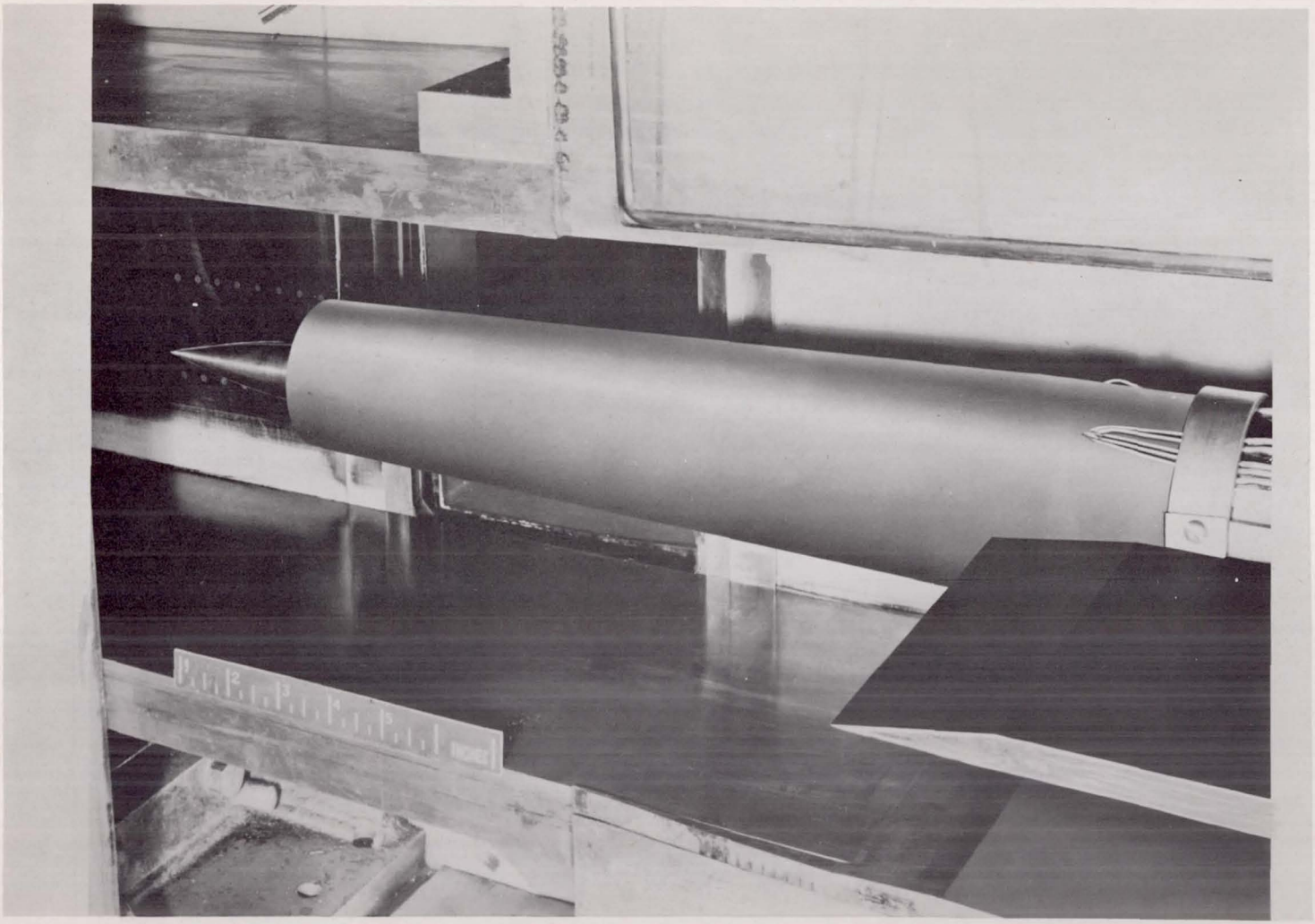

A-20675.2

Figure 2.- Photograph of typical small internal-compression inlet mounted in the Ames 8- by 8-inch wind tunnel.

CONFIDENTIAL

CONFIDENTIAL

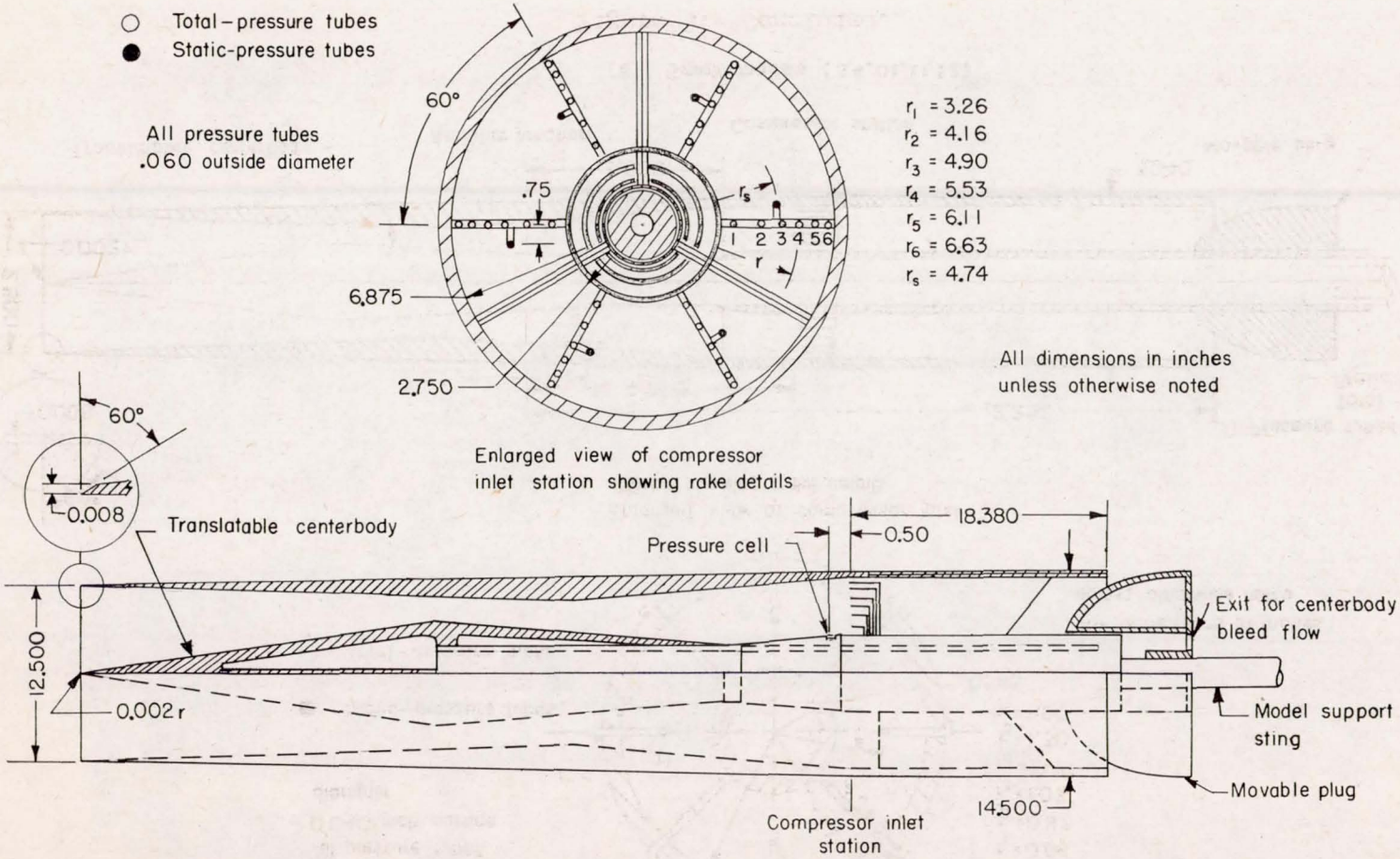

(a) Large models (S1, S2, S3)

Figure 3.- Sketches of the air-induction models.

CONFIDENTIAL

CONFIDENTIAL

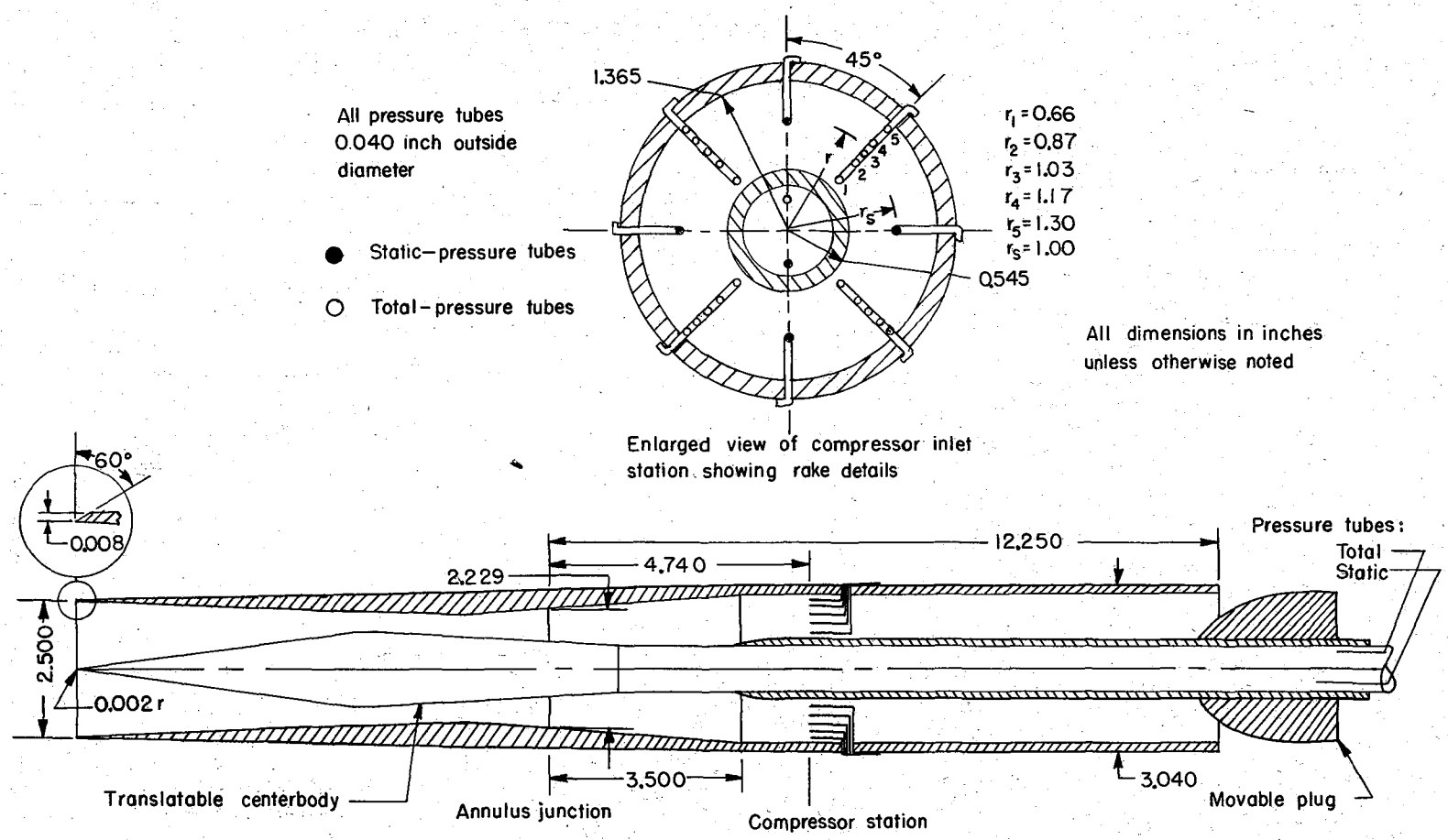

(b) Small models (S4,O1,I1,I2)

Figure 3.- Concluded.

CONFIDENTIAL

CONFIDENTIAL

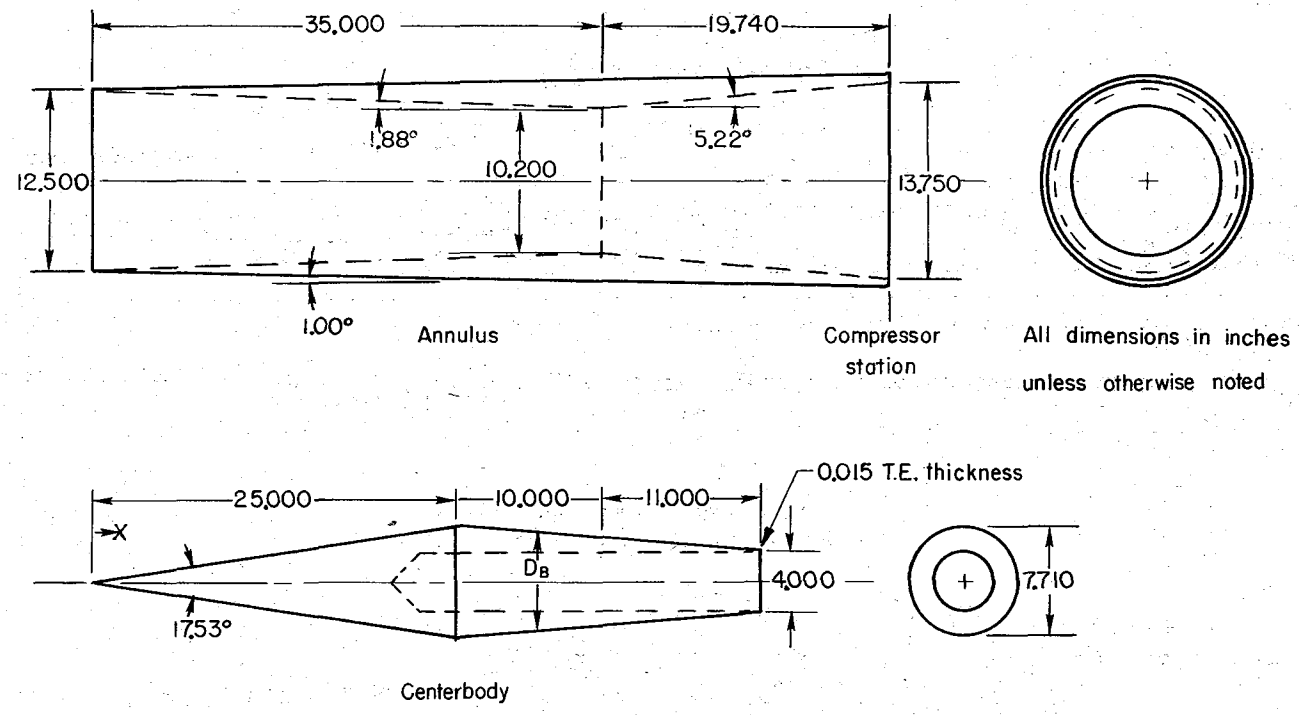

Coordinates of centerbody								
X	0	25.000	35.000	37.000	39.000	41.000	43.000	46.000
D_B	0	7.710	6.440	6.050	5.632	5.204	4.758	4.030

(a) Inlet S1

Figure 4.- Sketch of annulus and centerbody details of the seven inlets.

CONFIDENTIAL

CONFIDENTIAL

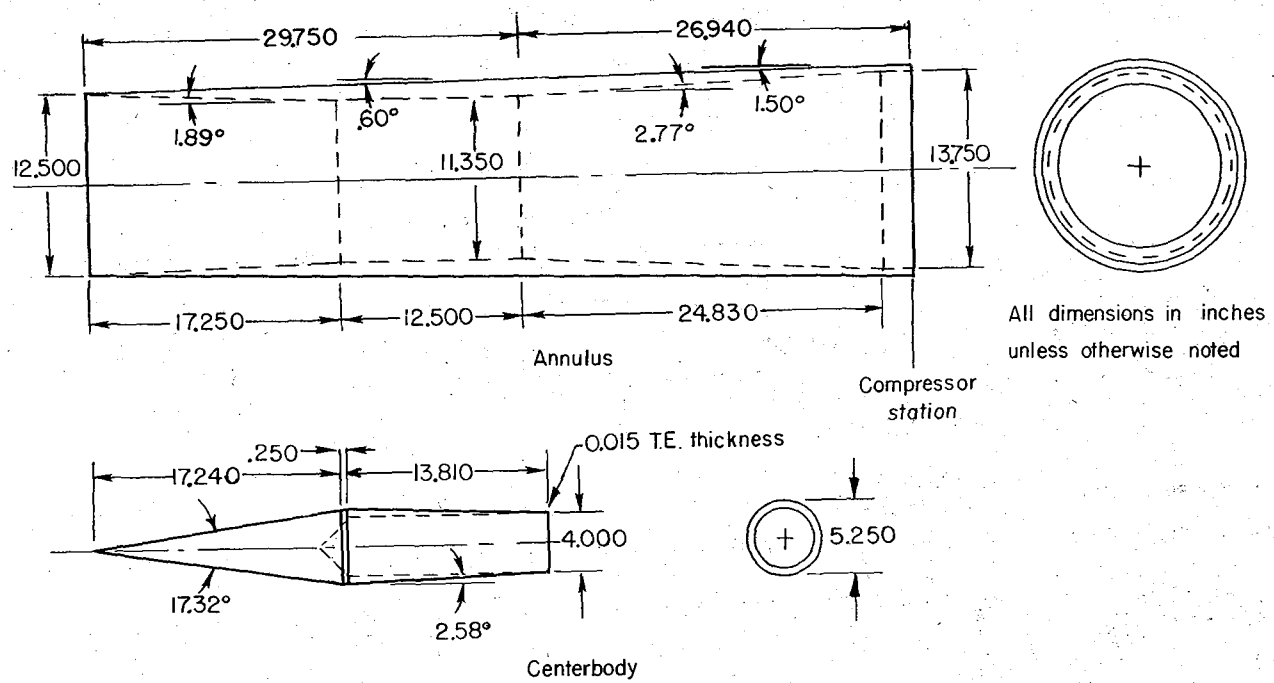

(b) Inlet S2

Figure 4.- Continued.

CONFIDENTIAL

CONFIDENTIAL

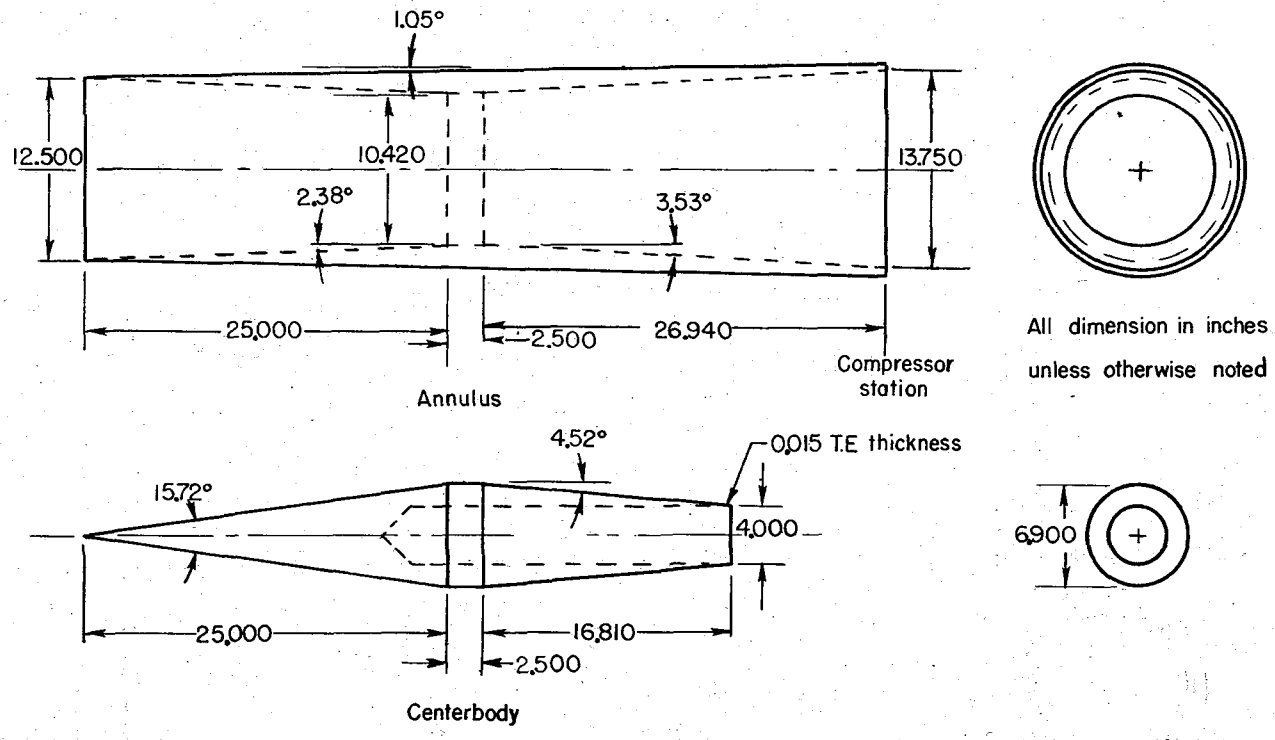

(c) Inlet S3

Figure 4.- Continued.

CONFIDENTIAL

CONFIDENTIAL

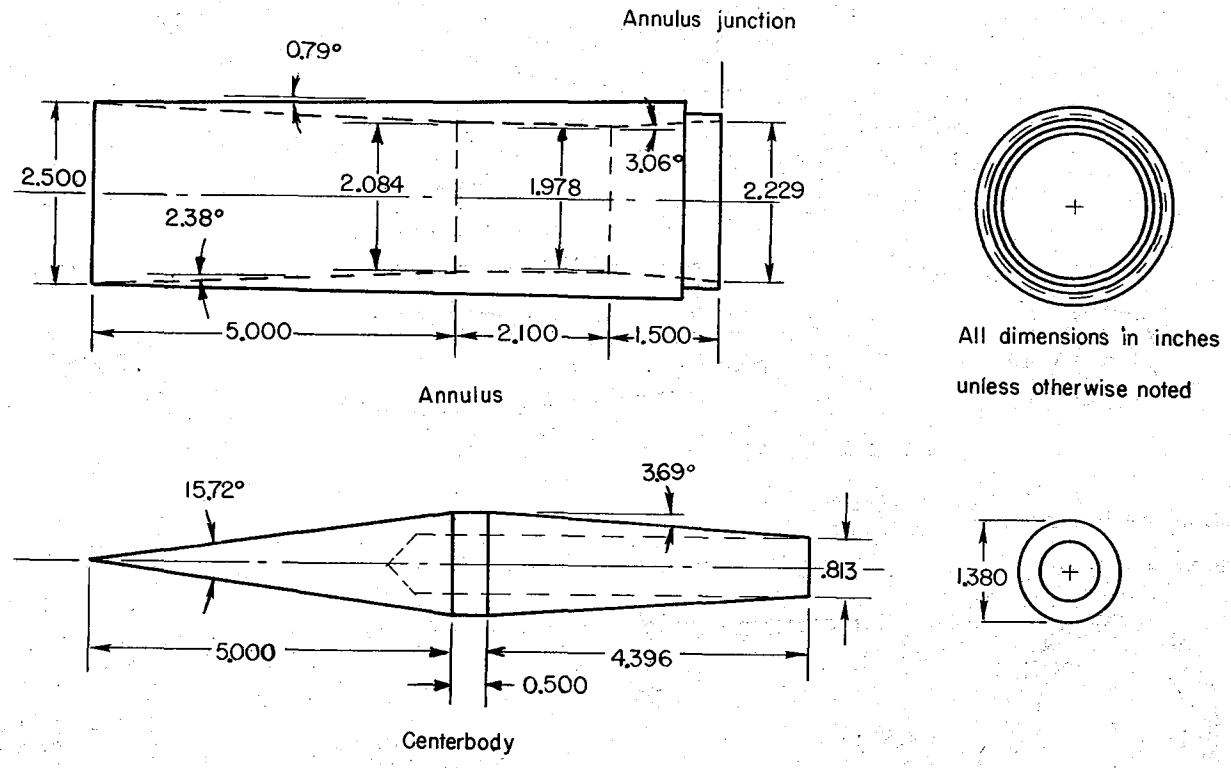

(d) Inlet S4

Figure 4.- Continued.

CONFIDENTIAL

CONFIDENTIAL

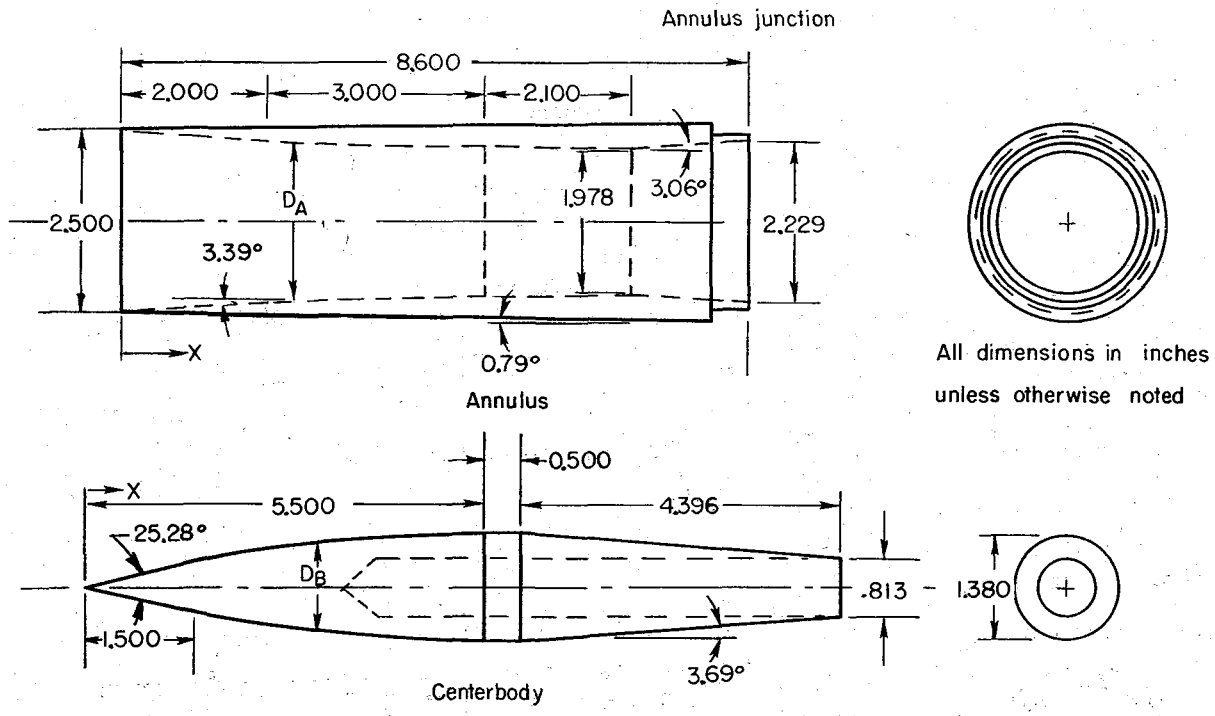

Coordinates of annulus and centerbody										
X	0	1.5	2.0	2.5	3.0	3.5	4.0	4.5	5.0	5.5
D_A	2.500	—	2.263	2.209	2.167	2.132	2.110	2.095	2.084	—
D_B	0	.671	.891	1.062	1.170	1.246	1.309	1.342	1.365	1.380

(e) Inlet 01

Figure 4.- Continued.

CONFIDENTIAL

CONFIDENTIAL

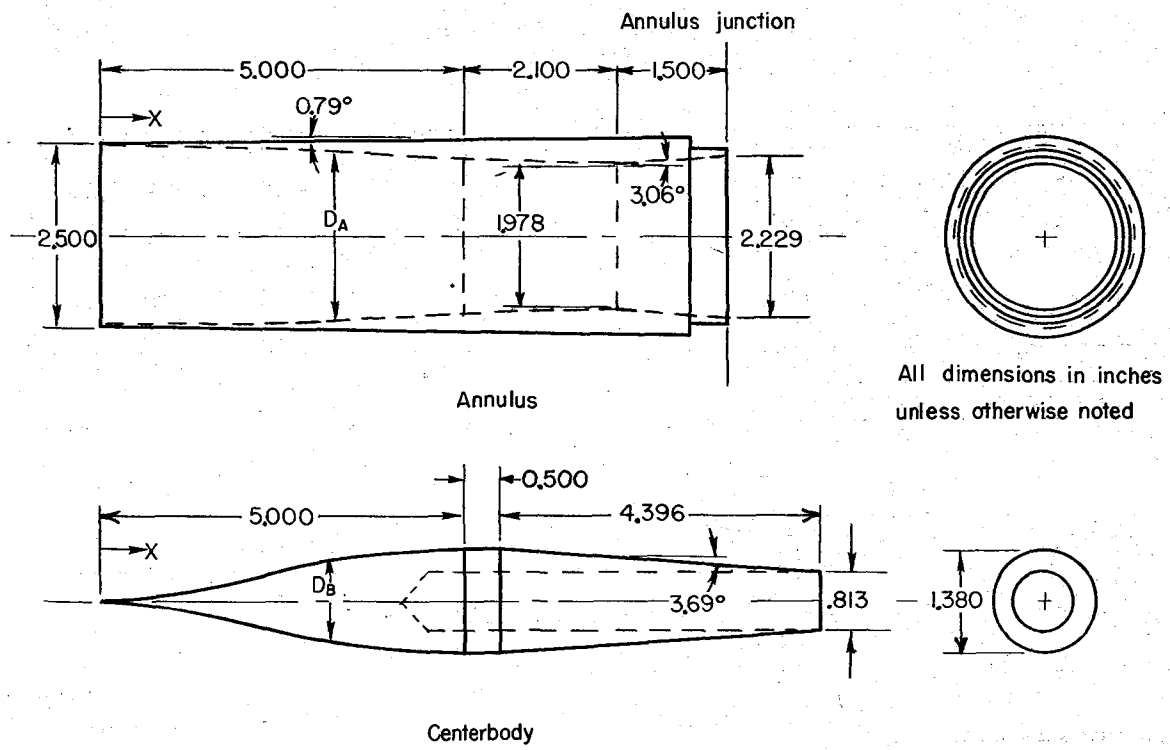

Coordinates of annulus and centerbody											
X	0	.500	1.000	1.500	2.000	2.500	3.000	3.500	4.000	4.500	5.000
D_A	2.500	2.480	2.466	2.448	2.416	2.362	2.294	2.212	2.142	2.100	2.076
D_B	0	.050	.156	.350	.600	.866	1.080	1.226	1.316	1.366	1.380

(f) Inlet I 1

Figure 4.- Continued.

CONFIDENTIAL

CONFIDENTIAL

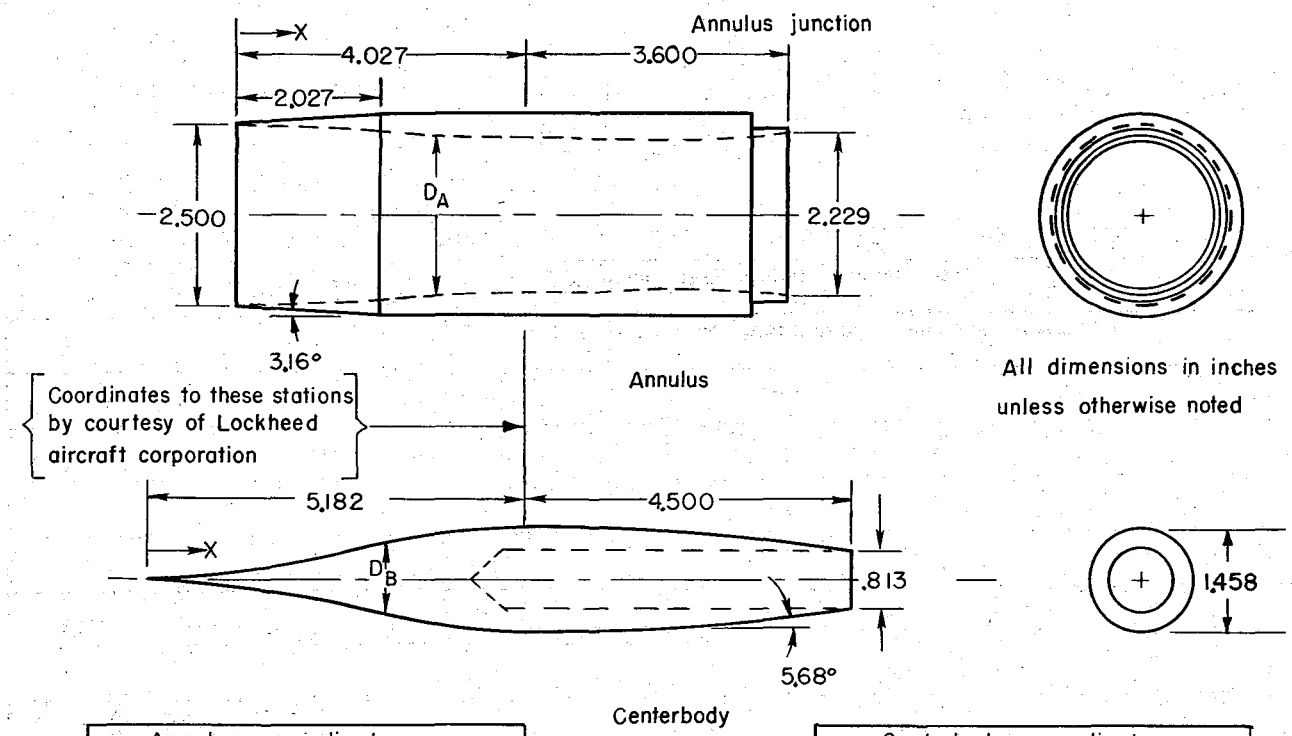

Annulus coordinates					
X	D_A	X	D_A	X	D_A
0	2.500	3.027	2.226	6.027	2.058
.527	2.492	3.527	2.176	6.527	2.080
1.027	2.464	4.027	2.158	7.027	2.138
1.527	2.418	4.527	2.154	7.627	2.229
2.027	2.356	5.027	2.136		
2.527	2.290	5.527	2.102		

Centerbody coordinates					
X	D_B	X	D_B	X	$-D_B$
0	0	3.182	.936	6.182	1.420
.682	.110	3.682	1.142	6.682	1.372
1.182	.238	4.182	1.312	7.182	1.306
1.682	.390	4.682	1.414	7.682	1.224
2.182	.560	5.182	1.458	9.682	.828
2.682	.740	5.682	1.448		

(g) Inlet I 2

Figure 4.- Concluded.

CONFIDENTIAL

CONFIDENTIAL

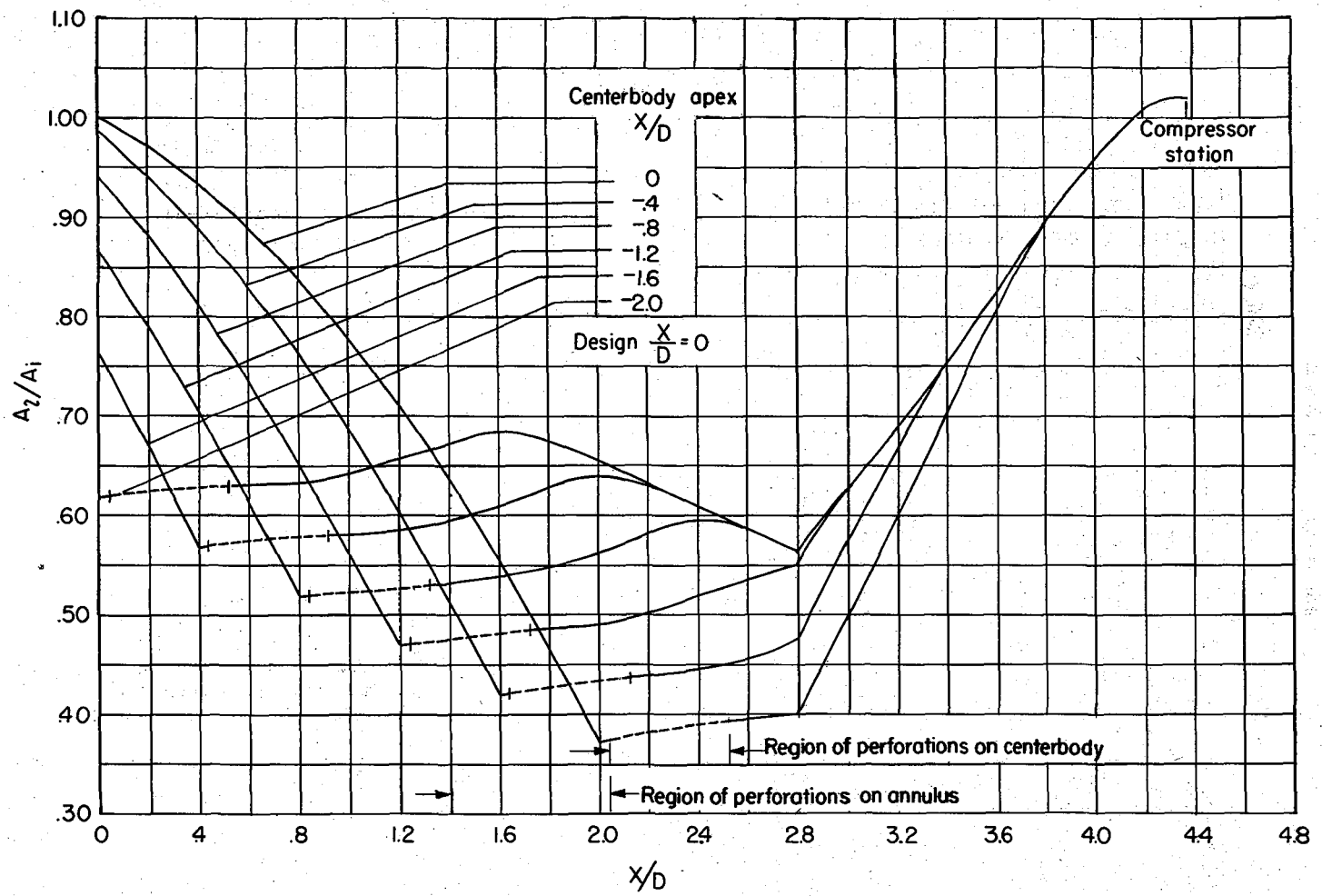

(a) Inlet S I

Figure 5.- Longitudinal area distribution of the seven inlets.

CONFIDENTIAL

CONFIDENTIAL

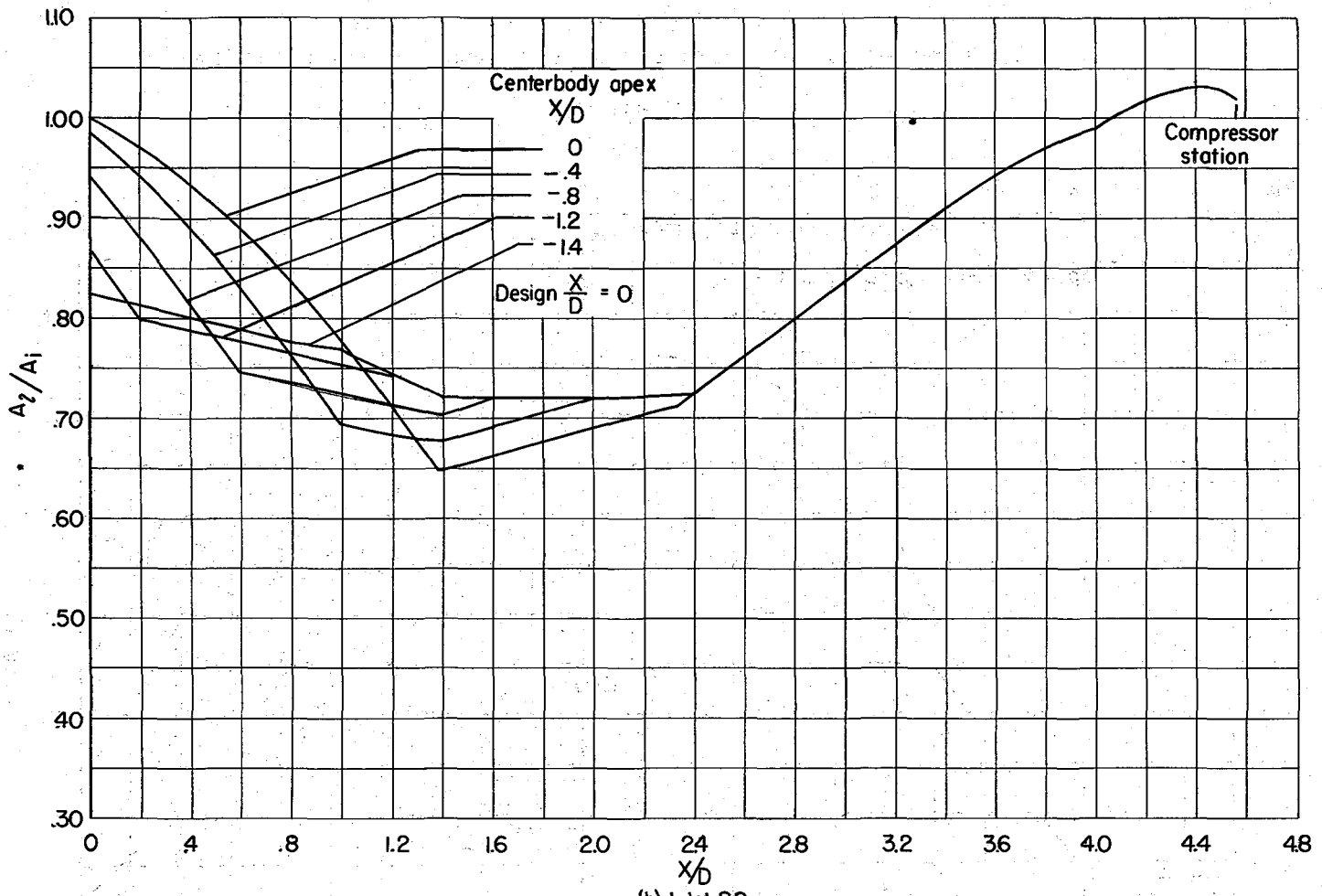

(b) Inlet S2

Figure 5.- Continued.

CONFIDENTIAL

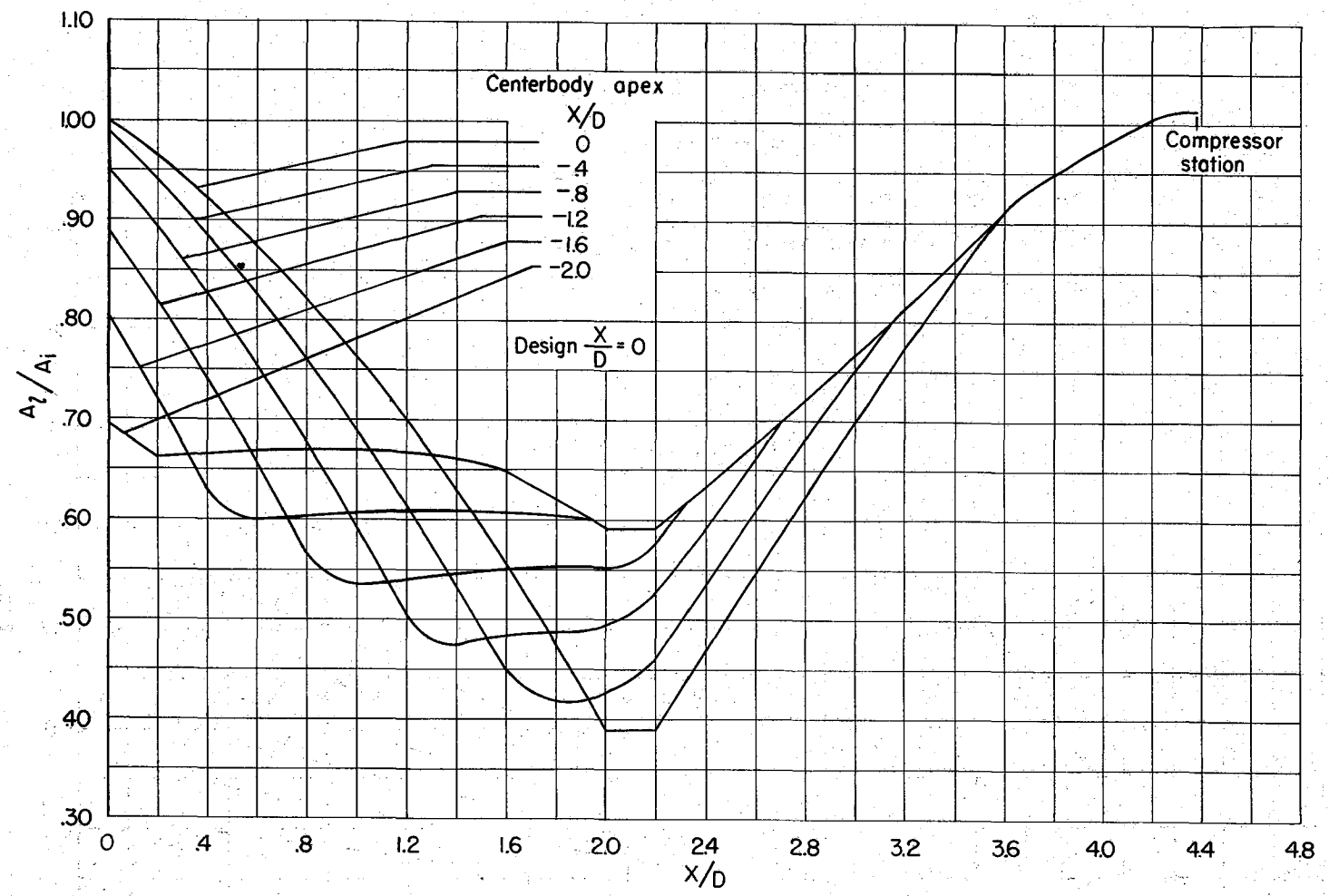

(c) Inlet S3

Figure 5.- Continued.

DECLASSIFIED

CONFIDENTIAL

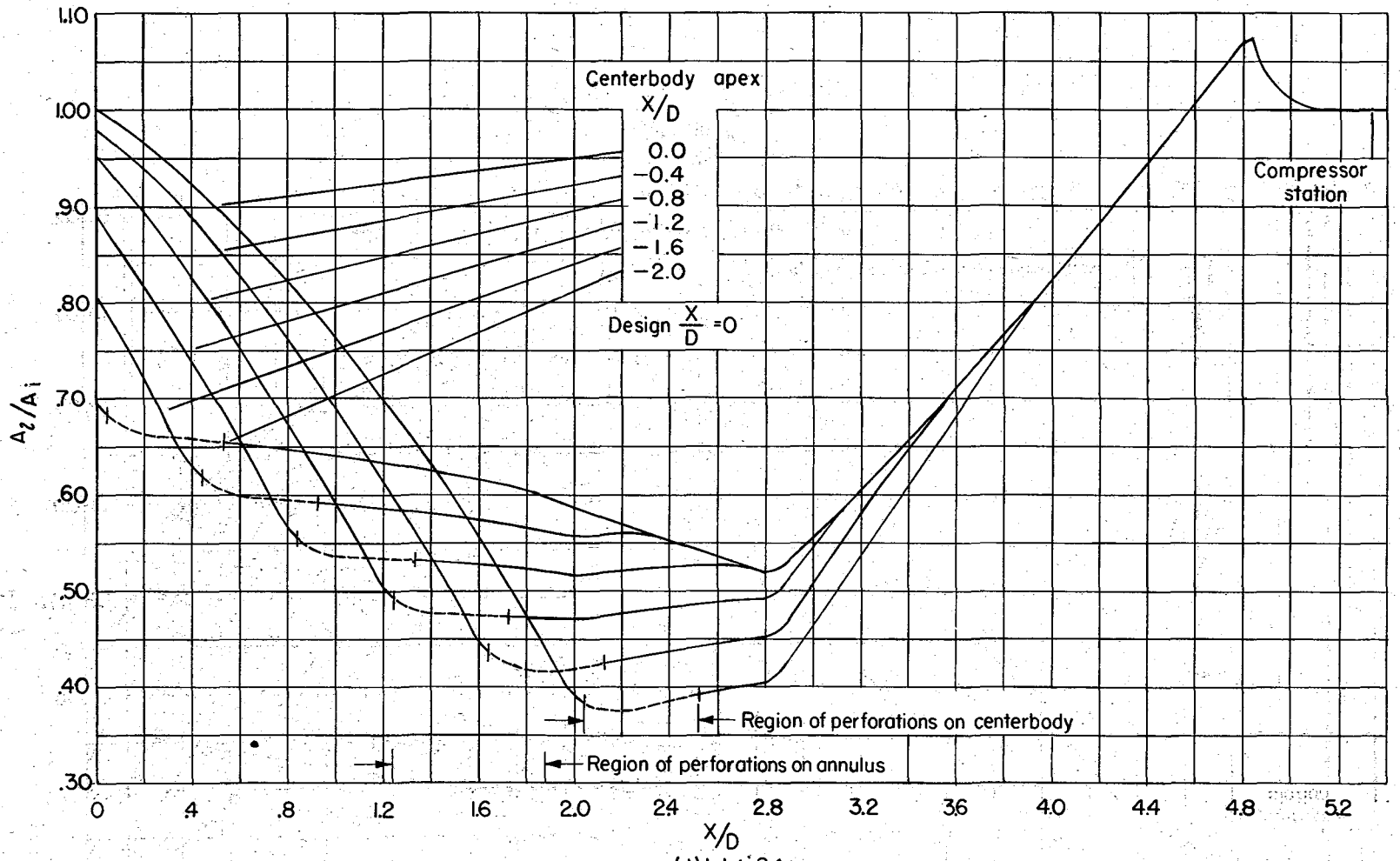

(d) Inlet S4

Figure 5.- Continued.

CONFIDENTIAL

CONFIDENTIAL

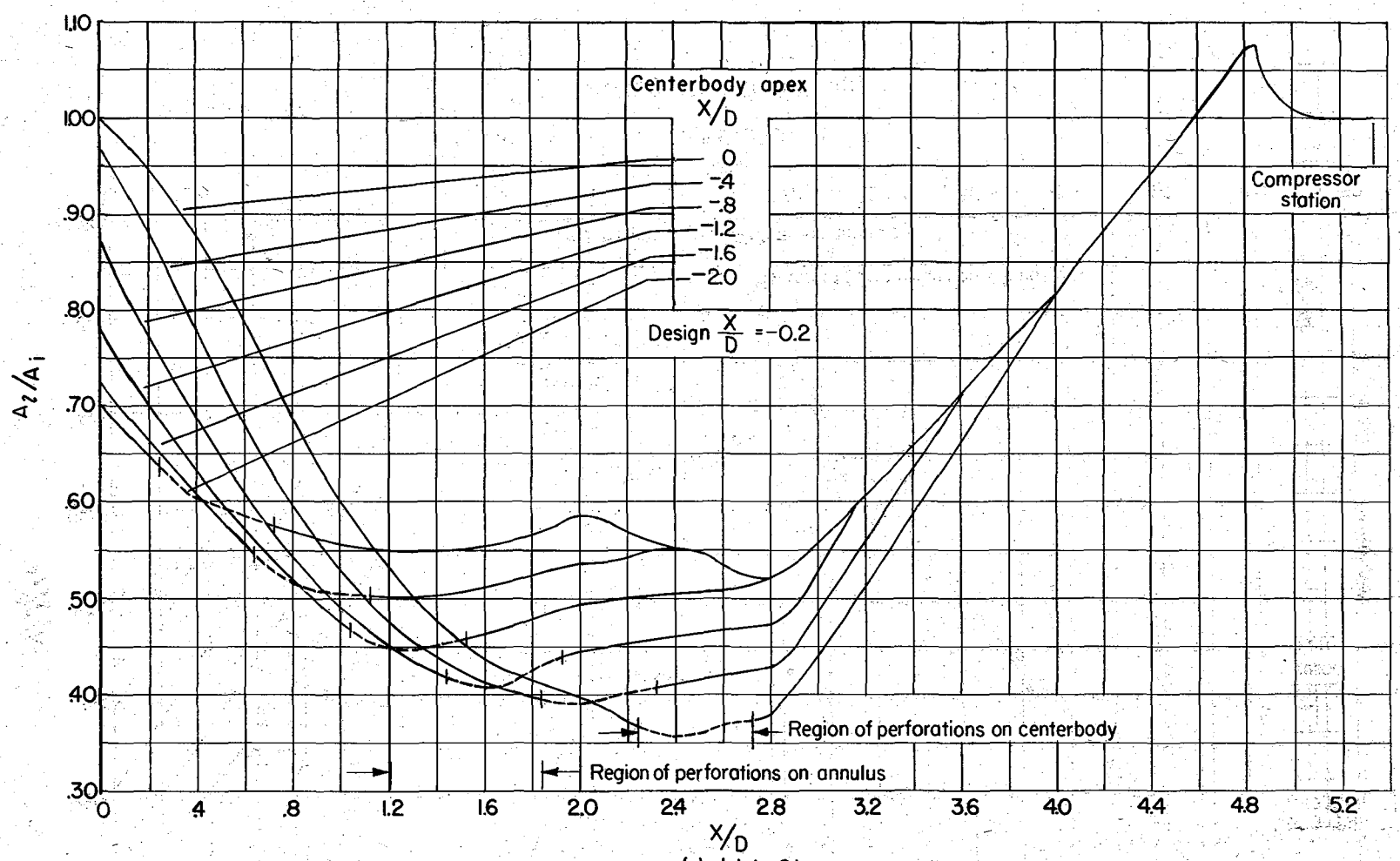

(e) Inlet 01

Figure 5.- Continued.

CONFIDENTIAL

CONFIDENTIAL

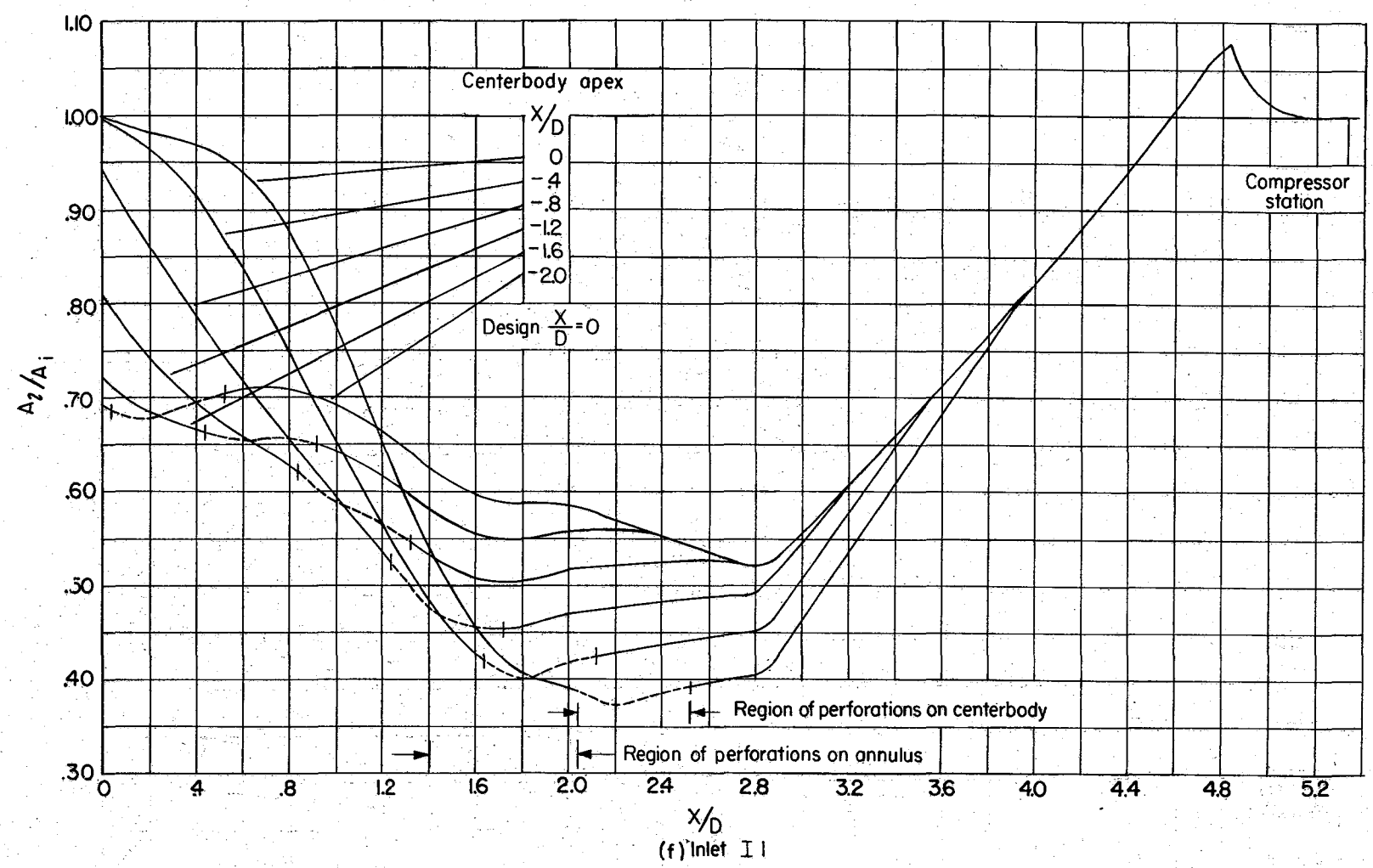

(f) Inlet I I

Figure 5.- Continued.

CONFIDENTIAL

CONFIDENTIAL

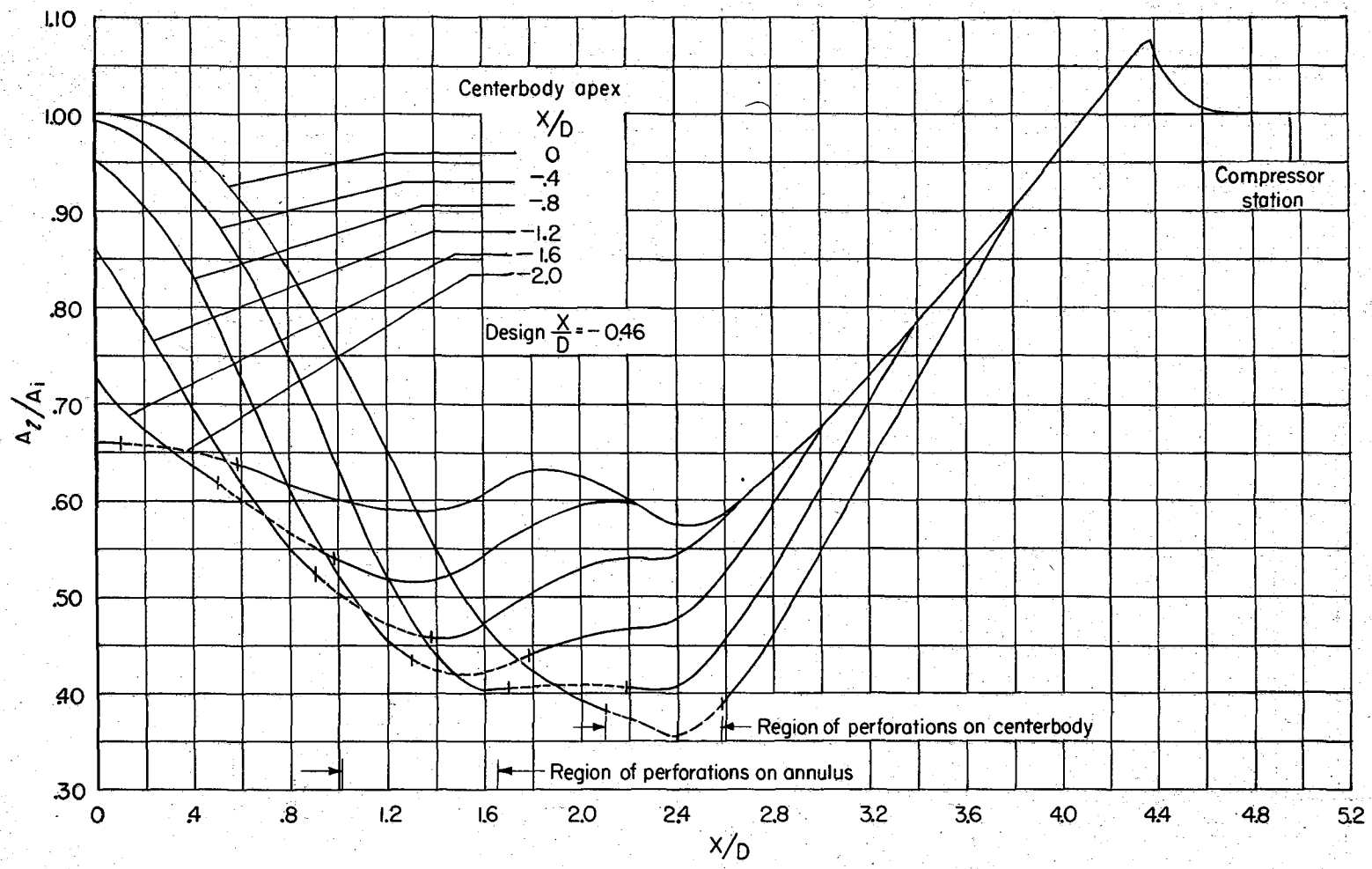

(g) Inlet I 2

Figure 5.- Concluded.

CONFIDENTIAL

UNCLASSIFIED

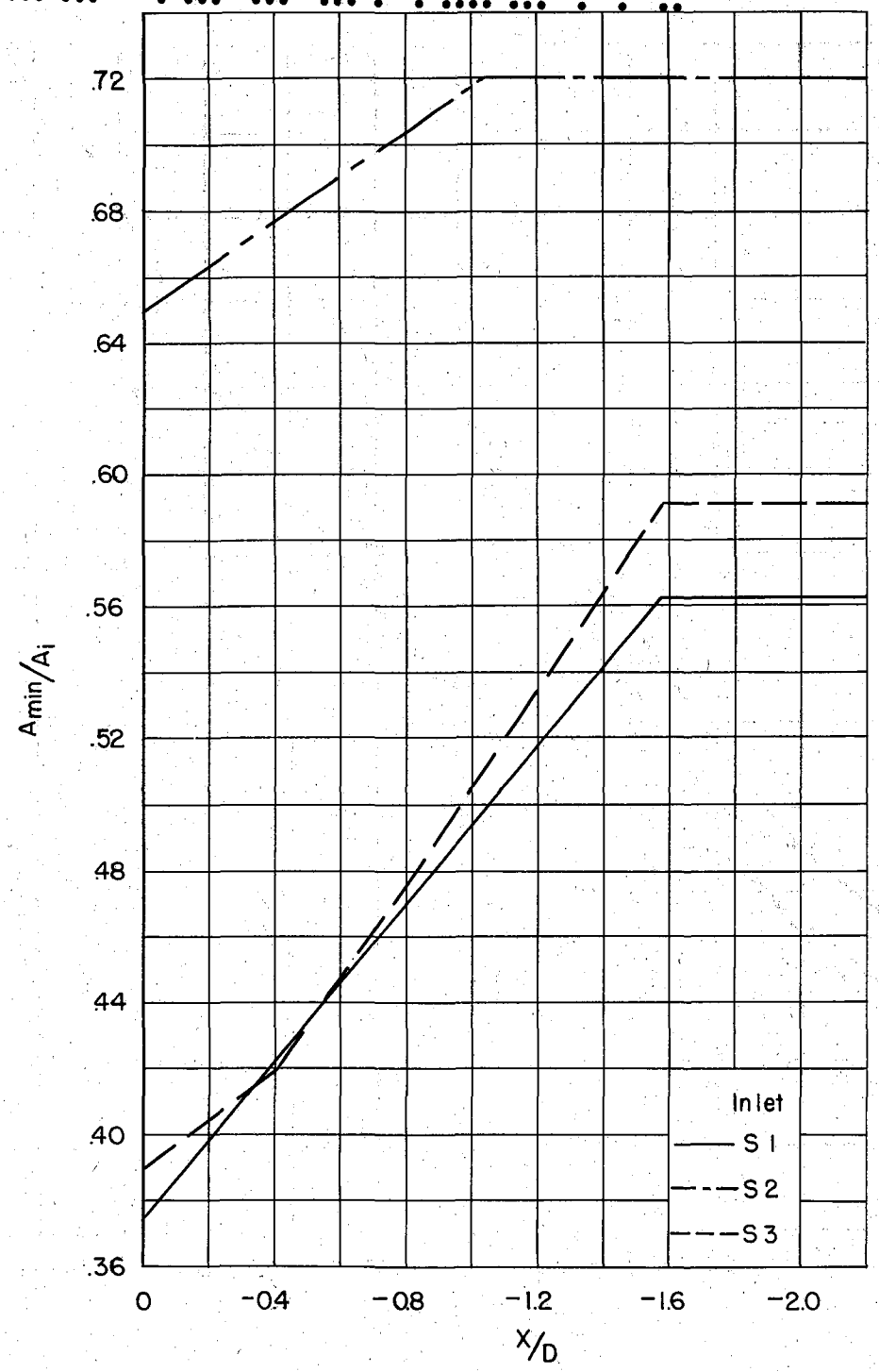

(a) Inlets S1, S2, S3

Figure 6.- Variation of contraction ratio with centerbody apex position.

UNCLASSIFIED

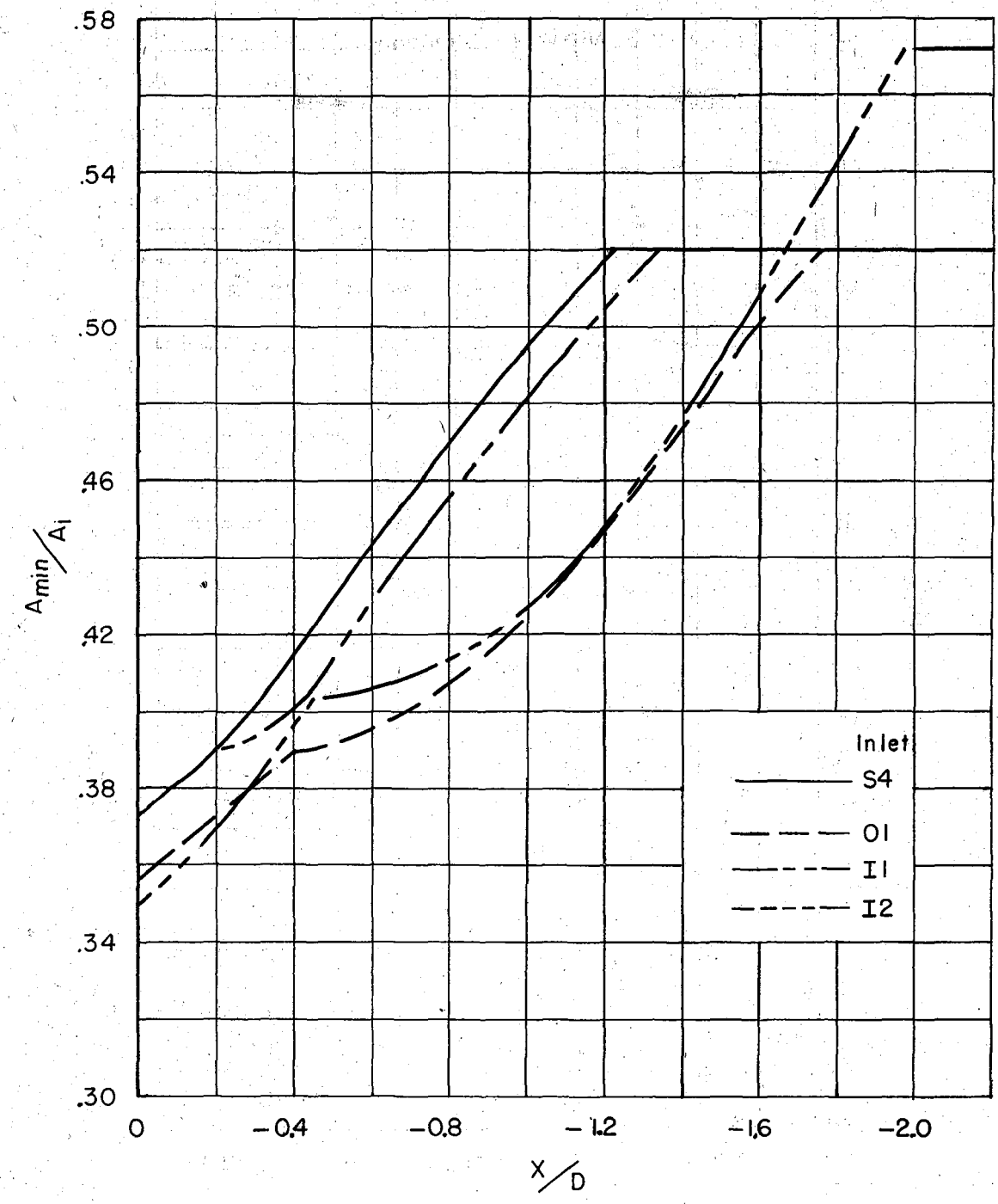

(b) Inlets S4, O1, I1, & I2

Figure 6.- Concluded.

Note ① 24 holes/row in all annuli, spaced equally; even numbered rows rotated 7 1/2°
Note ② 18 holes/row in all centerbodies, spaced equally; even numbered rows rotated 10°

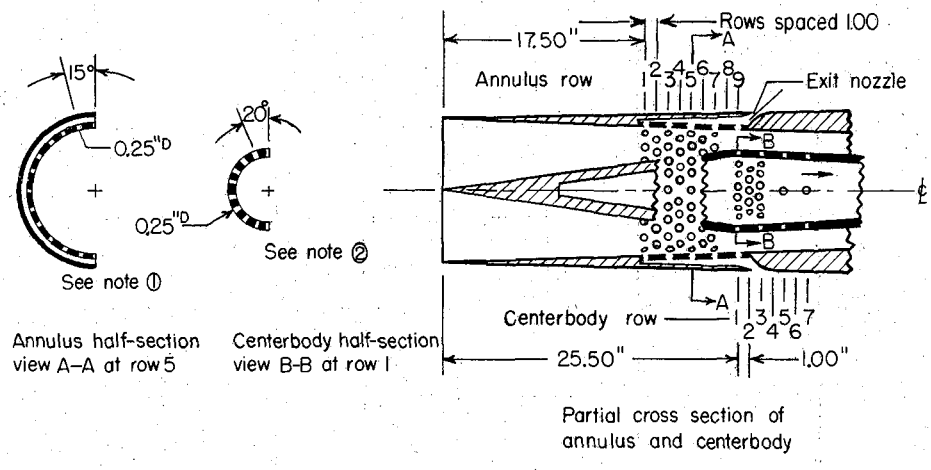

(a) Inlet SIP

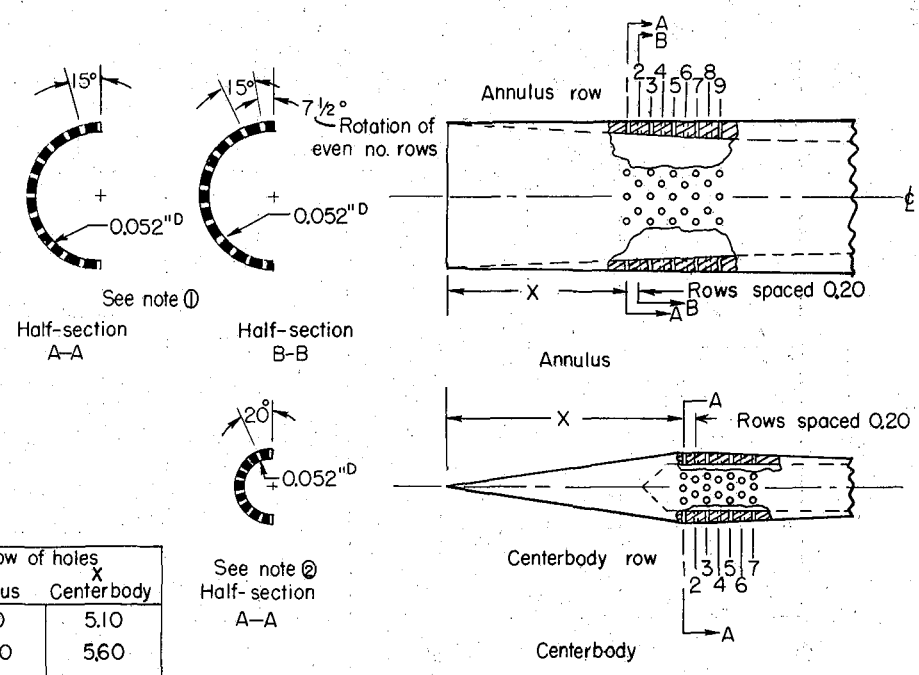

Location of first row of holes		
Inlet	X Annulus	X Centerbody
S4P	3.10	5.10
OIP	3.00	5.60
IIP	3.50	5.10
I2P	2.53	5.25

All dimensions in inches unless otherwise noted

(b) Inlets S4P, OIP, IIP, & I2P

Figure 7.- Details of the perforated inlets.

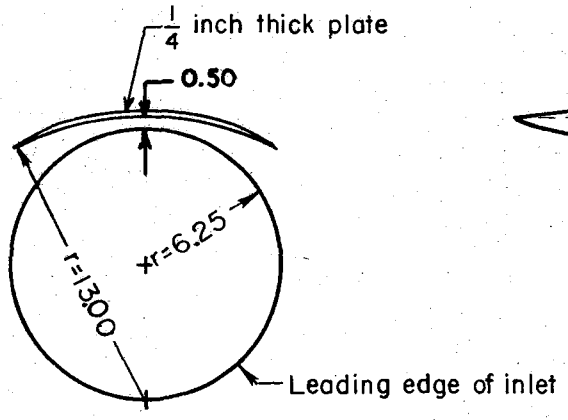

Front view

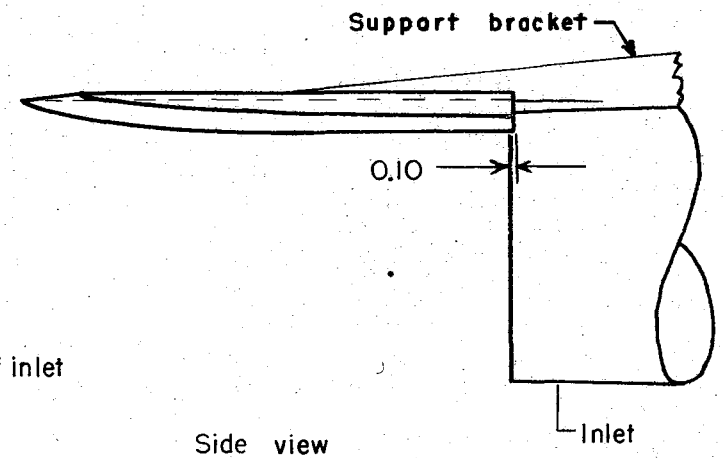

Side view

Coordinates			
a	±b	a	±b
0.50	1.50	8.00	5.71
1.00	2.21	9.00	5.98
2.00	3.07	10.00	6.22
3.00	3.71	11.00	6.44
4.00	4.25	12.00	6.54
5.00	4.70	13.00	6.58
6.00	5.07	↓	"
7.00	5.41	23.00	6.58

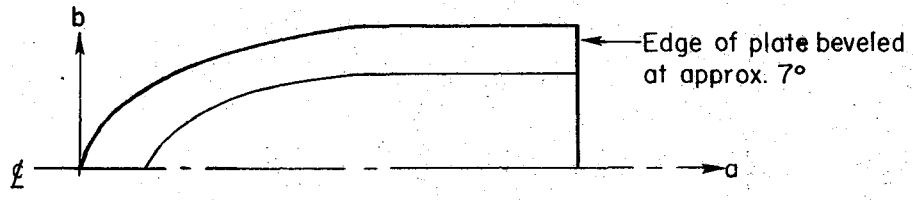

Half-plate development in a plane

All dimensions in inches unless otherwise noted

(a) Concave plate used with inlet S3

Figure 8.- Details of the flow deflector plate used with inlets S1 and S3.

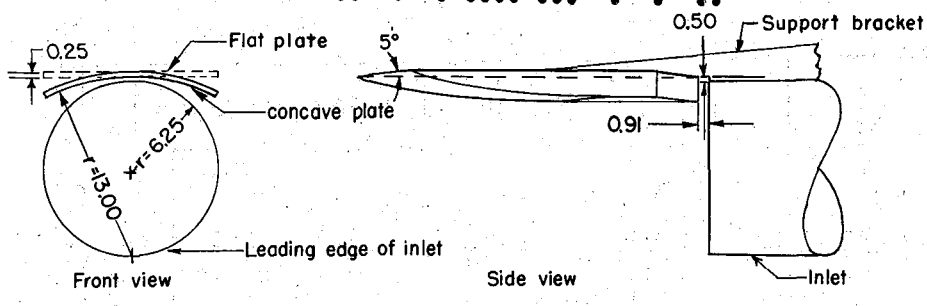

Coordinates for flat plate			
a	±b	a	±b
0	0	4.35	5.00
0.10	1.00	4.95	5.25
0.49	2.00	5.75	5.50
1.10	2.88	6.55	5.75
1.75	3.50	7.90	6.00
2.40	4.00	11.65	6.30
3.30	4.50	24.75	6.30

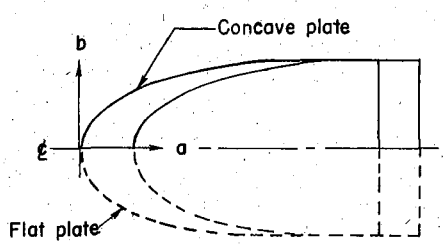

Top view

Coordinates for concave plate			
a	±b	a	±b
0	0	3.69	4.00
0.29	1.00	4.79	4.50
0.59	1.50	6.10	5.00
0.88	2.00	7.80	5.50
1.47	2.50	10.09	6.00
2.09	3.00	14.58	6.52
2.79	3.50	24.75	6.52

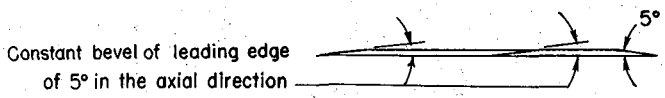

Side view (Flat plate only)
Half-plate development in a plane

(b) Concave and flat plates used with inlet S1

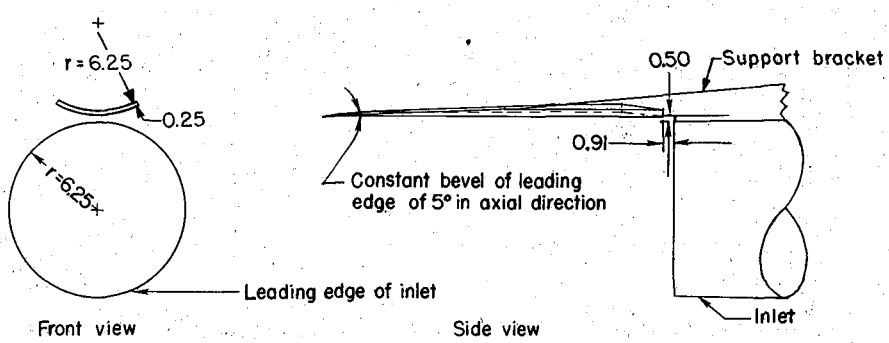

All dimensions in inches unless otherwise noted

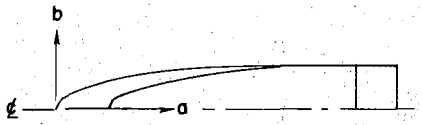

Half-plate development in a plane
Top view

Coordinates for convex plate			
a	±b	a	±b
12.00	0.00	6.30	2.42
0.72	.85	9.80	2.88
2.03	1.41	13.54	3.13
3.70	1.91	24.75	3.13

(c) Convex plate used with inlet S1

Figure 8.- Concluded.

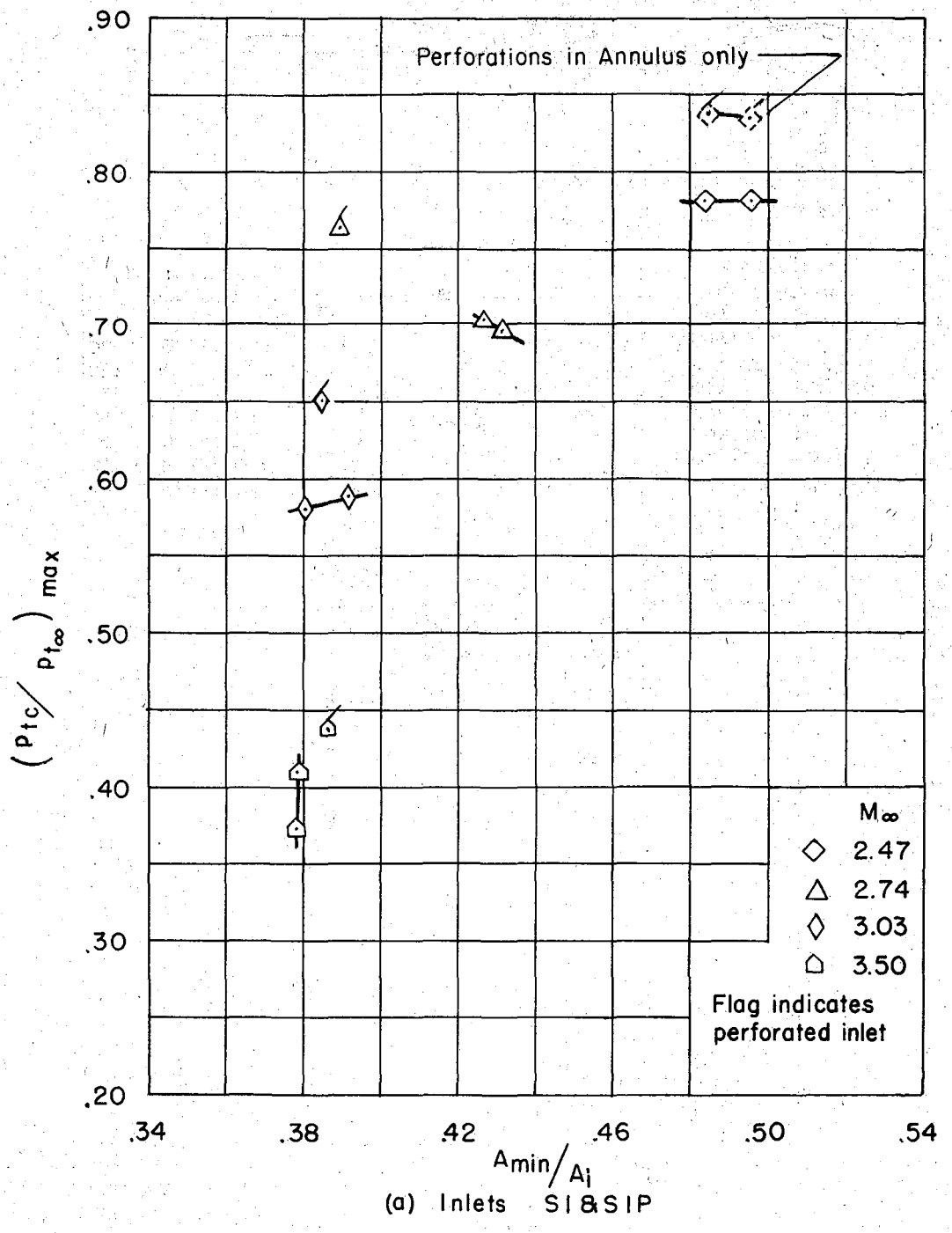

(a) Inlets S1 & S1P

Figure 9.- Pressure recovery as a function of the contraction ratio for the seven inlets.

UNCLASSIFIED

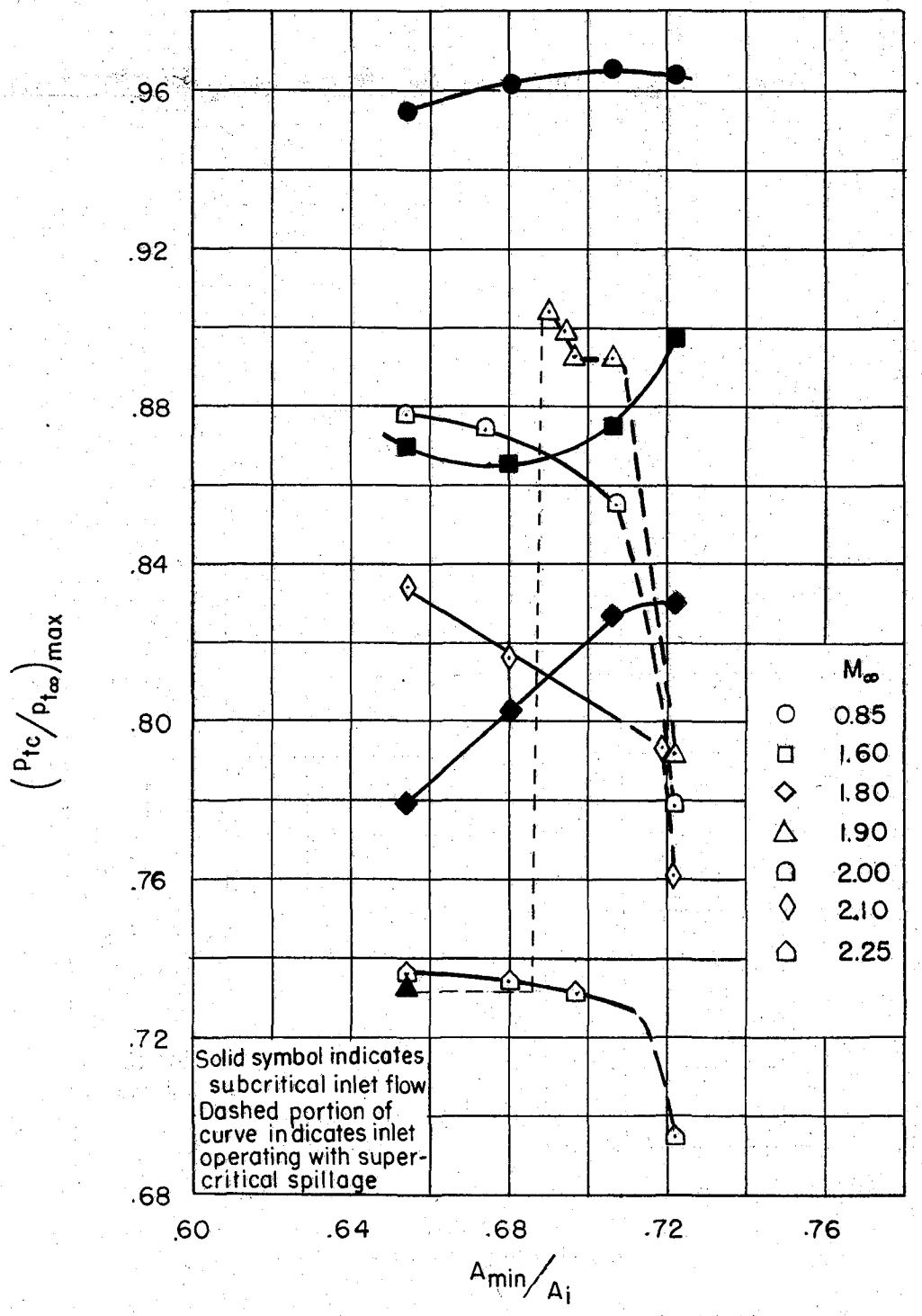

(b) Inlet S2

Figure 9.- Continued.

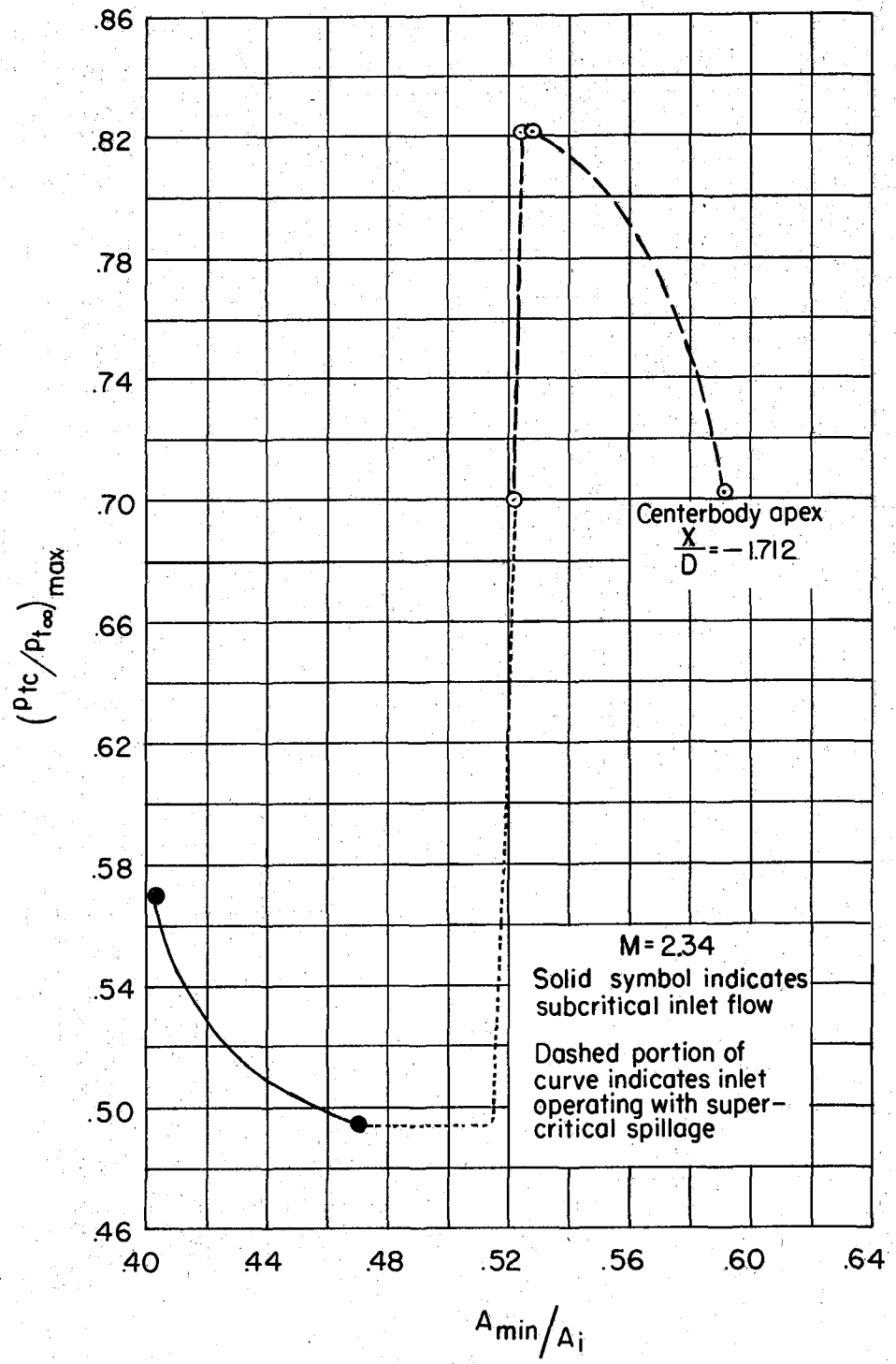

(c) Inlet S3

Figure 9.- Continued.

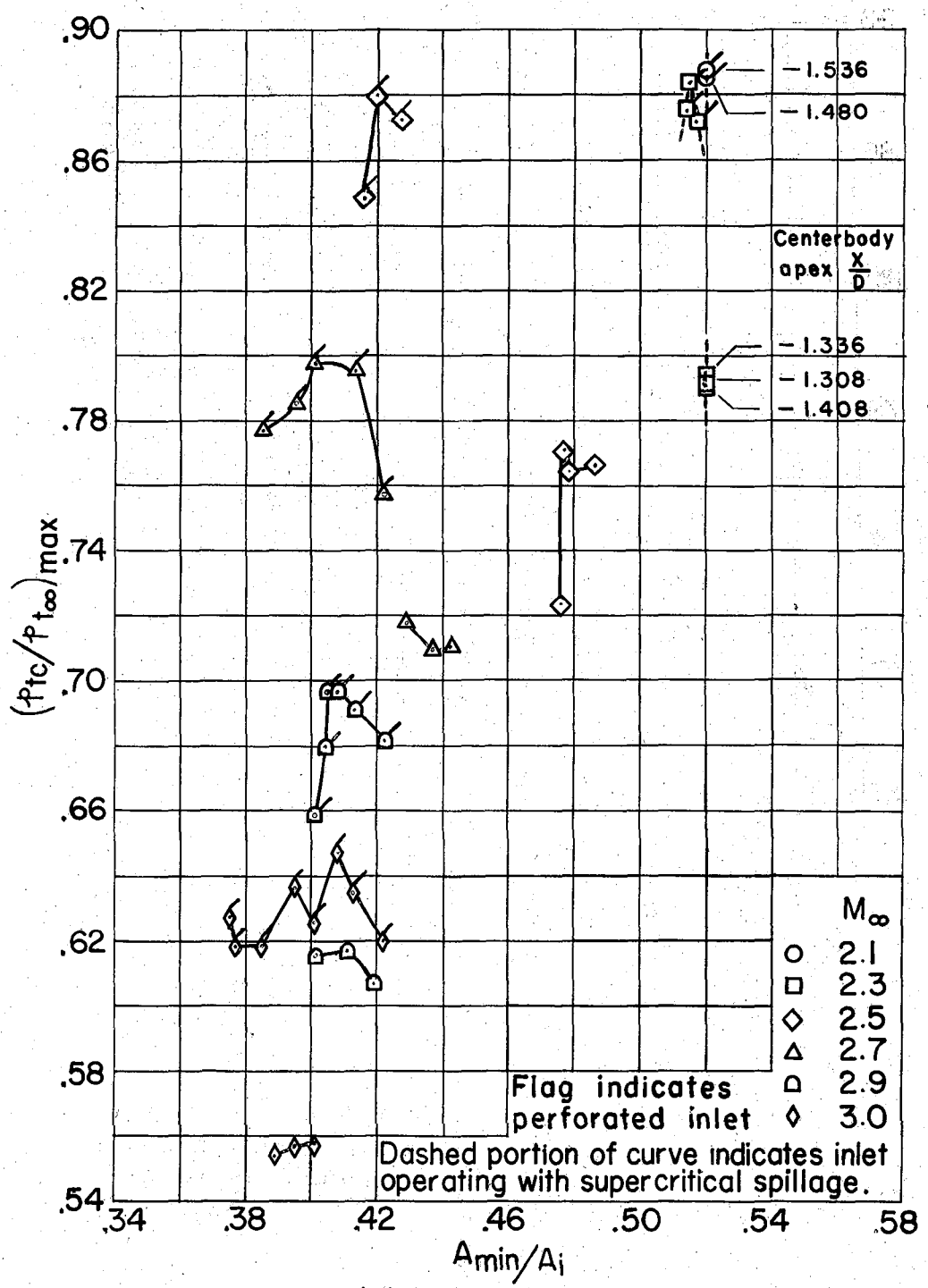

(d) Inlets S4 & S4P

Figure 9.- Continued.

UNCLASSIFIED

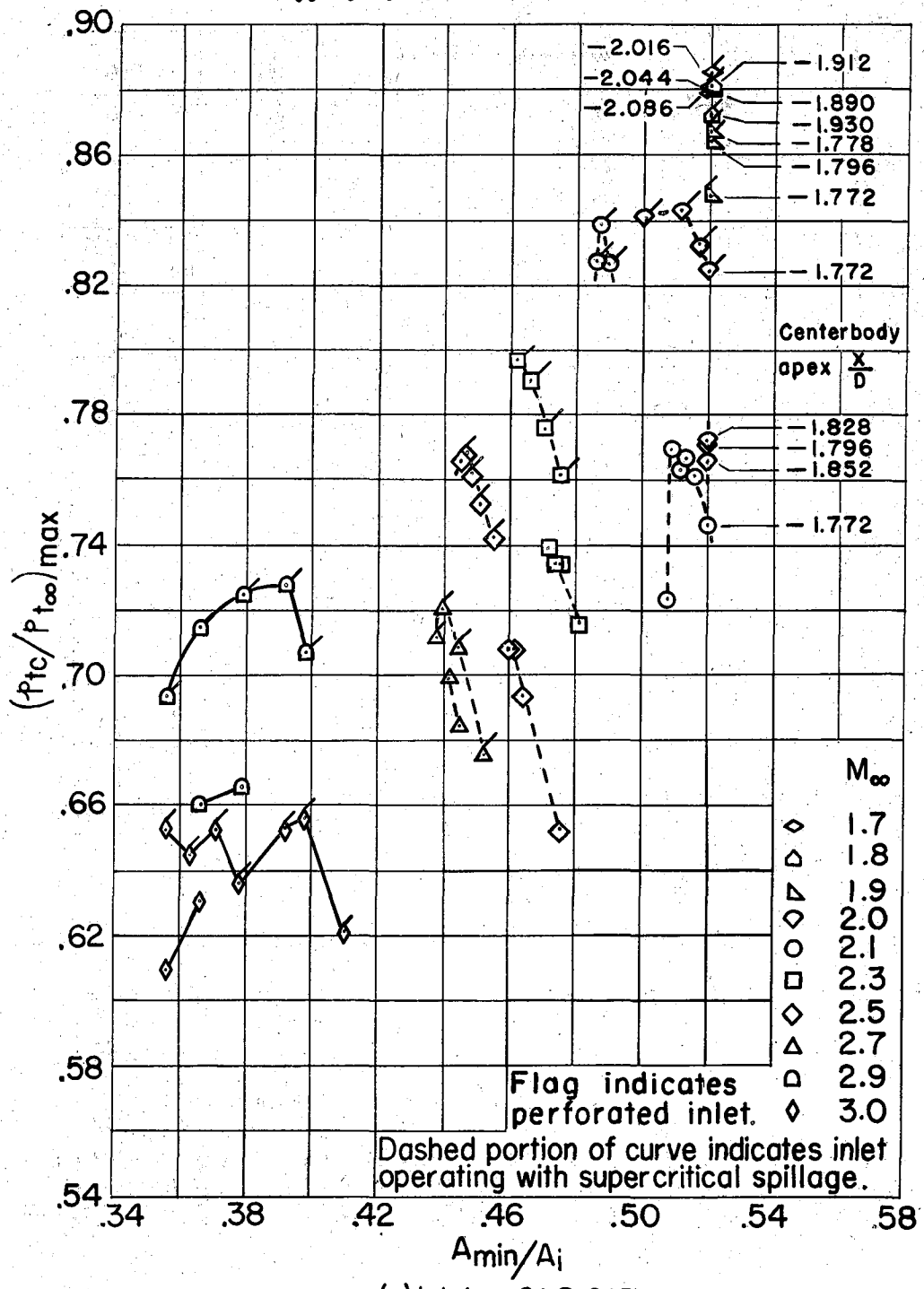

(e) Inlets 01 & 01P

Figure 9.- Continued.

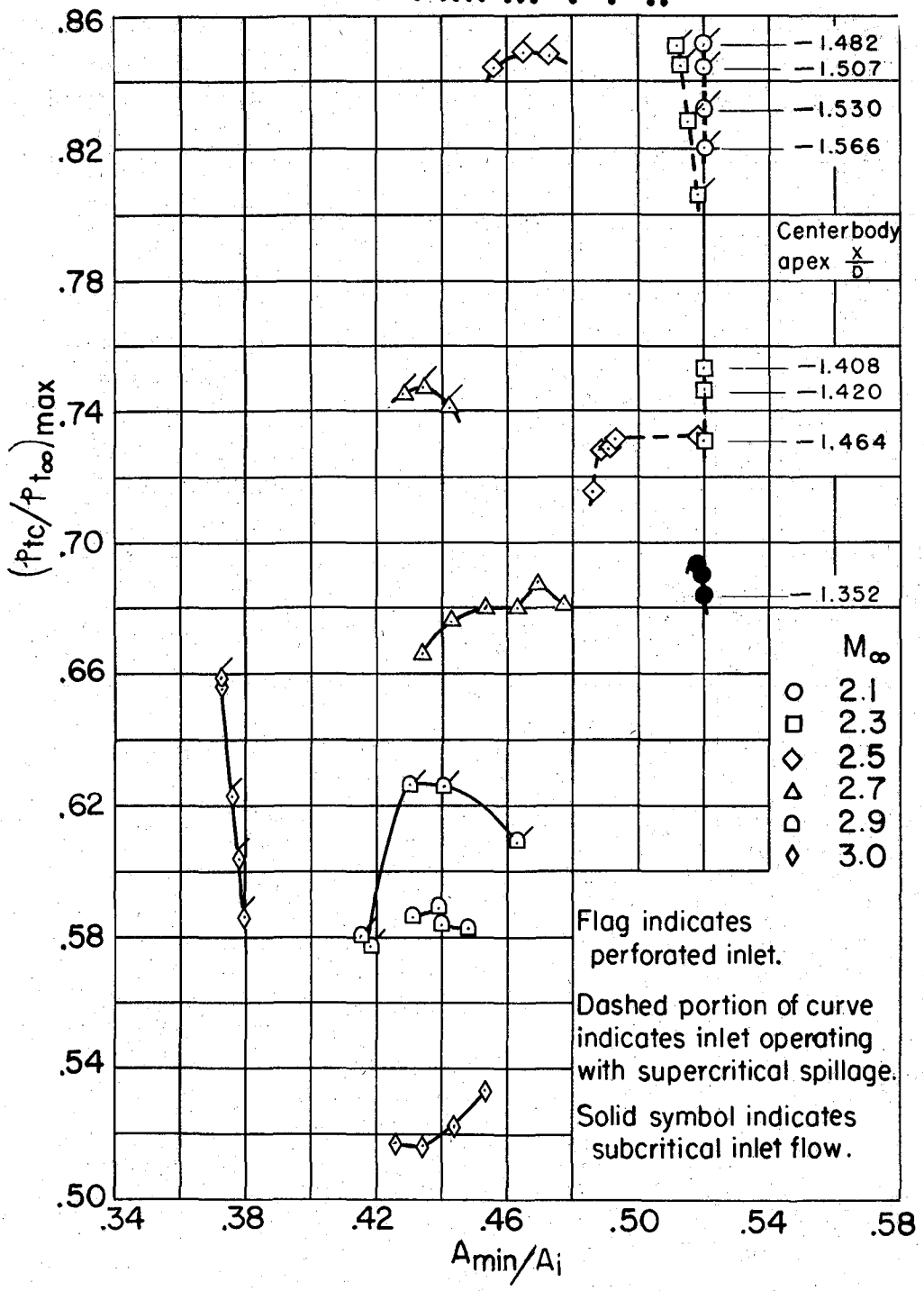

(f) Inlets II & II P

Figure 9.- Continued.

UNCLASSIFIED

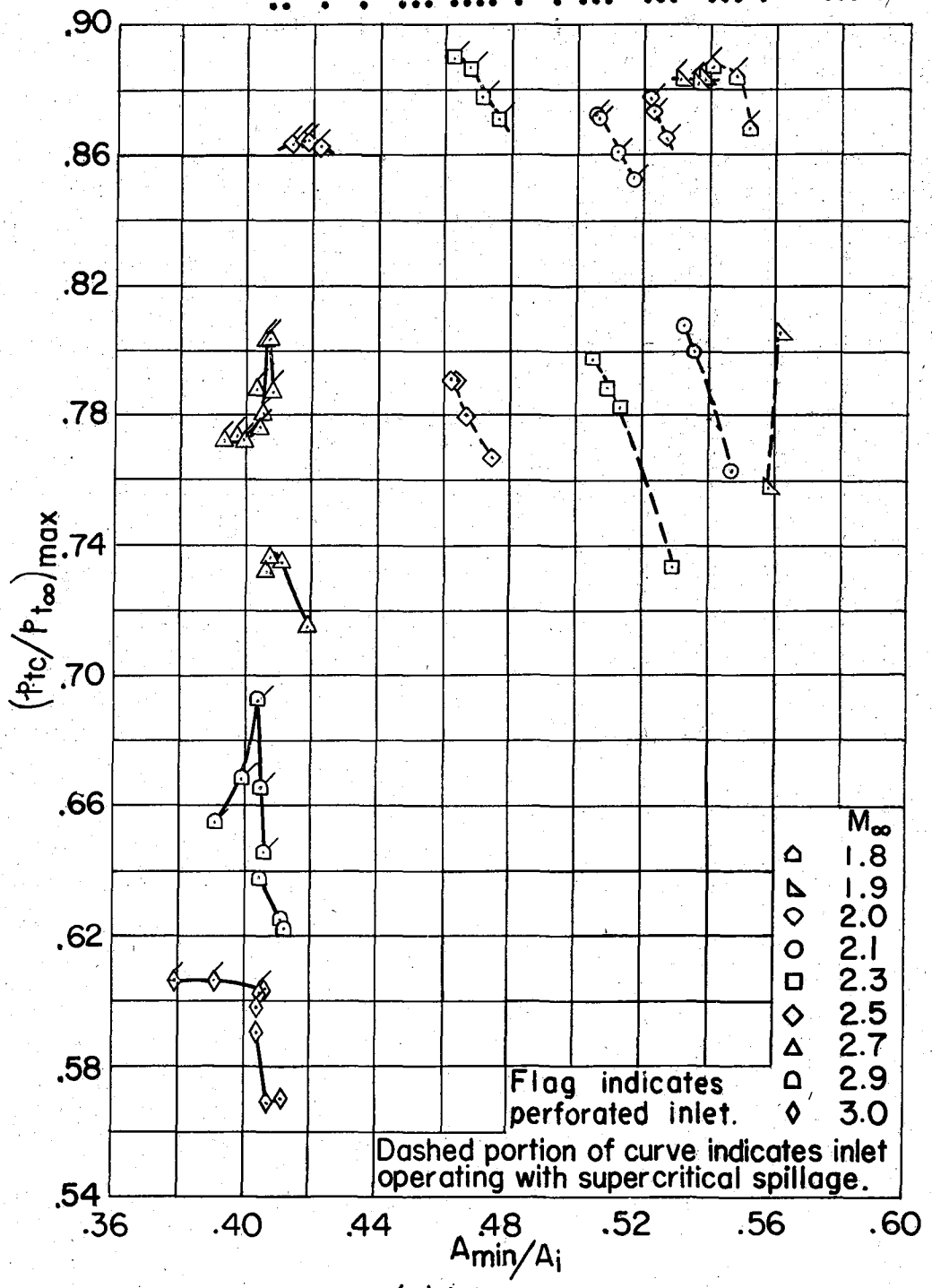

(g) Inlet I2&I2P

Figure 9.- Concluded.

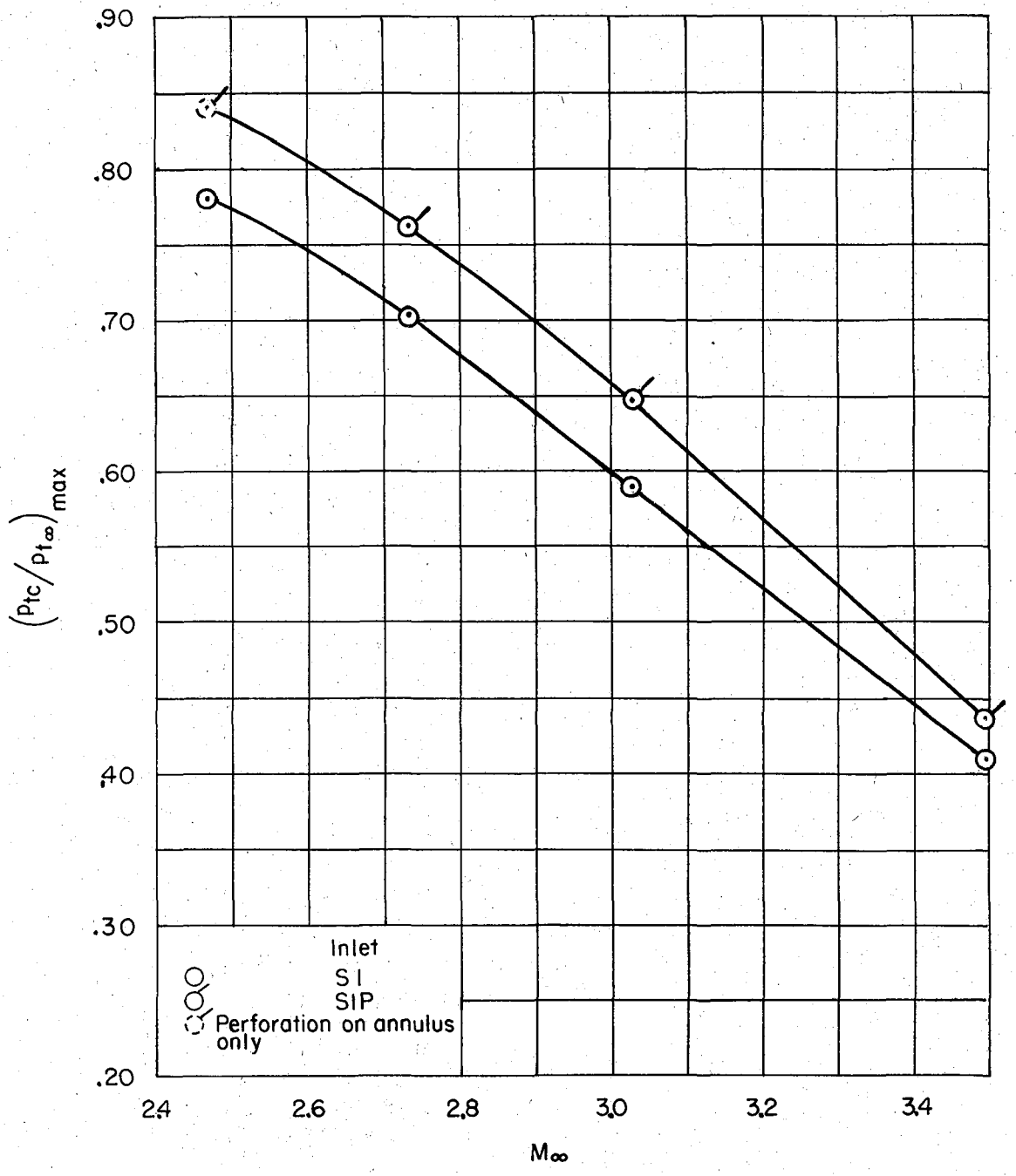

(a) Inlets S I & S I P

Figure 10.- Maximum pressure recovery as a function of Mach number for the seven inlets.

CONFIDENTIAL

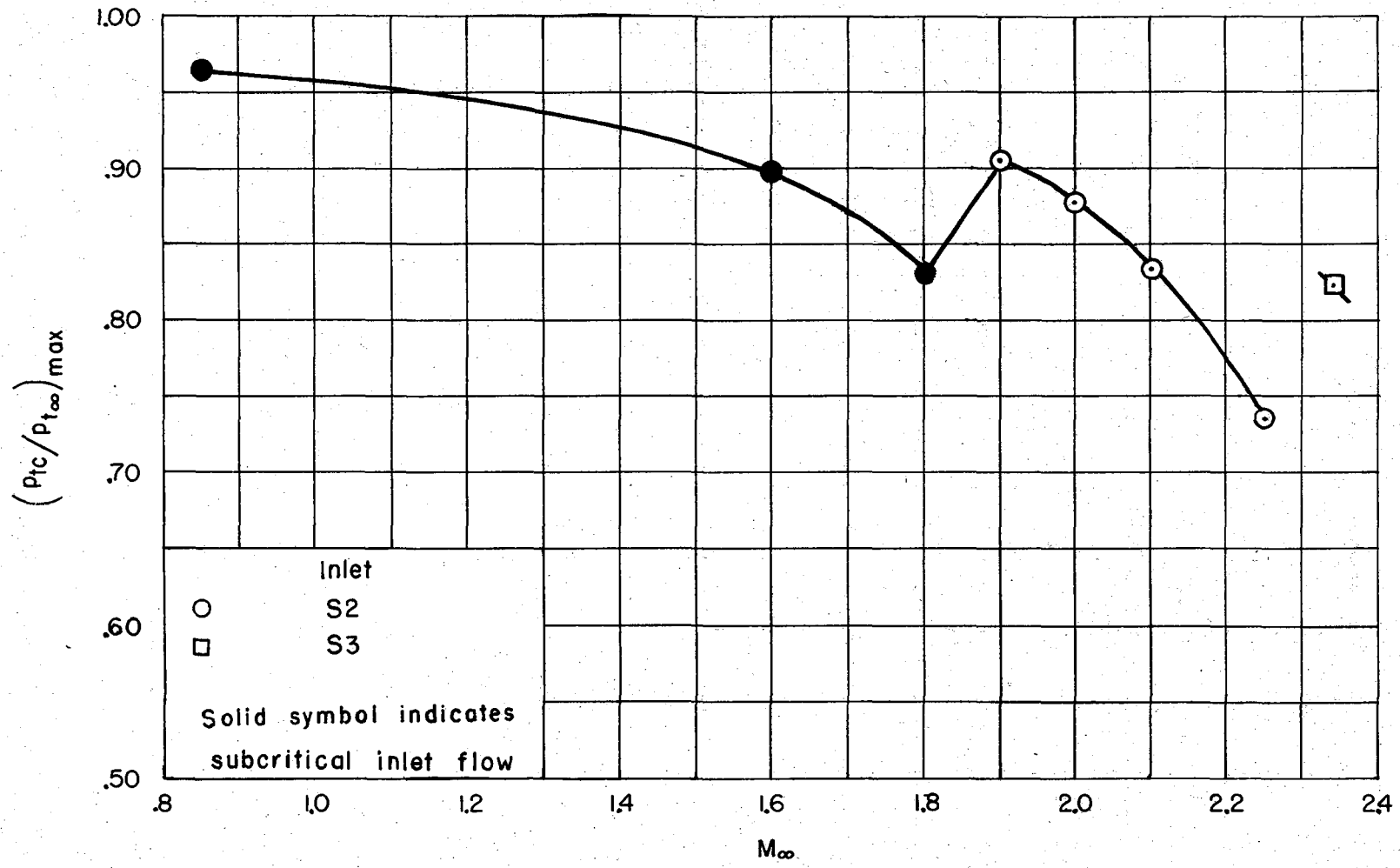

(b) Inlets S2 & S3

Figure 10.- Continued.

CONFIDENTIAL

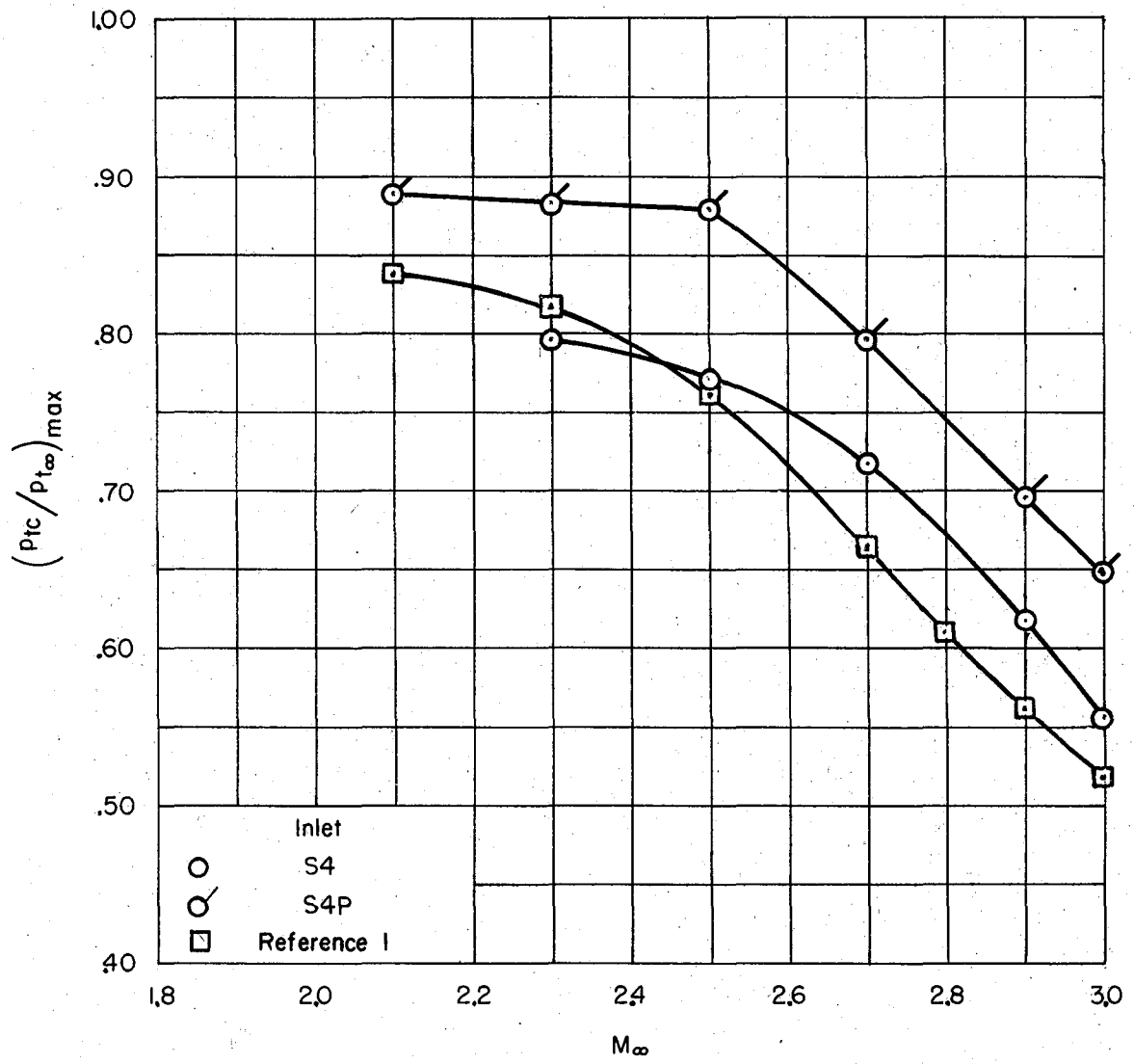

(c) Inlets S4&S4P

Figure 10.- Continued.

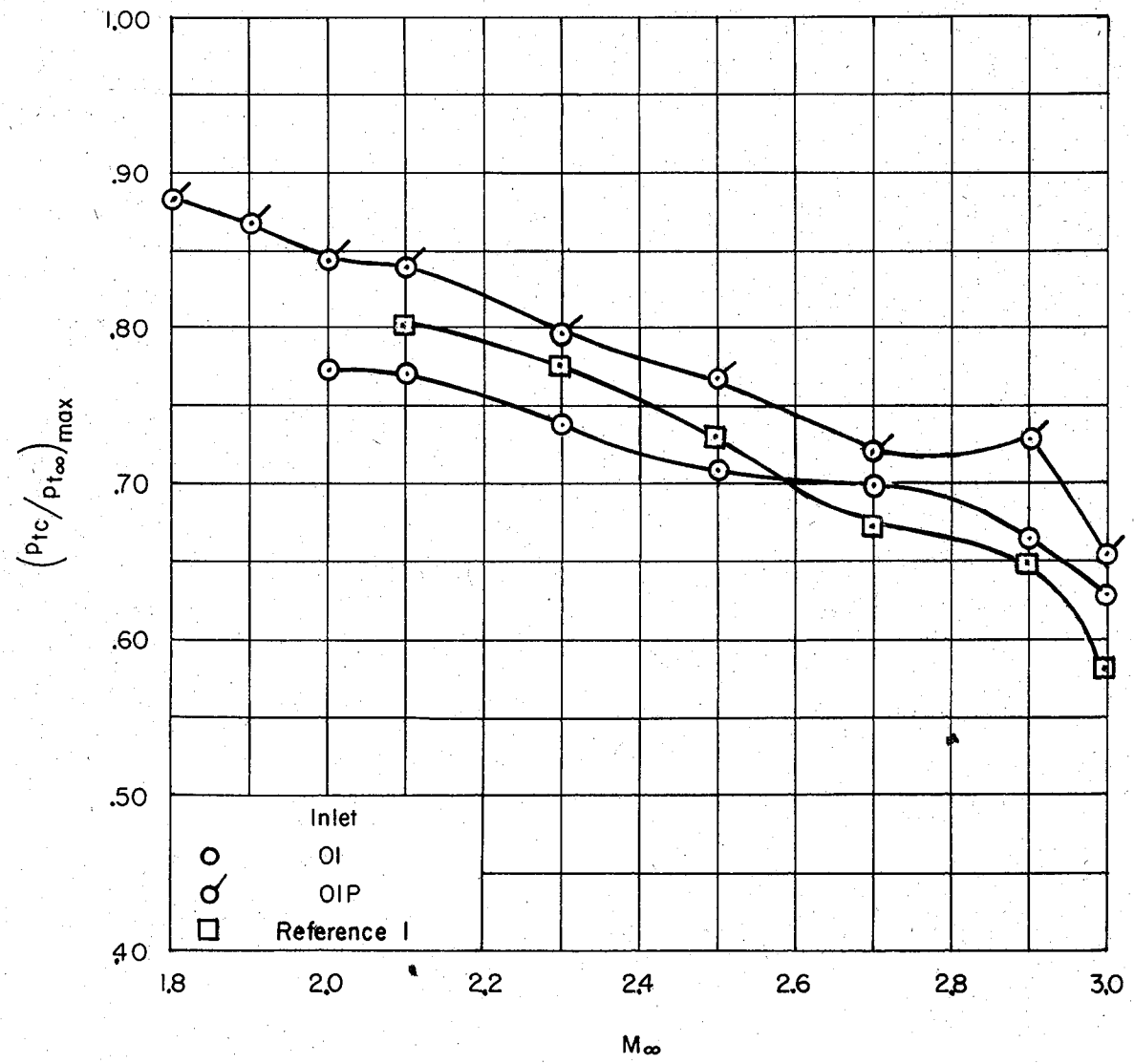

(d) Inlets OI & OIP

Figure 10.- Continued.

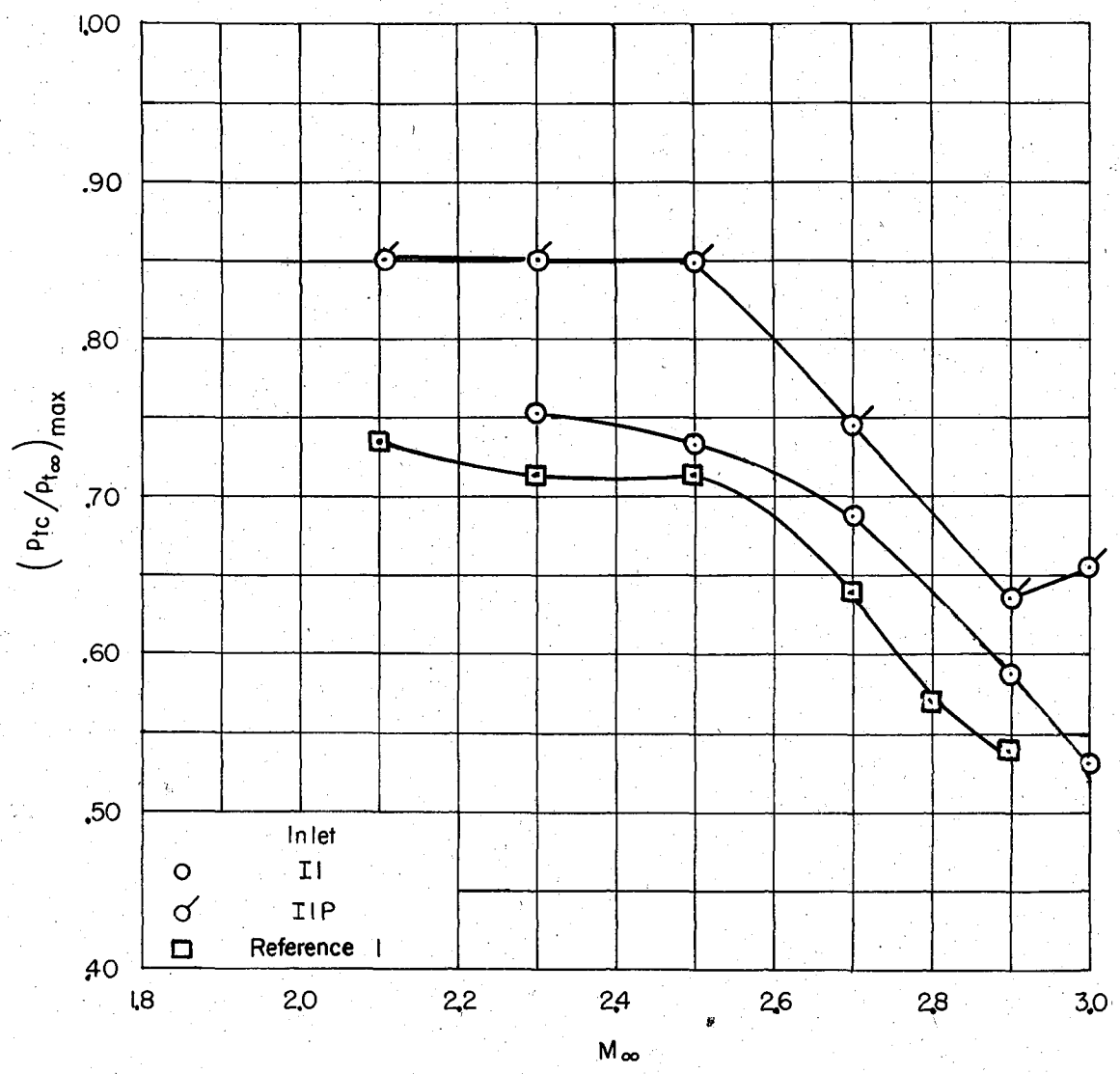

(e) Inlets II & IIP

Figure 10.- Continued.

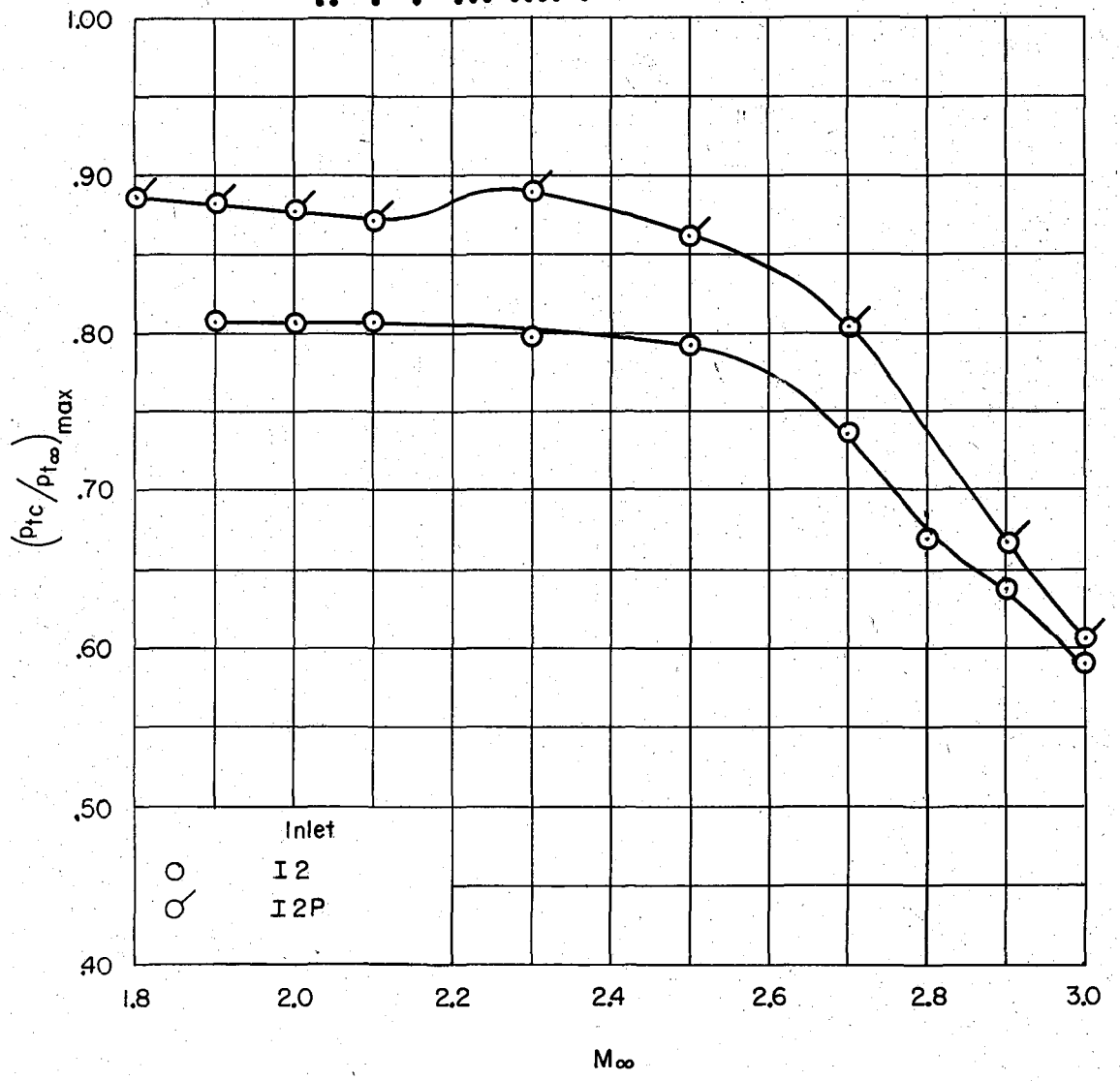

(f) Inlets I2 & I2P

Figure 10.- Concluded.

CONFIDENTIAL

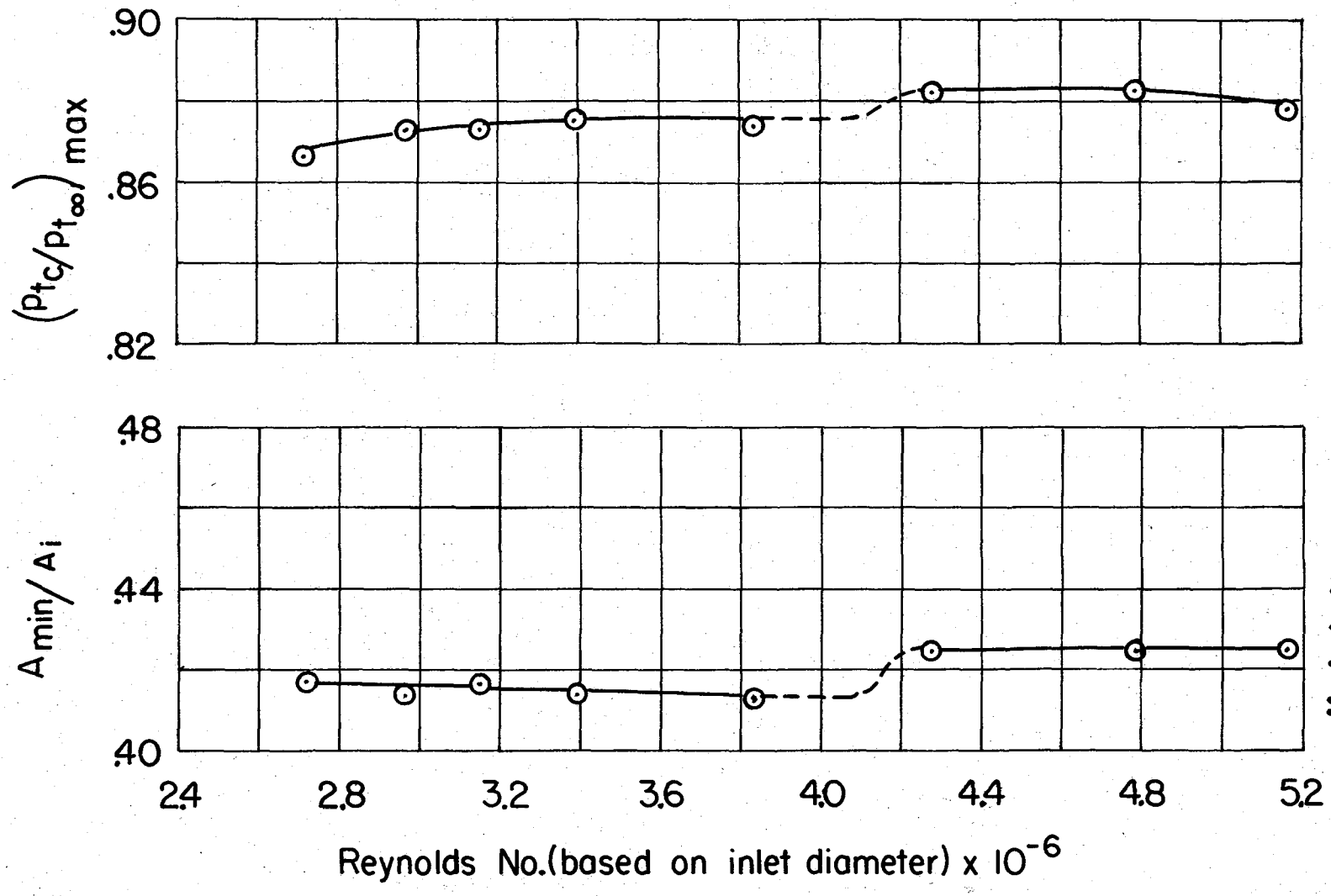

Figure 11.- Effect of Reynolds number on total-pressure recovery and contraction ratio; M = 2.5; $\alpha = 0^{\circ}$; Inlet I2P.

CONFIDENTIAL

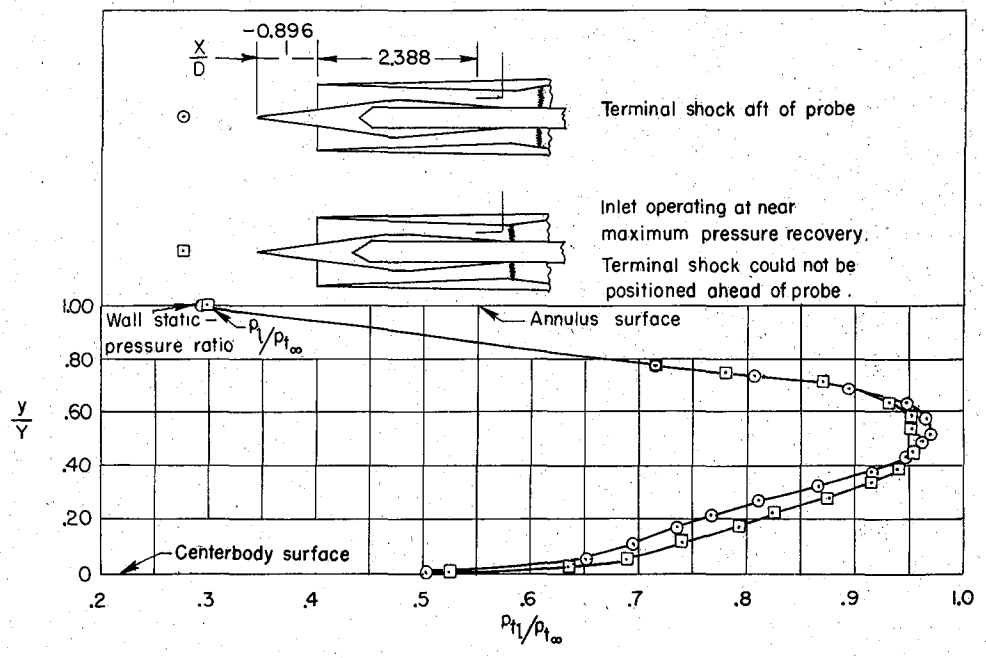

(a) Inlet S4

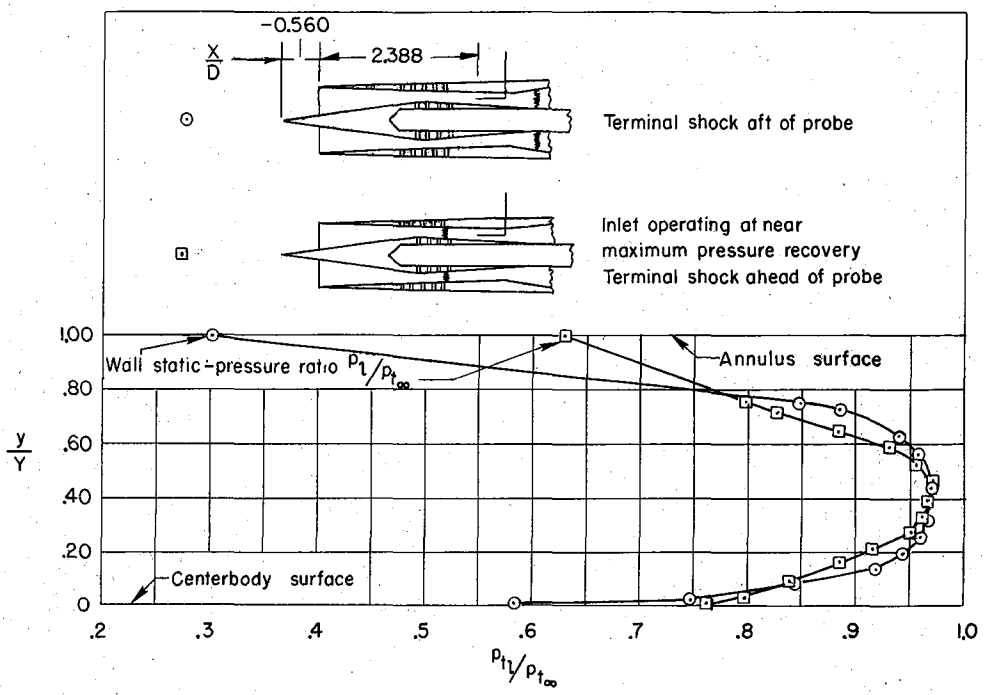

(b) Inlet S4P

Figure 12.- The distribution of the total-pressure ratio between the centerbody and annulus surfaces of inlets S4 and I2 with and without boundary-layer bleed; M = 2.5.

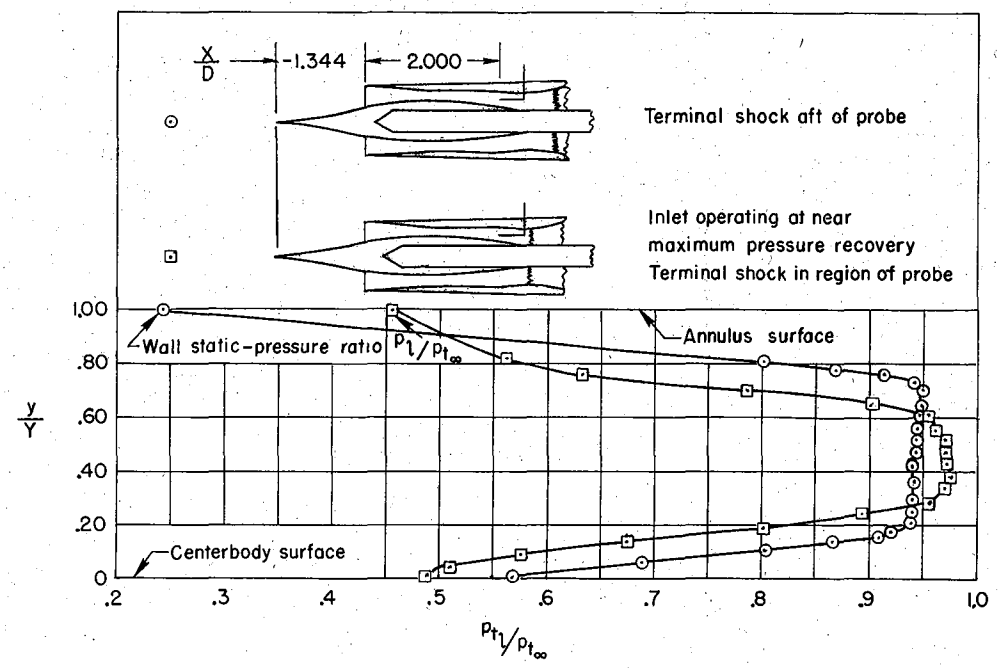

(c) Inlet I2

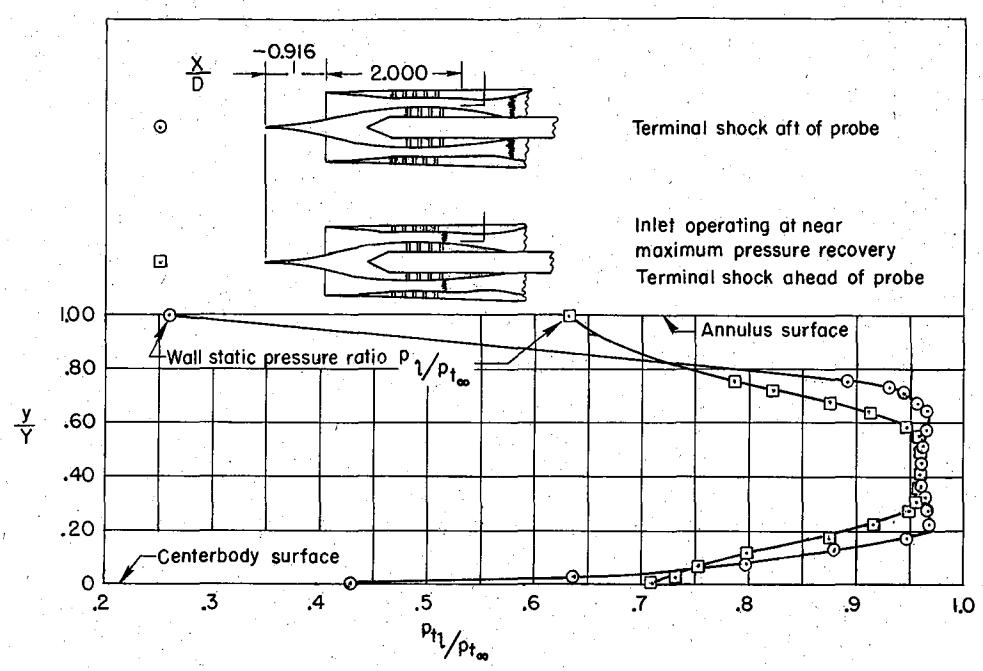

(d) Inlet I2 P

Figure 12.- Concluded.

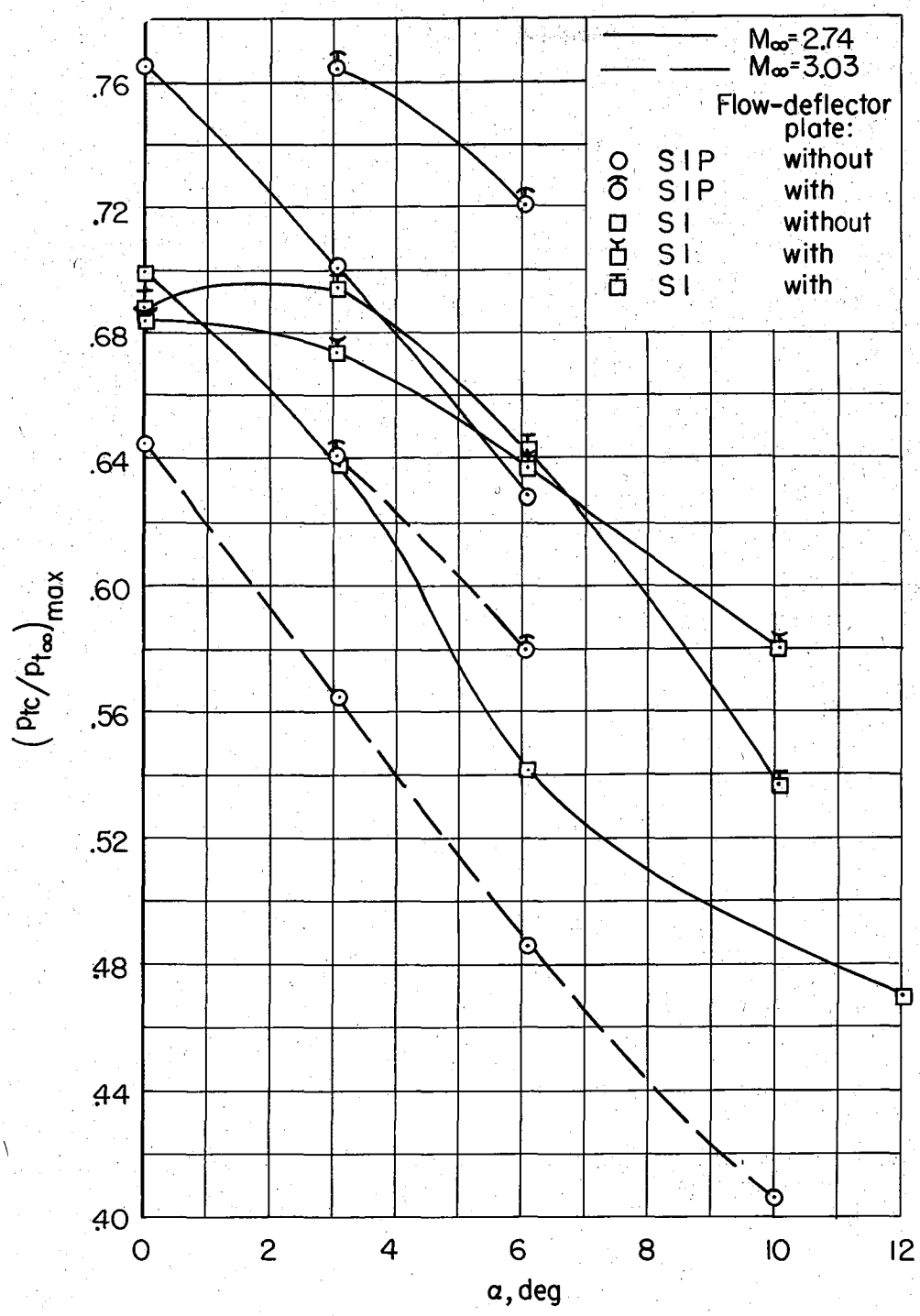

(a) Inlets SI & SIP

Figure 13.- Variation of maximum pressure recovery with angle of attack for two inlets.

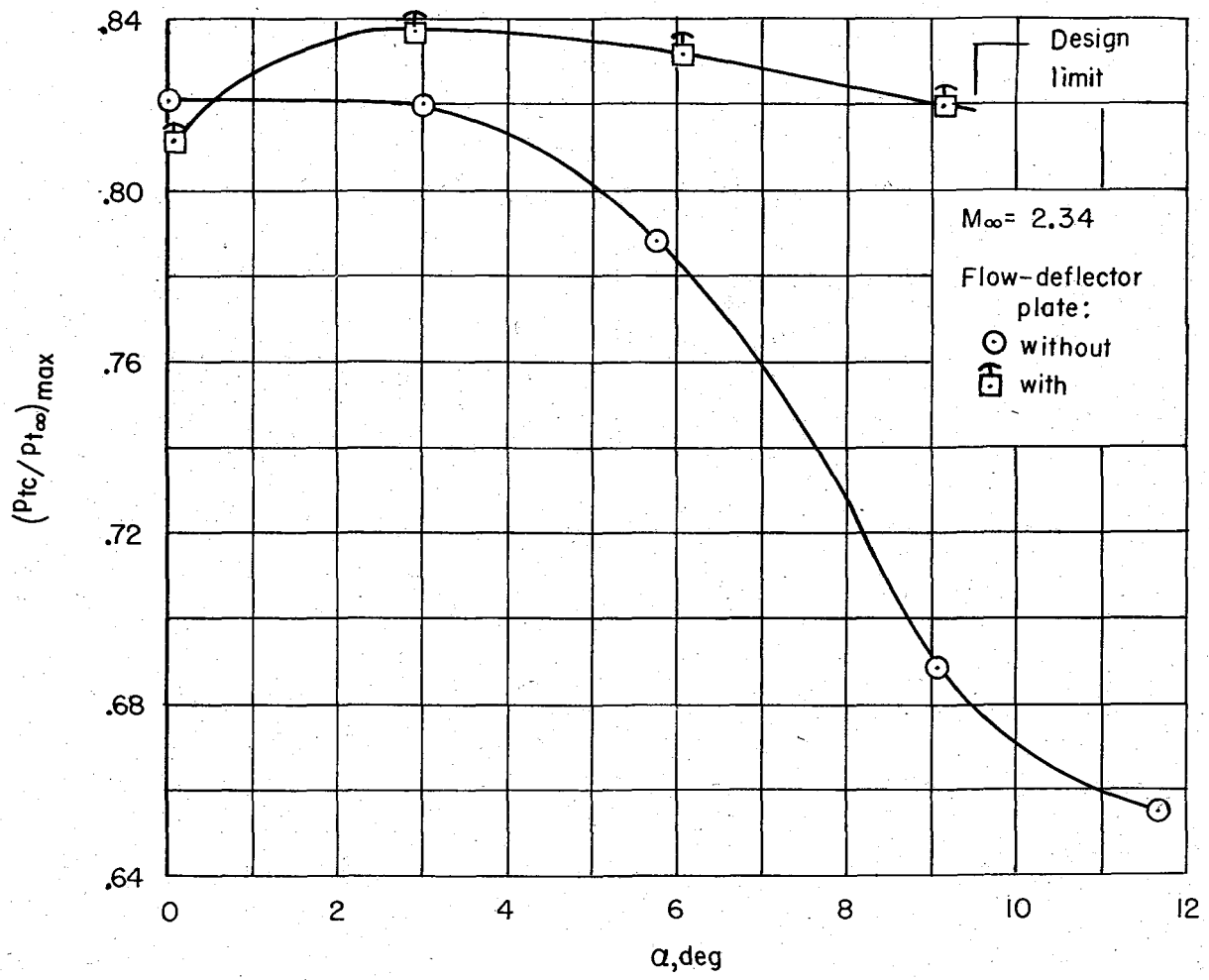

(b) Inlet S3

Figure 13.- Concluded.

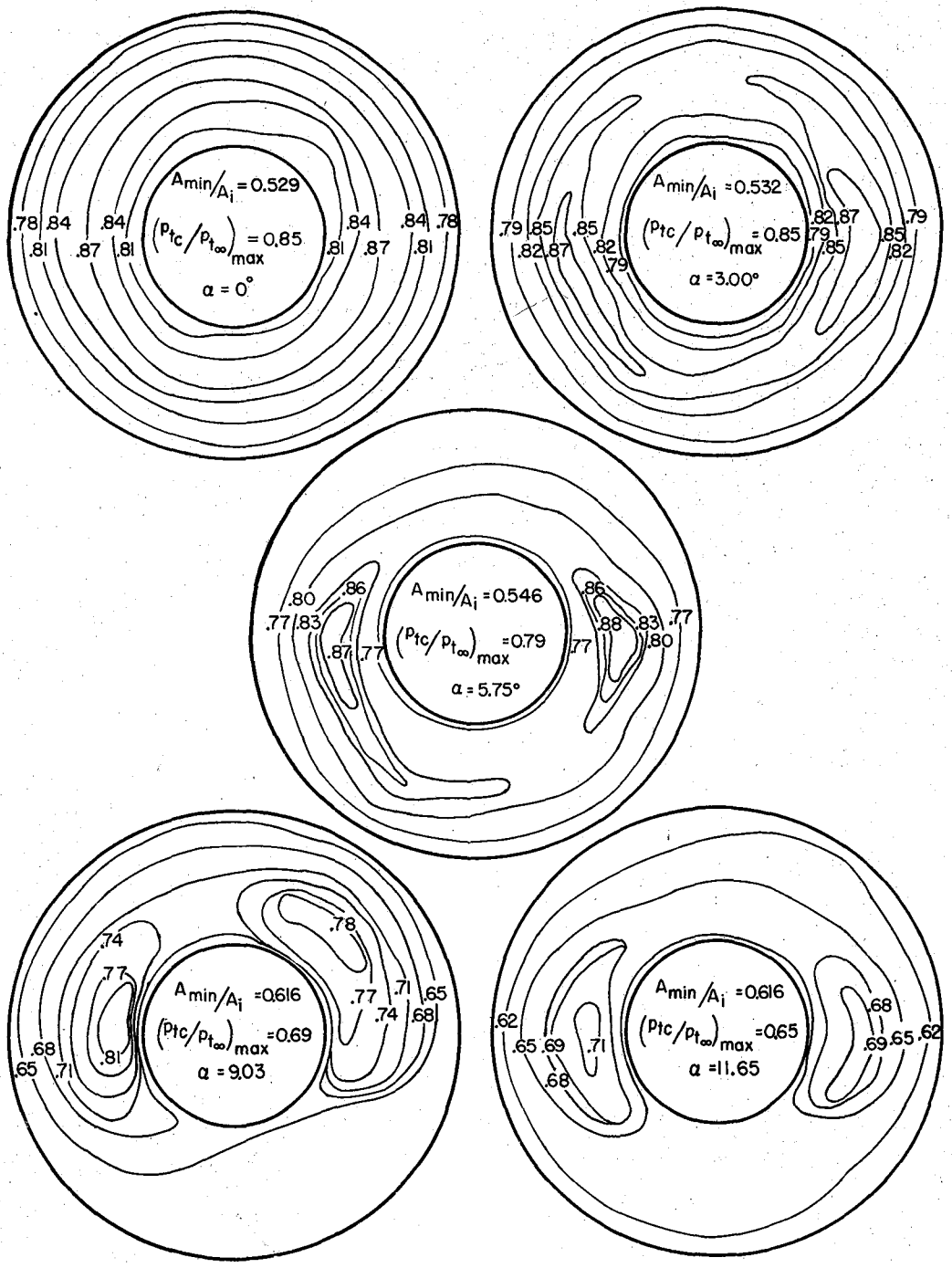

(a) Inlet S3 Without flow deflector plate, $M_\infty = 2.34$

Figure 14.- Contour lines of the total-pressure ratio at the compressor station for inlets S3 with and without a flow deflector plate and inlets S4, I2, and O1 with and without boundary-layer control.

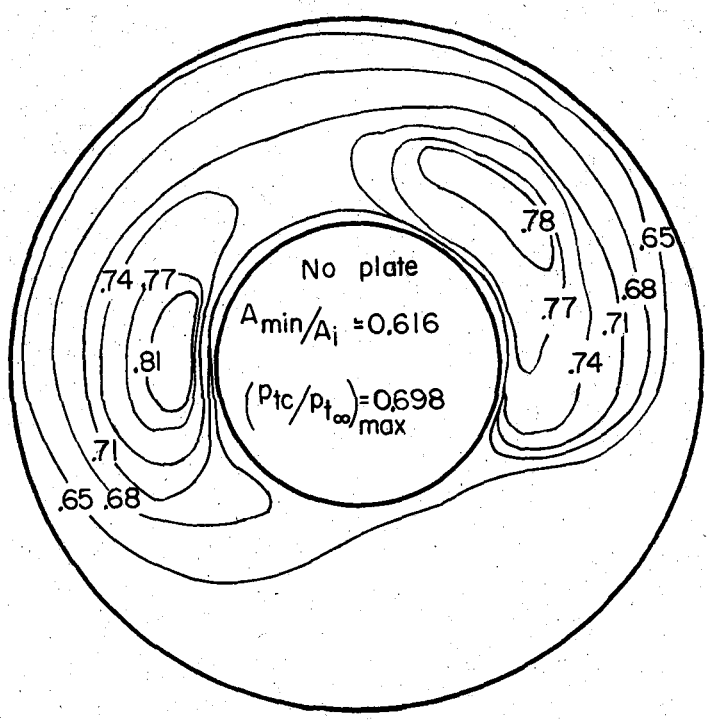

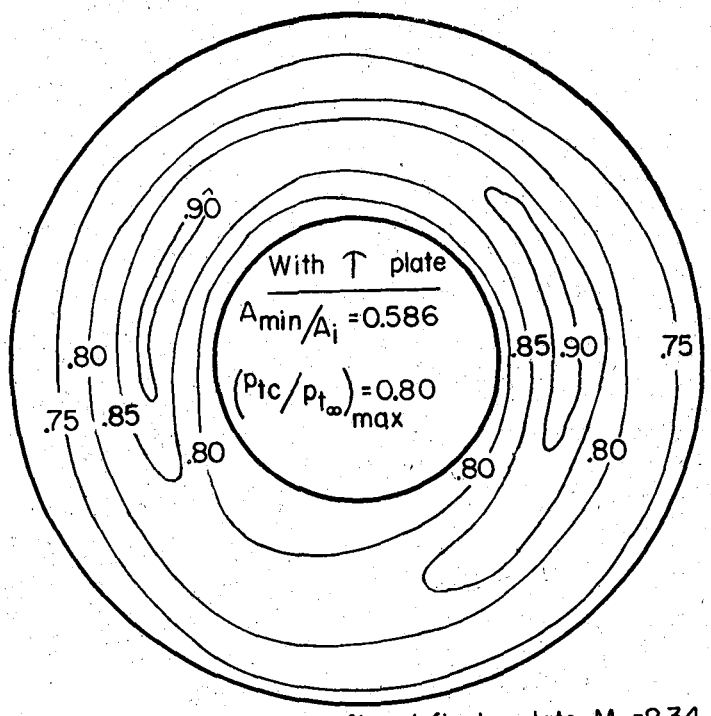

(b) Inlet S3 With & without flow deflector plate, M_∞=2.34 α=9°

Figure 14.- Continued.

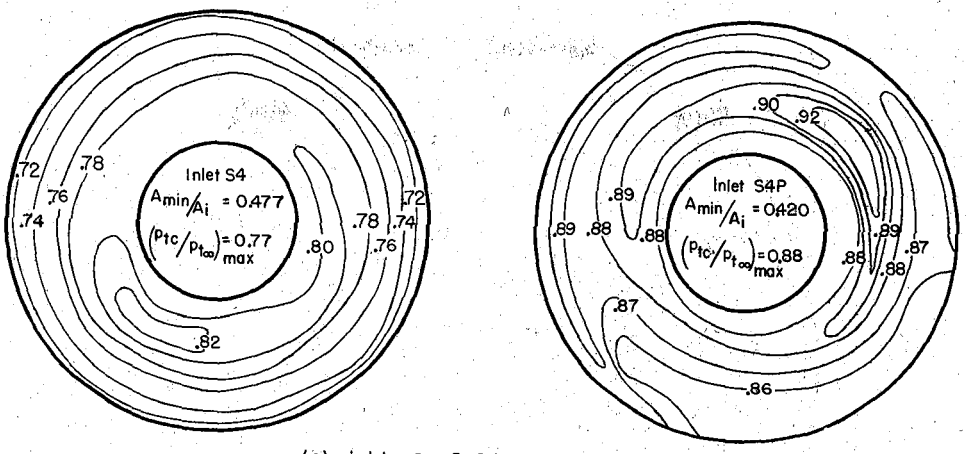

(c) Inlets S4 & S4P, $M_\infty = 2.5$, $\alpha = 0°$

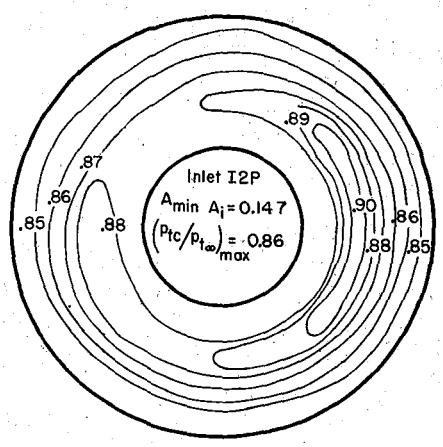

(d) Inlet I2P, $M_\infty = 2.5$, $\alpha = 0°$

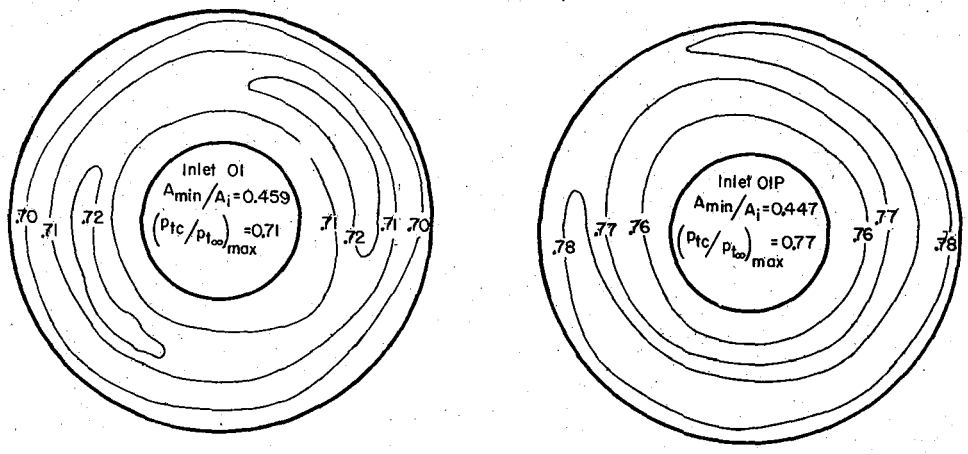

(e) Inlets OI & OIP, $M_\infty = 2.5$, $\alpha = 0°$

Figure 14.- Concluded.

CONFIDENTIAL

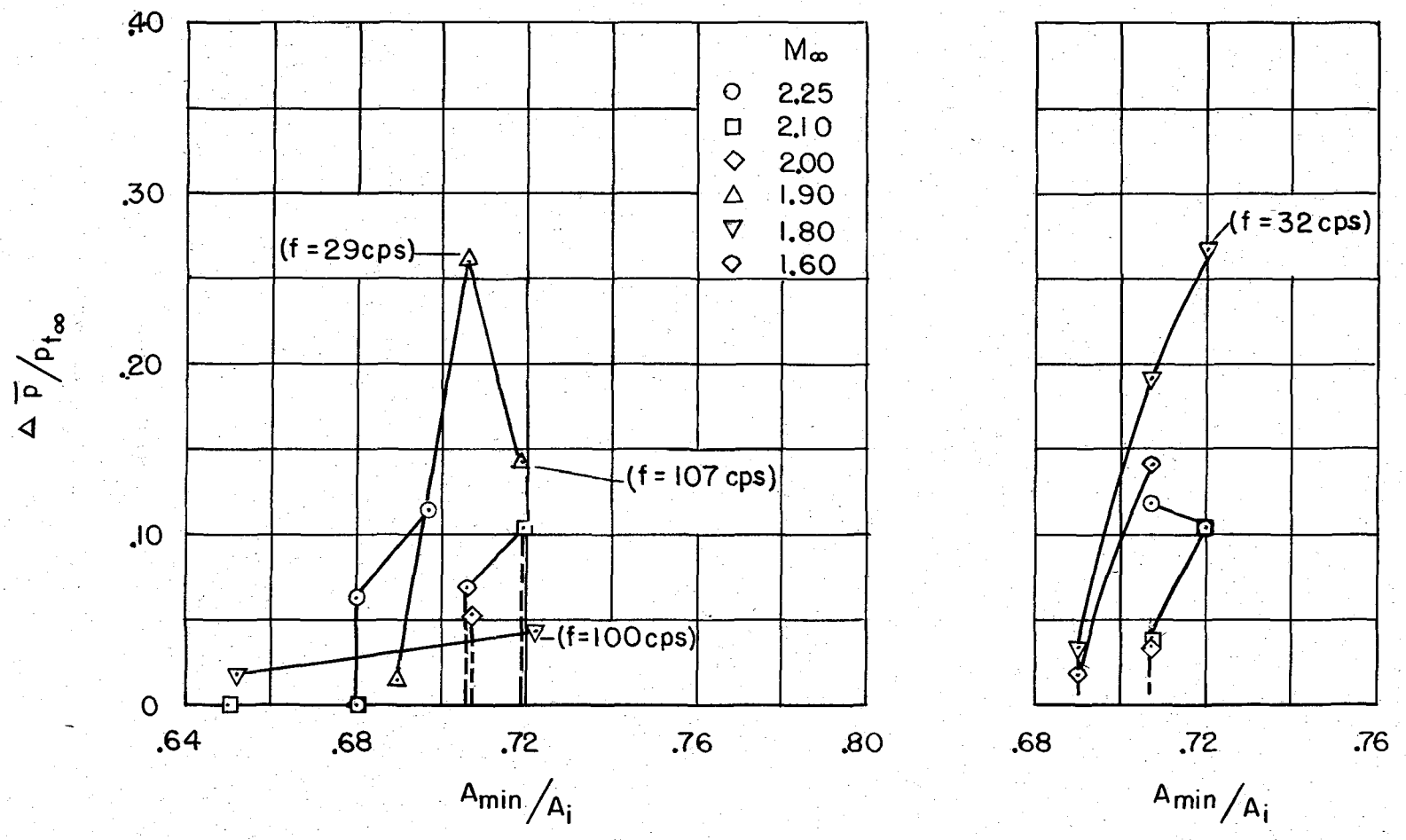

(a) $\alpha = 0°$

(b) $\alpha = 3.4°$

Figure 15.- Variation of air-flow unsteadiness with contraction ratio for inlet S2.

CONFIDENTIAL

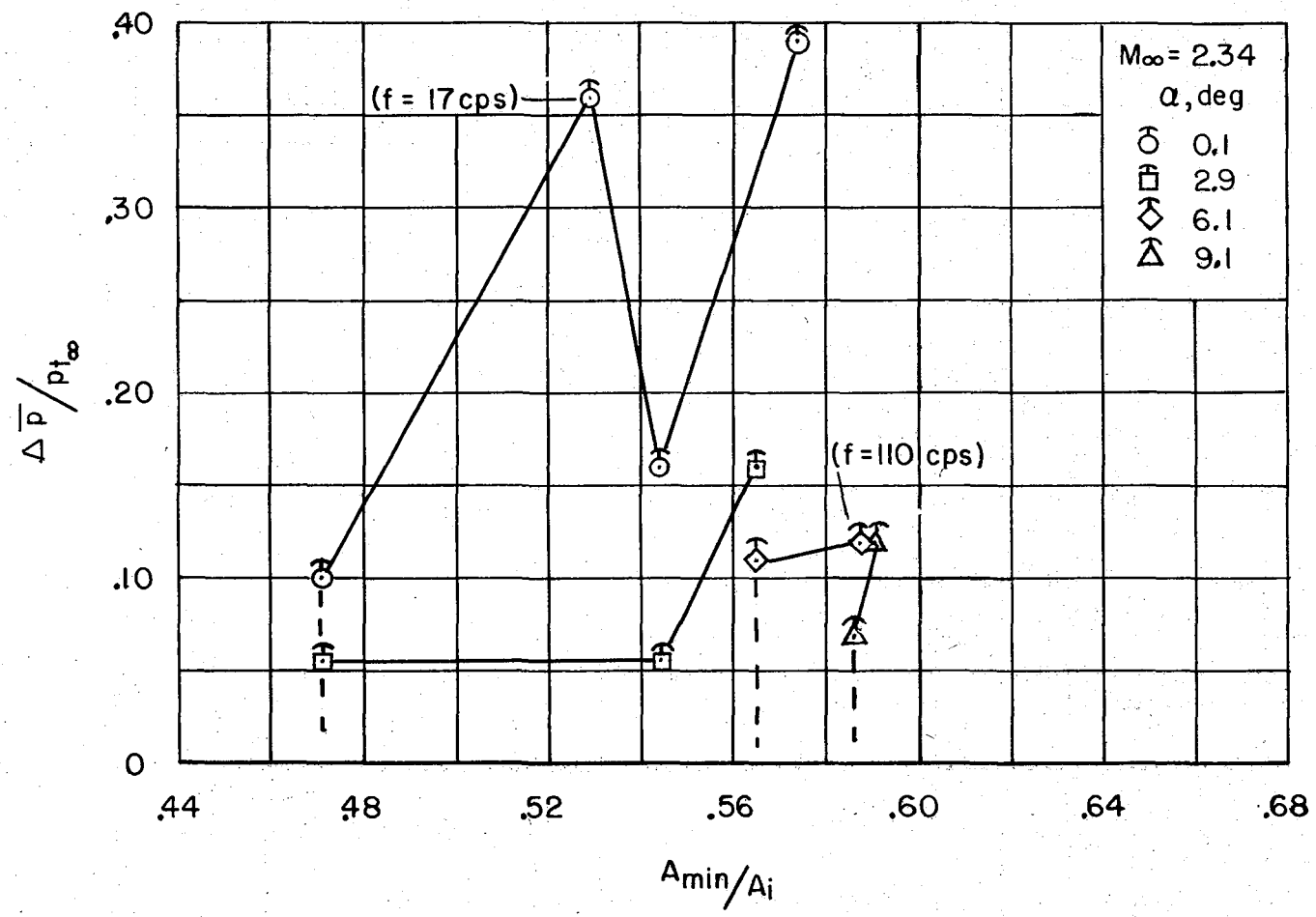

Figure 16.- Variation of air-flow unsteadiness parameter with contraction ratio for inlet S3 with flow deflector plate.

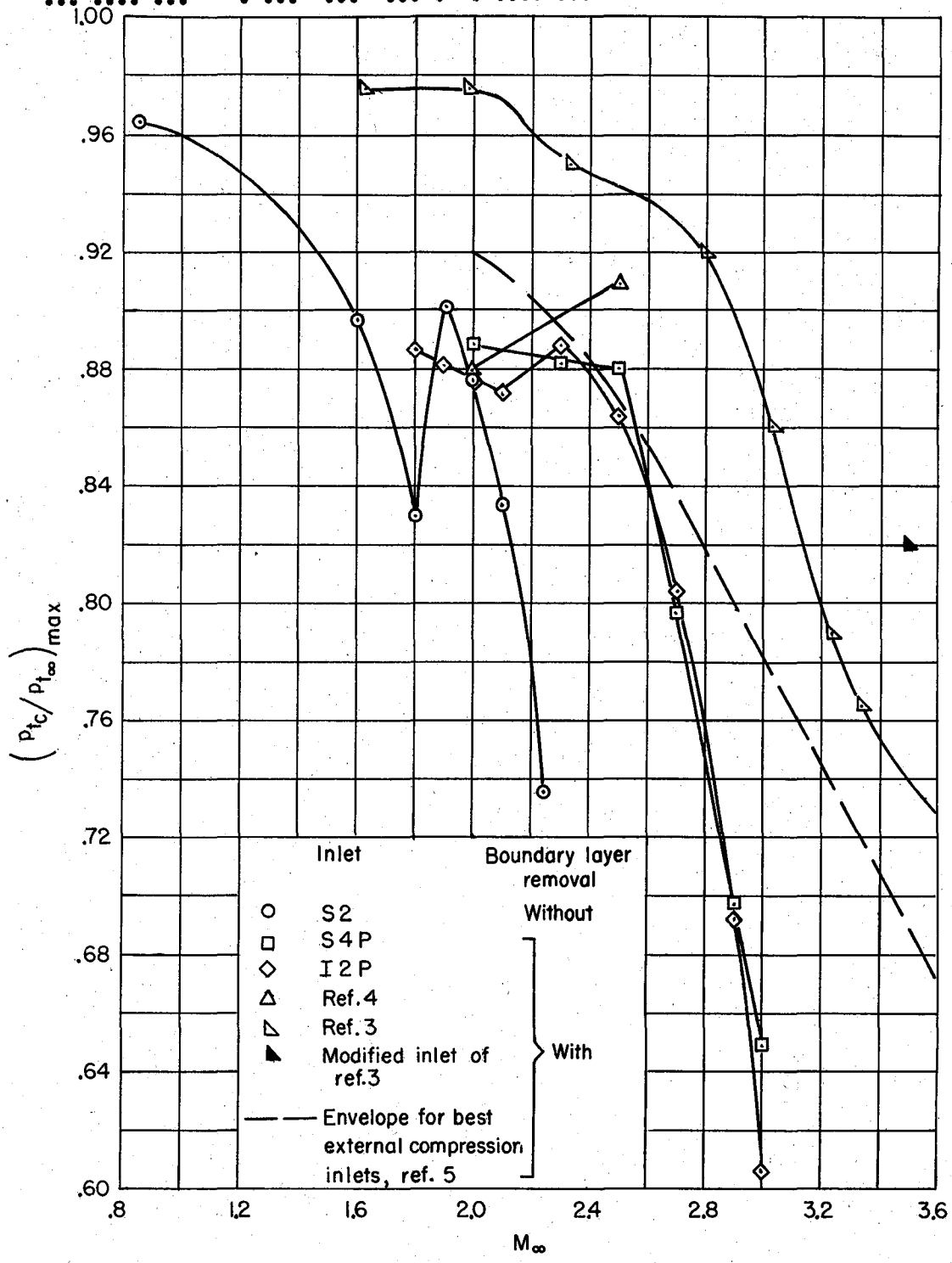

Figure 17.- Comparison of the maximum pressure recovery as a function of Mach number for several inlets.

UNCLASSIFIED

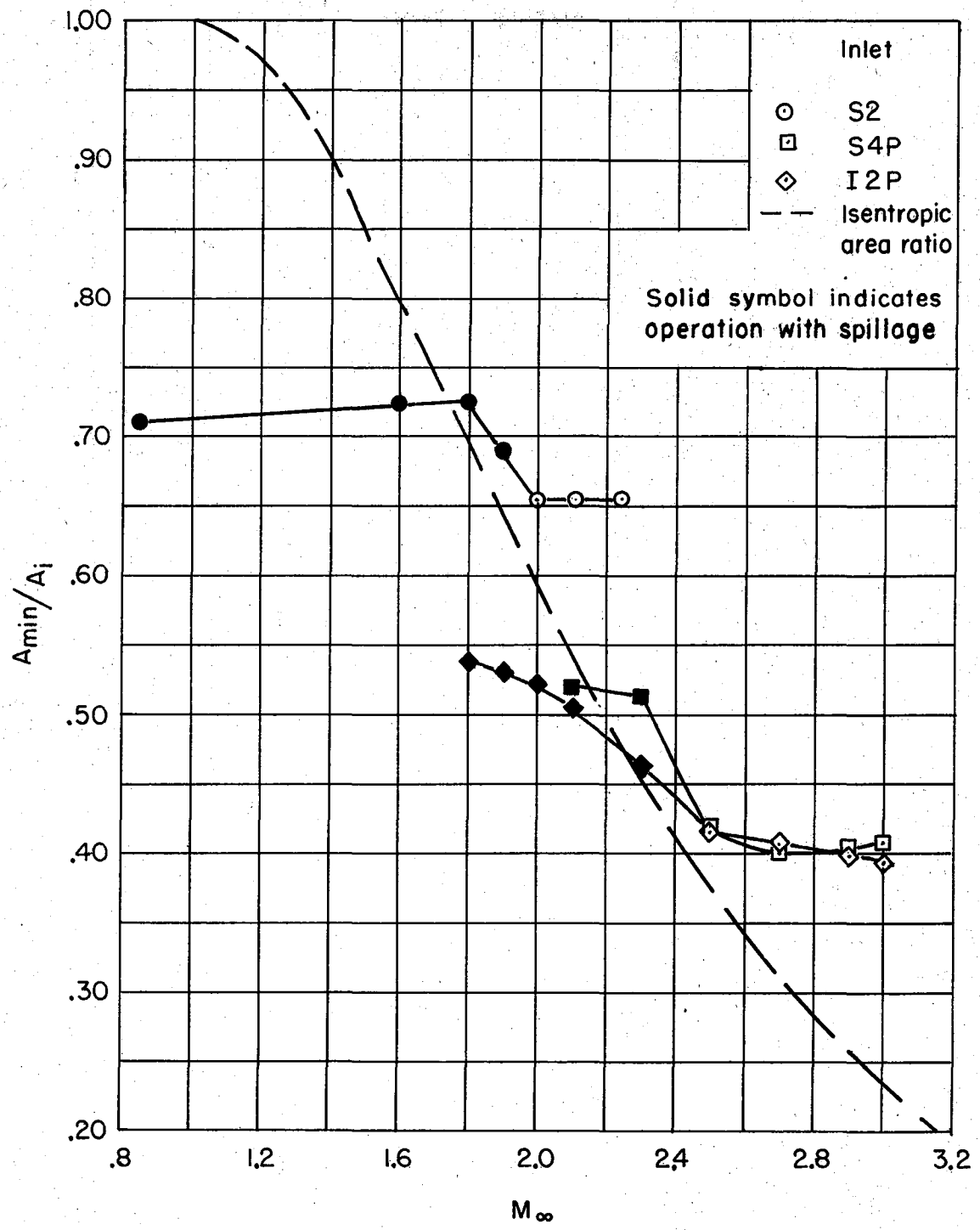

Figure 18.- Contraction ratio for maximum pressure recovery as a function of Mach number.

CONFIDENTIAL

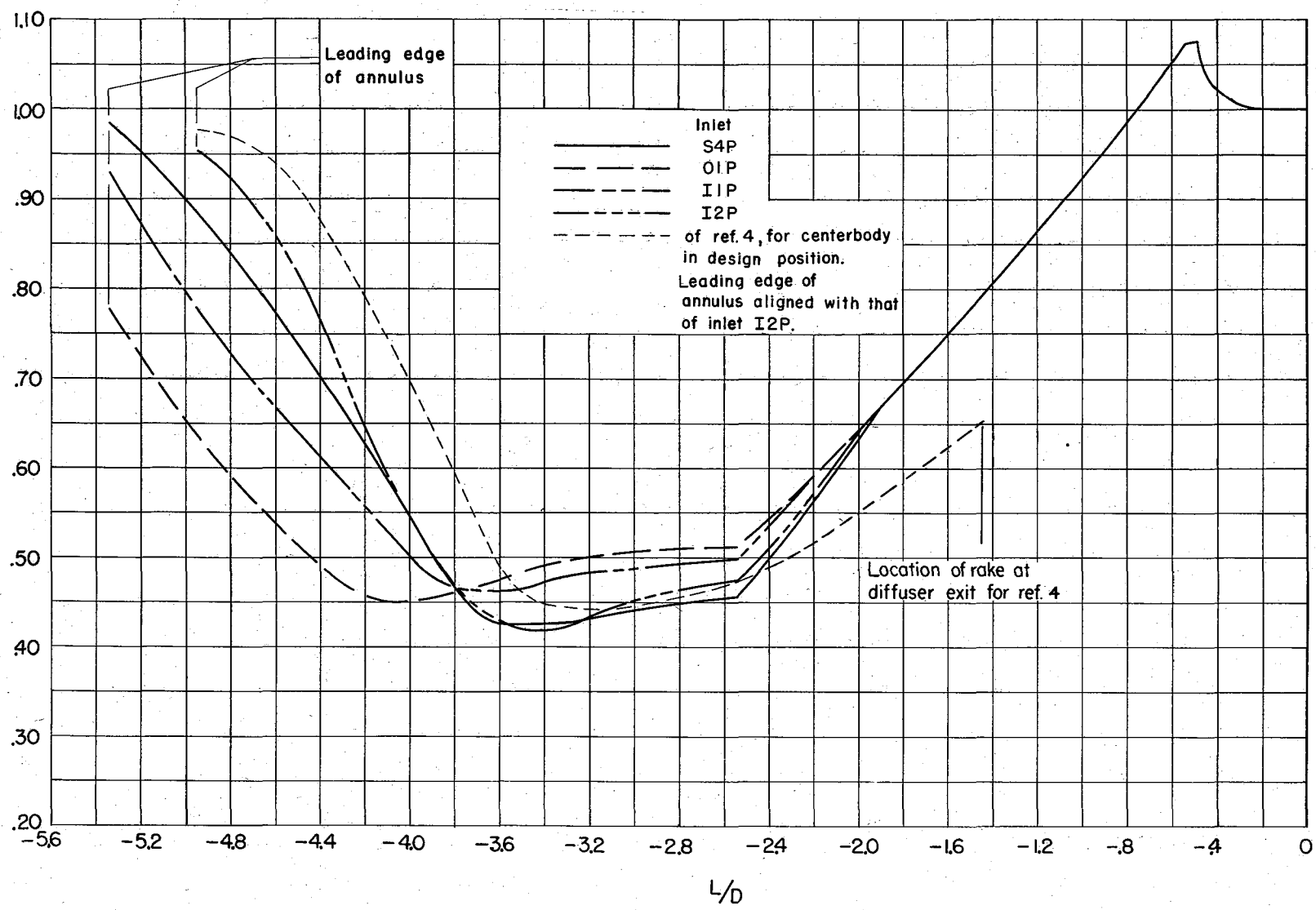

Figure 19.- Local internal area distribution as a function of the distance from the compressor station for the condition of maximum pressure recovery at M = 2.5.

CONFIDENTIAL

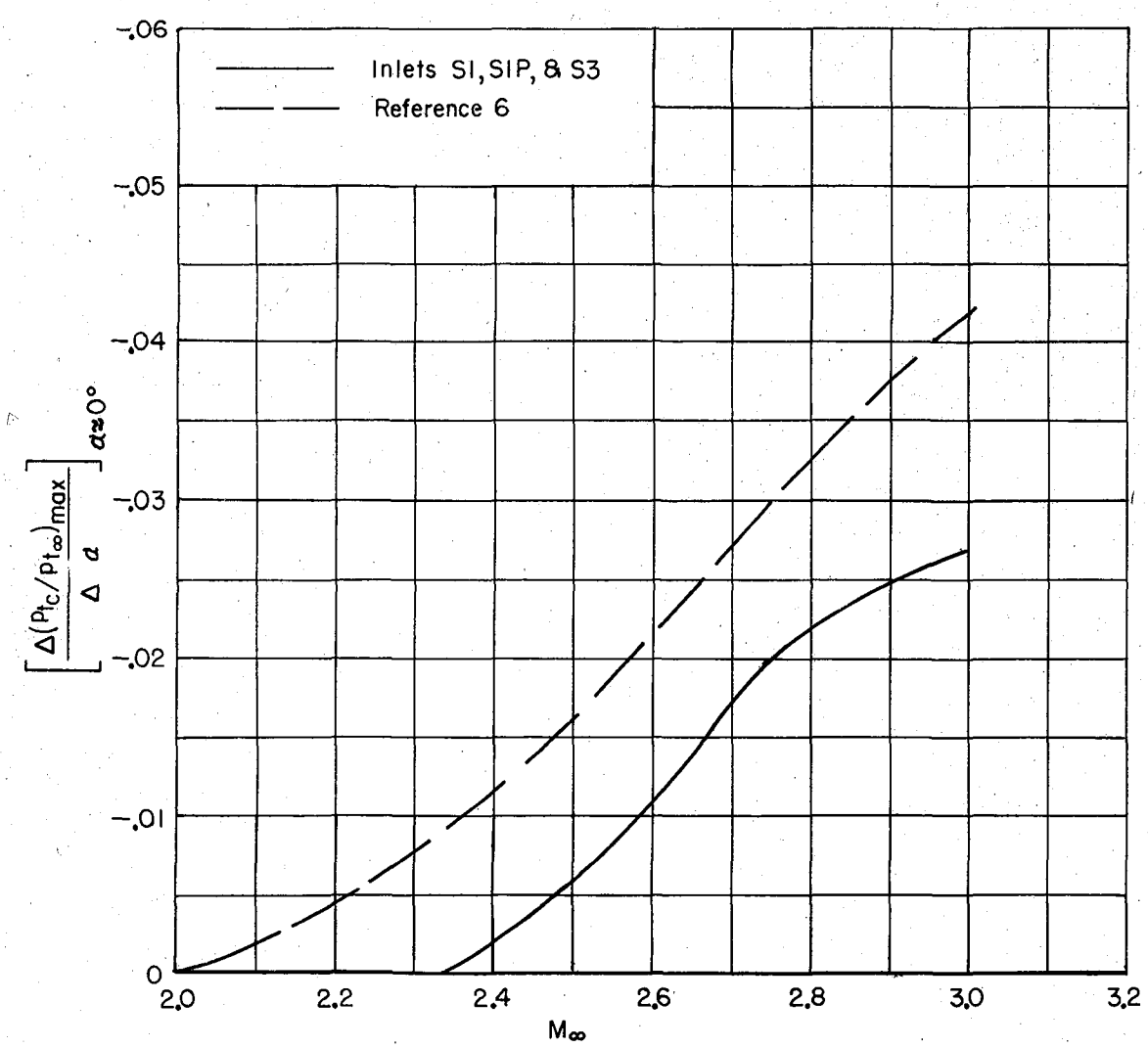

Figure 20.- The initial rate of change of pressure recovery with angle of attack as a function of Mach number.

NASA - Langley Field, Va. A-148

UNCLASSIFIED

NOTES: (1) Reynolds number is based on the diameter of a circle with the same area as that of the capture area of the inlet.

(2) The symbol * denotes the occurrence of buzz.

Report and facility	Description			Test parameters				Test data				Performance		Remarks
	Configuration	Number of oblique shocks	Type of boundary-layer control	Free-stream Mach number	Reynolds number $\times 10^{-6}$	Angle of attack, deg	Angle of yaw, deg	Drag	Inlet-flow profile	Discharge-flow profile	Flow picture	Maximum total-pressure recovery	Mass-flow ratio	
NASA MEMO 2-19-59A Ames 6- by 6-ft 8- by 7-ft 8- by 8-in wind tunnels	Straight inlet Ogival inlet Isentropic inlet	≅ 7 ≅ 7 isen-tropic	Holes drilled in annulus & centerbody (7 rows in annulus, 5 rows in centerbody)	0.85 to 3.50 1.8 to 3.0 1.8 to 3.0	0.6 to 3.0 2.0 to 3.0 2.0 to 5.2	0 to 12 0 0	0		x			M P.R. 2.1 0.89 2.5 .88 2.1 .84 2.5 .75 2.1 .87 2.5 .86	≈ 1.0	Seven models were tested with and without bleed. Flow deflector plates were effective in maintaining pressure recovery up to 90° angle of attack. A drag analysis and data for flow distortions, buzz, and Reynolds number, are presented.
NASA MEMO 2-19-59A Ames 6- by 6-ft 8- by 7-ft 8- by 8-in wind tunnels	Straight inlet Ogival inlet Isentropic inlet	≅ 7 ≅ 7 isen-tropic	Holes drilled in annulus & centerbody (7 rows in annulus, 5 rows in centerbody)	0.85 to 3.50 1.8 to 3.0 1.8 to 3.0	0.6 to 3.0 2.0 to 3.0 2.0 to 5.2	0 to 12 0 0	0		x			M P.R. 2.1 0.89 2.5 .88 2.1 .84 2.5 .75 2.1 .87 2.5 .86	≈ 1.0	Seven models were tested with and without bleed. Flow deflector plates were effective in maintaining pressure recovery up to 90° angle of attack. A drag analysis and data for flow distortions, buzz, and Reynolds number, are presented.
NASA MEMO 2-19-59A Ames 6- by 6-ft 8- by 7-ft 8- by 8-in wind tunnels	Straight inlet Ogival inlet Isentropic inlet	≅ 7 ≅ 7 isen-tropic	Holes drilled in annulus & centerbody (7 rows in annulus, 5 rows in centerbody)	0.85 to 3.50 1.8 to 3.0 1.8 to 3.0	0.6 to 3.0 2.0 to 3.0 2.0 to 5.2	0 to 12 0 0	0		x			M P.R. 2.1 0.89 2.5 .88 2.1 .84 2.5 .75 2.1 .87 2.5 .86	≈ 1.0	Seven models were tested with and without bleed. Flow deflector plates were effective in maintaining pressure recovery up to 90° angle of attack. A drag analysis and data for flow distortions, buzz, and Reynolds number, are presented.
NASA MEMO 2-19-59A Ames 6- by 6-ft 8- by 7-ft 8- by 8-in wind tunnels	Straight inlet Ogival inlet Isentropic inlet	≅ 7 ≅ 7 isen-tropic	Holes drilled in annulus & centerbody (7 rows in annulus, 5 rows in centerbody)	0.85 to 3.50 1.8 to 3.0 1.8 to 3.0	0.6 to 3.0 2.0 to 3.0 2.0 to 5.2	0 to 12 0 0	0		x			M P.R. 2.1 0.89 2.5 .88 2.1 .84 2.5 .75 2.1 .87 2.5 .86	≈ 1.0	Seven models were tested with and without bleed. Flow deflector plates were effective in maintaining pressure recovery up to 90° angle of attack. A drag analysis and data for flow distortions, buzz, and Reynolds number, are presented.

Bibliography

These strips are provided for the convenience of the reader and can be removed from this report to compile a bibliography of NACA inlet reports. This page is being added only to inlet reports and is on a trial basis.

CONFIDENTIAL

CONFIDENTIAL

CONFIDENTIAL

Restriction/Classification Cancelled